

BIOCHEMICAL AND BIOPHYSICAL CHARACTERIZATION OF THE
ALLOSTERIC EQUILIBRIUM OF THE
WISKOTT-ALDRICH SYNDROME PROTEIN

APPROVED BY SUPERVISORY COMMITTEE

Michael K. Rosen, Ph.D.

Melanie H. Cobb, Ph.D.

Kevin H. Gardner, Ph.D.

Philip J. Thomas, Ph.D.

This thesis is dedicated to my family

BIOCHEMICAL AND BIOPHYSICAL CHARACTERIZATION OF THE
ALLOSTERIC EQUILIBRIUM OF THE
WISKOTT-ALDRICH SYNDROME PROTEIN

by

Daisy W. Leung

DISSERTATION

Presented to the Faculty of the Graduate School of Biomedical Sciences

The University of Texas Southwestern Medical Center at Dallas

In Partial Fulfillment of the Requirements

For the Degree of

DOCTOR OF PHILOSOPHY

The University of Texas Southwestern Medical Center at Dallas

Dallas, Texas

December, 2005

Copyright

by

Daisy W. Leung, 2005

All Rights Reserved

Acknowledgements

I have many people to thank for making my graduate school experience so rewarding. First, I would like to express my sincerest gratitude to my mentor, Dr. Michael Rosen. His enthusiasm for science is particularly infectious and inspirational. I thank him for his many insightful comments and for challenging me to become a better biochemist everyday. I also thank him for the support and encouragement he has given to me throughout the years.

Second, I would like to thank all past and present members of the Rosen Lab. The lab has been a wonderful learning environment and I have truly benefited from interacting with everyone on a daily basis. In particular, I would like to thank Dr. Mara Kreishman-Deitrick, Dr. Gaya Amarasinghe, Dr. Eduardo Torres, and Daoqi You. These individuals, in particular, have provided many engaging scientific discussions, help, and support during our time together in New York and Dallas. I would like to thank Dr. Mara Kreishman-Deitrick and Dr. Gaya Amarasinghe for critical reading of my thesis. I would also like to acknowledge Drs. Annette Kim, Zehan Abdul-Manan, and Matthias Buck, whose work in the lab provided much of the foundation for my thesis.

I want to thank my thesis committee members Dr. Kevin Gardner, Dr. Melanie Cobb, and Dr. Philip Thomas for providing their advice, support, and encouragement over the course of my graduate studies.

My path to graduate school would not have been possible without the advice, support, and encouragement from Dr. Ernest Wright (UCLA). My gratitude and appreciation goes out to him for taking a chance on me and providing me with my first real opportunity to do research. I will always be indebted to him for that. I also have to

thank Drs. Donald Loo, Bruce Hirayama, and Eric Turk at UCLA for their scientific guidance.

Finally, I must thank my family and friends for all of their love, support, understanding, and patience over the last five years. Without their presence in my life, none of this work would have been possible. In particular, I have to especially thank both the Leung and Perez families: my parents, Shun and Yuk-Chun Leung, and members of my family, Anna Leung-Perez, Betty Leung, Celia Leung, Joey Perez, William Perez, and Katherine Perez. I also thank Gaya Amarasinghe for his support and encouragement.

Publications

- Leung, D. W., Morgan, D. M., and Rosen, M. K. (2006) Biochemical Properties and Inhibitors of (N-)WASP. *Methods Enzymol.* 406.
- Leung, D. W. and Rosen, M. K. (2005) The nucleotide switch in Cdc42 modulates coupling between the GTPase-binding and allosteric equilibria of Wiskott-Aldrich syndrome protein. *Proc. Natl. Acad. Sci.* 102(16): 5685-90.
- Labno, C. M., Lewis, C. M., You, D., Leung, D. W., Takesono, A., Kamberos, N., Seth, A., Finkelstein, L. D., Rosen, M. K., Schwartzberg, P. L., and Burkhardt, J. K. (2003) Itk functions to control actin polymerization at the immune synapse through localized activation of Cdc42 and WASP. *Curr. Biol.* 13(18): 1619-24.
- Leung, D. W., Turk, E., Kim, O., and Wright, E. M. (2002) Functional expression of the *Vibrio Parahaemolyticus* Na⁺/galactose (vSGLT) cotransporter in *Xenopus laevis* oocytes. *J. Membr. Biol.* 187: 65-70.
- Eskandari, S., Zampighi, G. A., Leung, D. W., Wright, E. M., and Loo, D. D. (2002) Inhibition of gap junction hemichannels by chloride channel blockers. *J. Membr. Biol.* 185: 93-102.
- Leung, D. W., Loo, D. D., Hirayama, B. A., Zeuthen, T., and Wright, E. M. (2000) Urea transport by cotransporters. *J. Physiol.* 528(2): 251-7.
- Panayotova-Heiermann, M., Leung, D. W., Hirayama, B. A., and Wright, E. M. (1999) Purification and functional reconstitution of a truncated human Na⁽⁺⁾/glucose cotransporter (SGLT1) expressed in *E. coli*. 459(3): 386-90.

BIOCHEMICAL AND BIOPHYSICAL CHARACTERIZATION OF THE
ALLOSTERIC EQUILIBRIUM OF THE
WISKOTT-ALDRICH SYNDROME PROTEIN

Publication No. _____

Daisy W. Leung, Ph.D.

The University of Texas Southwestern Medical Center at Dallas, 2005

Supervising Professor: Michael K. Rosen, Ph.D.

Proteins provide the essential building blocks of signal transduction pathways governing many biological processes. They are dynamic entities endowed with properties that allow them to respond to changes in the cell while maintaining specificity and fidelity of signaling in a crowded intracellular environment. Many signaling proteins are regulated by a subset of allostery where intramolecular interactions modulate the conformational equilibrium between an autoinhibited, inactive state and an active state. Relief of autoinhibition then requires that covalent modification or binding events shift

the equilibrium to favor the active state. However, the structural, biochemical, and biophysical properties of many autoinhibited systems have not been characterized. Thus, an understanding of how binding events are coupled to effector activation remains incomplete.

Previous work in our lab has described a framework based upon classical descriptions of allostery with which we can examine the regulation and activation of the Wiskott-Aldrich Syndrome protein (WASP) by the Rho-family GTPase Cdc42. Results from this work revealed that a simple two-state model can predict the hydrogen exchange behavior and binding affinity for Cdc42-GTP of WASP proteins over a range of folding stabilities. The goals of my thesis have been: 1) to further develop the quantitative two-state model of the allosteric regulation of WASP, 2) to understand how binding of Cdc42 is coupled to WASP activation toward Arp2/3 complex-mediated actin polymerization, and 3) to understand the implications of the GTPase nucleotide switch on effector activation.

In order to expand upon the range of WASP protein folding stabilities and to, more importantly, examine the relationship between Cdc42 binding and WASP activity towards the Arp2/3 actin nucleation complex, I generated a different series of WASP proteins by introducing mutations in the autoinhibited core of a more physiologically relevant WASP construct, which I used to parameterize our two-state model. Model predictions of WASP affinity for Cdc42, activity toward Arp2/3 complex, and activation by Cdc42 are all borne out experimentally and are functions of the two-state allosteric equilibrium of WASP. Application of the model to Cdc42-GDP revealed that the ratio of binding affinities for the inactive and active states of WASP is significantly smaller for

Cdc42-GTP than for Cdc42-GDP. Thus, the GTP-bound state of Cdc42 is more effective at distinguishing between the two states of WASP, converting Cdc42-GDP from a partial agonist to a full agonist of WASP. Therefore, the nucleotide switch in Cdc42 is not only based upon a change in affinity for the two states of WASP, but also the efficiency of coupling between the binding and allosteric equilibria of WASP. These properties have important implications for how specificity and fidelity of signaling can be maintained in a crowded intracellular environment, ensuring that only Cdc42-GTP can activate WASP and signal downstream.

Table of Contents

Title Fly.....	i
Dedication.....	ii
Title Page.....	iii
Copyright.....	iv
Acknowledgements.....	v
Publications.....	vii
Abstract.....	viii
Table of Contents.....	xi
List of Figures.....	xiii
List of Tables.....	xv
List of Abbreviations.....	xvi
 Chapter 1 Allosteric regulation of biological processes	 1
Introduction.....	1
Allosteric mechanisms.....	3
Coupled ligand equilibria.....	3
The MWC model.....	6
The KNF and general models.....	9
Classical allosteric systems.....	13
Modular allosteric systems.....	14
Conclusion.....	19
References.....	23
 Chapter 2 Regulation of the cellular actin cytoskeleton	 28
Introduction.....	28
Actin dynamics in the cell.....	28
Nucleators of actin polymerization.....	32
Regulation of the actin cytoskeleton by Rho GTPases and their effectors.....	35
WASP is an effector of the Rho GTPase Cdc42.....	40
Conclusion.....	63
References.....	65
 Chapter 3 Development of a two-state model describing the allosteric regulation and activation of WASP	 76
Introduction.....	76
Formulation of the WASP two-state model.....	76
Generation of mutations in WASP GBD-C.....	83
Biochemical characterization of WASP GBD-C mutants.....	87
Parameterization of the two-state model using WASP GBD-VCA mutant proteins.....	94
Development of a conformation specific antibody for the activated state of WASP.....	115
Conclusion.....	120

Materials and Methods.....	124
References.....	153
 Chapter 4 Modulation of the allosteric equilibrium of WASP by Cdc42	157
Introduction.....	157
The biophysical basis of the Cdc42 nucleotide switch on the activation of WASP	158
Conclusion	180
Materials and Methods.....	186
References.....	189
 Chapter 5 Conclusion of thesis work	192
References.....	202
 Appendix I Derivation of Equations	204

List of Figures

Figure 1-1	Basic features of allostery	2
Figure 1-2	Free energy diagram describing the binding to two ligands, L1 and L2, to a protein, P	5
Figure 1-3	MWC model of allostery	8
Figure 1-4	KNF model of allostery	10
Figure 1-5	A general model for allostery proposed by Eigen	12
Figure 1-6	Features of autoinhibition	15
Figure 2-1	Dendritic nucleation/array treadmilling model for actin polymerization at the leading edge of motile cells	31
Figure 2-2	GTPase cycle	36
Figure 2-3	Actin cytoskeletal signaling pathways regulated by the Rho GTPases Cdc42, Rac, and Rho	39
Figure 2-4	Domain organization of WASP family proteins	41
Figure 2-5	Examples of proteins that interact with WASP domains	43
Figure 2-6	Structure of autoinhibited WASP	50
Figure 2-7	Autoinhibition and activation of WASP	55
Figure 3-1	Allosteric regulation and activation of WASP by Cdc42	78
Figure 3-2	Western blot of WASP expression	84
Figure 3-3	WASP residues that were mutated in this study	86
Figure 3-4	Domain organization of WASP constructs	88
Figure 3-5	Limited proteolysis of GBD-C wildtype and mutant proteins	91
Figure 3-6	¹ H NMR spectra of GBD-C wildtype and mutant proteins	92
Figure 3-7	Thermal denaturation of GBD-VCA wildtype and mutant proteins using CD spectroscopy	95
Figure 3-8	Biochemical characterization of GBD-VCA and GBD-VCA I290Q	98
Figure 3-9	Urea denaturation of GBD-VCA proteins	99
Figure 3-10	Binding affinity of GBD-VCA M307A for Cdc42-mantGMPPNP	103
Figure 3-11	Affinity of WASP proteins for Cdc42-GMPPNP as a function of stability	105
Figure 3-12	Activity of WASP proteins using the Arp2/3 complex mediated pyrene-actin polymerization assay	106
Figure 3-13	Activity of WASP proteins as a function of stability	107
Figure 3-14	Effect of the basic region on the activity of WASP	110
Figure 3-15	Binding affinities of BGBD-VCA and BGBD-VCA I290Q for Arp2/3 complex	112
Figure 3-16	Pyrene-actin polymerization curves of VCA titration	113
Figure 3-17	Development of a monoclonal antibody that preferentially binds to active WASP	117
Figure 3-18	ELISA results indicate that 26E6 binds specifically to active WASP	118
Figure 3-19	Activated Cdc42-GTP and WASP are colocalized at the immunological synapse	121

Figure 3-20	WASP is recruited to the immunological synapse independently of Cdc42.....	122
Figure 3-21	Purification of His ₆ -tagged GBD-VCA	129
Figure 3-22	Purification of Cdc42	132
Figure 3-23	Purification of Cdc42 loaded with GMPPNP	134
Figure 3-24	Purification of mant-GMPPNP	135
Figure 3-25	Source 15Q purification of bArp2/3 complex from calf thymus.....	140
Figure 3-26	MonoS 10/10 purification of bArp2/3 complex.....	141
Figure 3-27	Final purification of bArp2/3 complex using gel filtration (Sephadex 200)	142
Figure 3-28	Purification of actin and pyrene-labeled actin	145
Figure 4-1	Activation of WASP mutants by Cdc42-GMPPNP	160
Figure 4-2	FRET based assay to measure the binding affinity of Cdc42-GDP for CFP-GBD-VCA-YFP.....	163
Figure 4-3	Differential activation of GBD-VCA M307A by Cdc42-GDP or Cdc42-GMPPNP	165
Figure 4-4	WASP activity in the presence of Cdc42-GDP or Cdc42-GMPPNP	166
Figure 4-5	¹ H/ ¹⁵ N TROSY HSQC spectra of ² H/ ¹⁵ N GBD-VCA in the presence of Cdc42-GMPPNP or Cdc42-GDP	168
Figure 4-6	NMR assignment of ² H/ ¹⁵ N/ ¹³ C-labeled GBD-VCA in the presence of Cdc42-GDP	171
Figure 4-7	¹ H/ ¹⁵ N TROSY HSQC spectrum of ² H/ ¹⁵ N Cdc42-GDP in the presence of increasing concentrations of GBD-VCA	173
Figure 4-8	Intensity ratios of WASP residues upon binding to Cdc42-GDP	177
Figure 4-9	NMR analysis of WASP binding interface with Cdc42-GTP and Cdc42-GDP	178
Figure 4-10	Biological implications for the GTPase nucleotide switch.....	185
Figure 5-1	Predicted WASP activity in the presence of activators and inhibitors ...	194
Figure 5-2	Evolvability of protein behavior in a modular system.....	199

List of Tables

Table 1-1	Examples of proteins regulated by autoinhibition	21
Table 3-1	Temperature denaturation of GBD-C constructs as determined by CD spectroscopy.....	89
Table 3-2	Temperature denaturation of GBD-VCA constructs as determined by CD spectroscopy	96
Table 3-3	Measured values of ΔG , K_{eq} , and K_D	100
Table 4-1	Chemical shifts (ppm) of Cdc42 residues whose $^1H/^{15}N$ TROSY HSQC resonances decrease in intensity by >60% in the presence of 50 μM GBD-VCA	175
Table 4-2	Chemical shifts (ppm) of Cdc42 residues whose $^1H/^{15}N$ TROSY HSQC resonances shift by >0.033 ppm in the presence of 300 μM GBD-VCA	176

List of Abbreviations

λ_{em}	emission wavelength
λ_{ex}	excitation wavelength
°C	degrees Celsius
A.U.	arbitrary units
APC	antigen presenting cell
Arp2/3	Actin-related protein 2/3
BR	basic region
CD	circular dichroism
Cdc42	Cell division cycle 42
CFP	cyan fluorescent protein
CRIB	Cdc42/Rac interacting binding
DTT	dithiothreitol
ELISA	enzyme-linked immunosorbant assay
EVH1	Ena/VASP homology 1
F-actin	filamentous actin
FRET	fluorescence resonance energy transfer
G-actin	globular or monomeric actin
GAP	guanine nucleotide activating protein
GBD	GTPase binding domain
GDI	guanine nucleotide inhibitor
GdnHCl	guanidine hydrochloride

GDP	guanosine diphosphate
GEF	guanine nucleotide exchange factor
GTP	guanosine triphosphate
HSQC	heteronuclear spin quantum correlation
IPTG	isopropyl- β -D-thiogalactopyranoside
IS	immunological synapse
kcal	kilocalorie
K _D	equilibrium dissociation constant
kDa	kiloDalton
K _{eq}	equilibrium constant
KNF	Koshland, Némethy, and Filmer
mAb	monoclonal antibody
mg	milligrams
min	minutes
mol	mole
MWC	Monod, Wyman, and Changeux
nm	nanometer
nM	nanomolar
NMR	nuclear magnetic resonance
N-WASP	neuronal Wiskott-Aldrich syndrome protein
P	proline rich region
PAK	p21-activated kinase
PIP2	phosphatidylinositol 4,5-bisphosphate

ppm	parts per million
Rho	Ras homology
sec	seconds
Scar	suppressor of cyclic AMP receptor
SH2	Src homology 2
SH3	Src homology 3
TCR	T-cell receptor
TROSY	transverse relaxation optimized spectroscopy
VCA	verprolin homology/central domain/acidic region
WAS	Wiskott-Aldrich syndrome
WASP	Wiskott-Aldrich syndrome protein
WAVE	WASP family verprolin homologous
WIP	WASP interacting protein
XLN	X-linked neutropenia
XLT	X-linked thrombocytopenia
YFP	yellow fluorescent protein
ΔG	Gibbs' free energy
μM	micromolar

Chapter 1 Allosteric regulation of biological processes

Introduction

Allostery is a universal phenomenon that is important to many cellular processes governing biological systems. The unifying concept of allostery (translation from Greek, *allos* = other, *stereos* = shape) by convention describes the intrinsic property of a protein where two distinct binding sites are coupled through conformational space (Figure 1-1). Binding of a ligand to a regulatory site on a protein causes conformational changes that are propagated to an active site distant from the regulatory site. Thus, the conformational modification of protein induced upon binding of an allosteric ligand results in a change in protein activity. Application of this versatile concept expands upon the number of regulatory interactions observed that influence protein behavior, and which underlie signal transduction and changes in cellular function. Allostery has traditionally been used to describe classical metabolic or multimeric systems, including how metabolic enzymes work, how oxygen binds to hemoglobin, and how gene expression is regulated. But the concept of allostery has more recently been adapted to explain the diversity and regulatory strategies of many other biological processes, including the function of modular proteins that gate signal transduction pathways. The understanding of how allostery is intimately involved in all of these processes may provide the “second secret of life” (Monod *et al.* 1963), after the structure of DNA, which holds the other key to our biological existence.



Figure 1-1. Basic features of allostery. A ligand (green hexagon) binds to a regulatory site (a) on a protein that is distinct from the active site (b) resulting in conformational changes that affect activity.

Allosteric mechanisms

Proteins are flexible, dynamic entities that are endowed with properties that allow them to respond to interactions with other proteins, nucleic acids, or ligands. Proteins receive, process, and transmit information, which ultimately affects specificity and activity. In particular, specificity is important for proper functioning in the crowded intracellular environment where proteins must be able to discriminate among a variety of inputs in order to properly direct information flow. Thus, a detailed understanding of a protein's properties and its interactions with ligands is essential toward gaining insight to its significance in biological function.

Coupled ligand equilibria

Many biological processes depend upon interactions between proteins and ligands. In many cases, protein-ligand interactions do not occur in isolation but as a part of a larger protein network, providing a mechanism through which specificity of signaling response is maintained. There are several descriptions of protein-ligand interactions, including those based upon thermodynamics and structure. Gregorio Weber proposed one of the more widely accepted frameworks incorporating energetics in order to understand the thermodynamic properties of a system and how ligand interactions can be allosterically coupled (Weber 1972; Weber 1975). In a simple system where a protein (P) binds two ligands (L1 and L2), the reactions of the system can be described by free energies in the following relationships:

$$\Delta G_1^0 \quad \text{P} + \text{L1} \rightleftharpoons \text{PL1} \quad (\text{Eqn. 1-1})$$

$$\Delta G_2^0 \quad \text{P} + \text{L2} \rightleftharpoons \text{L2P} \quad (\text{Eqn. 1-2})$$

$$\Delta G_1^0(2) \quad \text{L2P} + \text{L1} \rightleftharpoons \text{L2PL1} \quad (\text{Eqn. 1-3})$$

$$\Delta G_2^0(1) \quad \text{PL1} + \text{L2} \rightleftharpoons \text{L2PL1} \quad (\text{Eqn. 1-4})$$

$$\Delta G(1,2) \quad \text{P} + \text{L1} + \text{L2} \rightleftharpoons \text{L2PL1} \quad (\text{Eqn. 1-5})$$

where ΔG is the standard free energy for each reaction and $\Delta G_2^0(1)$ describes the standard free energy change for binding L2 to P saturated with L1. Application of the conservation of free energy then states that the free energy to reach one state is independent of the path taken, which is described by (Figure 1-2):

$$\Delta G_1^0 + \Delta G_2^0(1) = \Delta G_2^0 + \Delta G_1^0(2) = \Delta G(1,2) \quad (\text{Eqn. 1-6})$$

It is not required that $\Delta G_2^0 = \Delta G_2^0(1)$ or that $\Delta G_1^0 = \Delta G_1^0(2)$. Rearrangement of Equation 1-6 gives rise to:

$$\Delta G_1^0(2) - \Delta G_1^0 = \Delta G_2^0(1) - \Delta G_2^0 = \Delta G_{12}^0 \quad (\text{Eqn. 1-7})$$

Equation 1-6 describes then that the energetic effect of L1 on the binding of L2 is the same as the energetic effect of L2 on the binding of L1, which is encompassed in the coupling free energy term ΔG_{12}^0 . Thus, the term ΔG_{12}^0 describes if ligand interactions are linked. If ligand interactions are not coupled, then $\Delta G_2^0 = \Delta G_2^0(1)$ and $\Delta G_1^0 = \Delta G_1^0(2)$, and

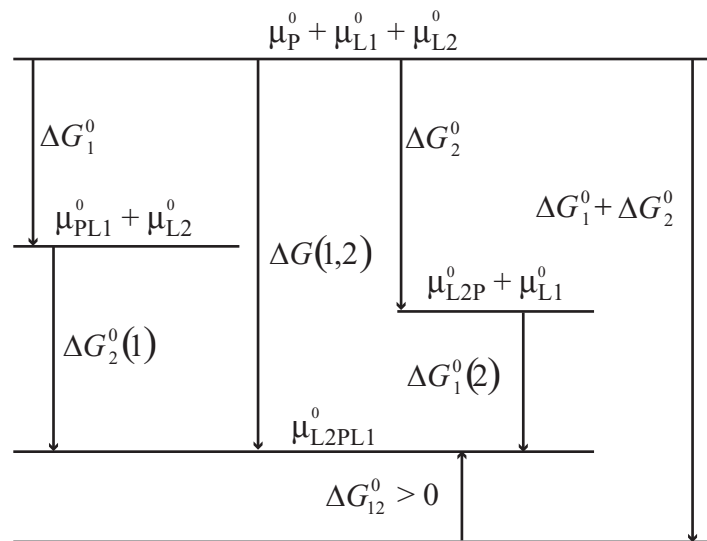


Figure 1-2. Free energy diagram describing the binding of two ligands, L1 and L2, to a protein, P. μ^0 is the standard chemical potential. ΔG_1^0 and ΔG_2^0 are the free energies of binding ligands L1 and L2 to P. $\Delta G_1^0(2)$ and $\Delta G_2^0(1)$ are the free energies of binding L1 and L2, respectively, when P is saturated with L2 and L1, respectively. ΔG_{12}^0 is the coupling free energy. When $\Delta G_{12}^0 < 0$, which is indicated in the above figure, there is positive cooperativity between ligands. (Adapted from Weber 1975.)

$\Delta G_{12}^0 = 0$ describes the system where there is no interaction between ligands. If $\Delta G_{12}^0 \neq 0$, then cooperativity is established between binding interactions. If $\Delta G_{12}^0 > 0$, then there is antagonistic effects between ligand interactions or negative cooperativity. However, if $\Delta G_{12}^0 < 0$, then binding of one ligand facilitates binding of another ligand, referred to as positive cooperativity. Furthermore, equations 1 and 2 can be subtracted from Equation 1-5, such that:



$$\Delta G^0(1,2) - \Delta G_1^0 - \Delta G_2^0 = \Delta G_{12}^0 \quad (\text{Eqn. 1-9})$$

The change in free energy in the above reaction (Equation 1-8) has an equilibrium constant, K_{12} , which can be described by:

$$K_{12} = e^{-\Delta G_{12}^0 / RT} \quad (\text{Eqn. 1-10})$$

When $K_{12} > 1$, formation of L2PL1 and P are strongly favored than the partially bound L2P and PL1. Therefore, the energetic framework outlined by Weber provides a thermodynamic rationale for allosteric interactions observed in many systems with multiple ligand binding (Weber 1972; Weber 1975).

The MWC model

Monod, Wyman, and Changeux provided a simple structural approach toward examining protein-ligand interactions to explain the intrinsic properties of a protein,

referred to as the MWC model (Monod *et al.* 1965). Briefly, this allosteric model provides a framework for describing the coupling of conformational changes between two topologically distinct sites on a protein with activity. Central to this concept of allostery is the assumption of a pre-existing equilibrium between two conformational states, designated the T (tense) and R (relaxed) states (Figure 1-3). For a protein composed of four protomers, each protomer can exist in two conformations that freely interconverts between one another. The protein is assumed to be symmetrical and all ligand binding sites on each protomer are equivalent. In the absence of ligand, all the protomers in the protein predominantly exist in the inactive T state. Binding of an activating ligand modulates the conformational equilibrium such that a ligand, which preferentially binds to the active R state, shifts the overall T-R equilibrium to favor the R state. Because the conformational change in the quaternary structure of the protein is concerted, binding of one ligand to one protomer of a protein causes all other protomers to occupy the R state. As a result, there is a rapid increase in the number of protomer ligand binding sites made available in the R state than there are proteins occupying the R state, giving rise to cooperativity where binding of the first ligand enhances the binding of subsequent ligands. As the concentration of ligand increases, all of the protein will eventually shift to the R state. The structural framework of the MWC model can be described quantitatively using only three variables: K_T , K_R , and L . K_T and K_R are the dissociation constants of ligand for the T and R states of the protein, respectively. L is the allosteric constant that is equal to the concentration ratio of the T to R states ($L = [T]/[R]$). An additional term, the C parameter, is equal to the ratio of binding affinities of a ligand for the R and T states, where $C = K_{D,R}/K_{D,T}$, and that describes the extent to

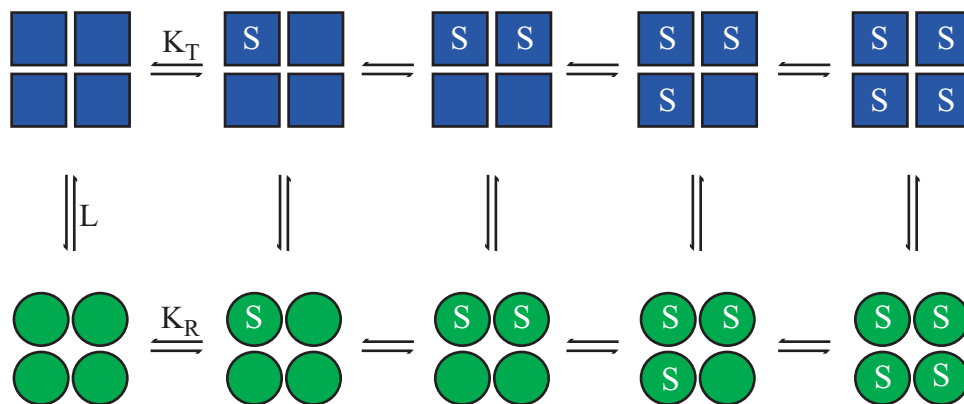


Figure 1-3. MWC model of allostery. A protein consisting of four equivalent protomers exist in one of two states, an inactive T state (blue square) or an active R state (green circle), which is described by the allosteric constant, L . Substrate, S , can bind to the T state, K_T , but has a higher affinity for the active R state, K_R . Binding of substrate favors the active state and shifts the equilibrium towards the active state.

which binding of a ligand shifts the T-R equilibrium. The equilibrium between the ligand-bound T and ligand-bound R states is then described by the product of the allosteric constant and the C parameter or $L^*(K_R/K_T)$. Thus, using only three parameters, the MWC model provides a simplified explanation of how protein function is modulated by the conformational properties of a protein.

The KNF and general models

The assumption of a concerted change occurring in the quaternary structure restricts the number of protein conformations that could exist to two, which is only an approximation of the number of conformations that a protein can sample. Alternative models have been formulated to address this issue. In the Koshland-Némethy-Filmer (KNF) model, the change in protomer conformations from the T state to the R state occurs in a sequential process giving rise to multiple conformations that an oligomeric protein can sample (Figure 1-4) (Koshland *et al.* 1966). In the absence of any ligand, all the protomers exist in the T state. Binding of the first ligand to a protomer causes a conformational change in the bound protomer from the T state to the R state, the effect of which then can be transmitted to a neighboring subunit. These interactions lead to a change in affinity of the next protomer for ligand, providing the basis for cooperativity. The notion of induced fit results in changes only in the tertiary structure of the protein and allows for the existence of intermediate thermodynamic states that have been experimentally identified for some proteins. For example, crystallographic data reveal the presence of intermediate states in hemoglobin and ATCase, and electrophysiological data indicate the existence of subconducting states in non-nicotinic channels that are

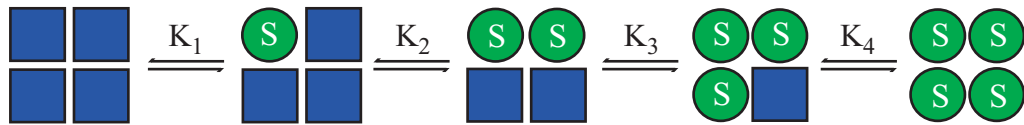


Figure 1-4. KNF model of allostery. A homotetramer protein becomes activated in a sequential manner upon binding to ligand. Substrate, S, binds to one subunit at a time, causing the transition of a subunit from an inactive T state (blue square) to an active R state (green circle). The three conformations in the middle represents the presence of intermediate thermodynamic states. K_1 , K_2 , K_3 , and K_4 represent different substrate dissociation constants for each empty substrate site in the intermediate states.

consistent with predictions from the KNF model (Changeux and Edelstein 1998; Changeux and Edelstein 2005). Furthermore, the KNF model allows for negative cooperativity where binding of one ligand decreases the binding affinity of subsequent ligands, which has been observed for tyrosyl-tRNA synthetase and glyceraldehyde 3-phosphate dehydrogenase (Irwin *et al.* 1976; Biesecker *et al.* 1977). The MWC model cannot account for negative cooperativity since ligand binding can only shift the conformational equilibrium towards the state that it preferentially binds to and there are no conditions that allow for decreasing binding affinities as ligand concentration increases. However, in the mathematical formulation of the KNF model, the number of constants required to parameterize the model is the same as that of binding events. Therefore, in the activation pathway, the complexity of the KNF model provides a more accurate measurement describing the molecular events involved in allosteric interactions but may be limited by what can be observed or determined experimentally. Similarly, a general model incorporating both MWC and KNF assumptions or simplifications has been proposed by Eigen to generate a more encompassing model where the MWC and KNF models represent extreme cases in a larger scheme, as shown in Figure 1-5 (Eigen 1967; Herzfeld and Stanley 1974). However, the analysis of such a system is far too complex. Thus, interpretations and simplifications like the MWC and KNF models, which have been shown to account for complex protein behaviors, become easier to process and experimentally test and therefore are more widely used.

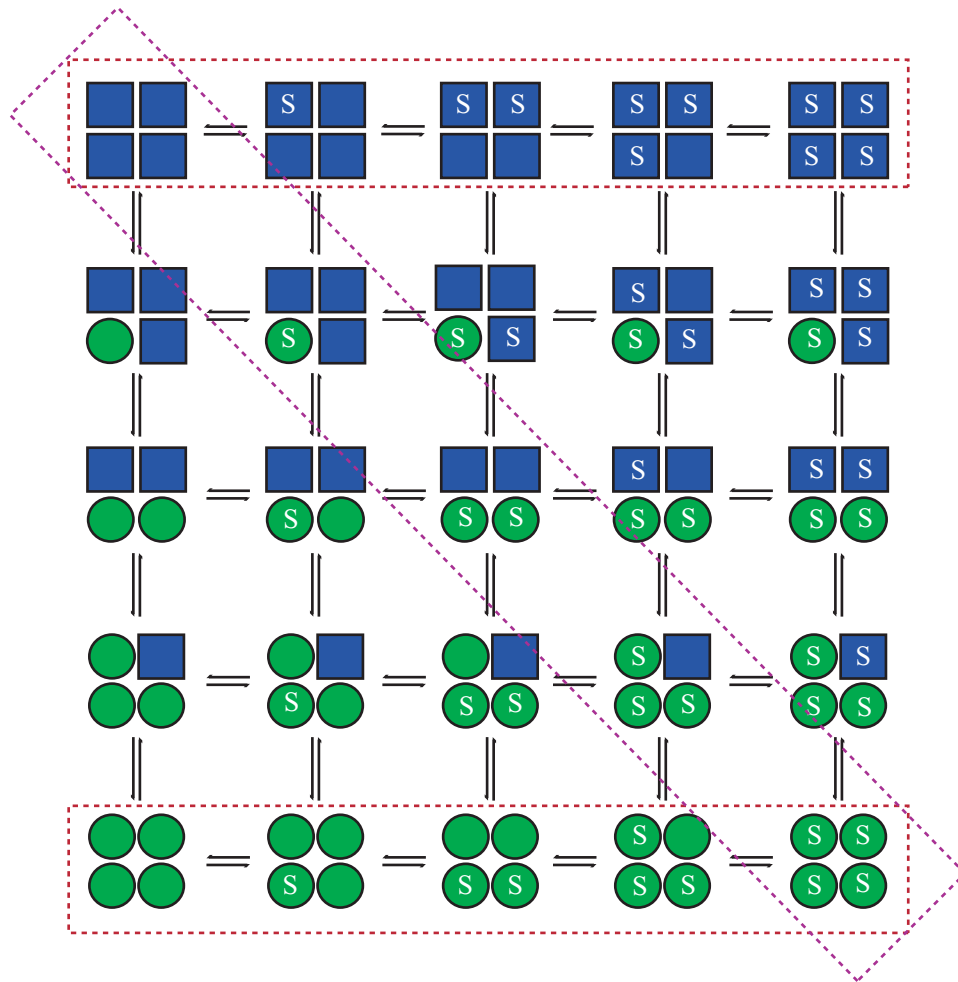


Figure 1-5. A general model for allostery proposed by Eigen. The top and bottom rows represent the MWC model (red dashed lines). The diagonal represents the KNF model (purple dashed lines).

Classical allosteric systems

Both the MWC and KNF models have provided mathematical descriptions of the mechanistic behavior observed in many proteins. Classical allosteric systems encompass proteins that typically form an individual cooperatively folding structure that contains both a regulatory site and an active site and exists in two conformations, an inactive T state and an active R state (Figure 1-1). The prototypical example is that of hemoglobin (Perutz *et al.* 1964). Hemoglobin is composed of four subunits arranged symmetrically, where each subunit contains a heme functionality that can bind to an oxygen molecule. Binding of the first oxygen molecule causes an increase in binding affinities for subsequent oxygen molecules to the other three subunits in the protein complex. Even though the binding sites are distant from one another, the change in affinity suggested that the binding sites were interacting with one another and changed behavior in the presence of ligand. Application of the MWC model described how hemoglobin binds to four molecules of oxygen in a cooperative manner by establishing an equilibrium between the unbound T state and ligand-bound R state. Binding of the first oxygen molecule stabilizes the R state of one hemoglobin subunit and biases the conformational equilibrium towards the R state, thus increasing the affinity for subsequent oxygen molecules to bind cooperatively to other subunits. The KNF model similarly accounts for the oxygen binding behavior observed in hemoglobin but uses four binding constants in its description. Binding of an oxygen molecule induces conformational changes in the tertiary structure of that subunit, increasing the affinity of the next subunit to bind to oxygen.

The mechanism of allosteric interactions also provided an explanation that clarified how metabolic enzymes can be regulated through feedback inhibition. Aspartate transcarbamylase (ATCase) is a metabolic enzyme composed of six catalytic and six regulatory subunits and that is involved in pyrimidine synthesis. ATCase activity is inhibited by its own product, CTP, which is structurally distinct from the substrates, carbamyl phosphate and aspartate, and activated by the product of purine synthesis, ATP (Gerhart and Pardee 1962). This observation did not fit into classical inhibition models of steric hinderance, where a substrate with a similar structure (pseudo-substrate) directly blocks access to the active site. Instead, application of the MWC model accounted for the cooperative binding of CTP, which stabilizes the T state of the multimeric protein, and activation by ATP, which stabilizes the R state. The biasing of the conformational equilibrium provided a mechanism through which enzyme response to synthesize pyrimidines becomes amplified when purine concentrations are high. Thus, biochemical analysis of ATCase using the classical allosteric framework was sufficient to explain the biological function of the protein.

Modular allosteric systems

Unlike classical allosteric systems where a single folding structure contains both the regulatory and catalytic sites and are multimeric, there are many other examples of proteins where the regulatory and catalytic sites are individually located on independently folding domains (Figure 1-6A) (Kobe and Kemp 1999; Lim 2002; Pawson and Nash 2003; Dueber *et al.* 2004). These domains can be physically detached and when isolated form autonomously folding units that can still participate in functional interactions

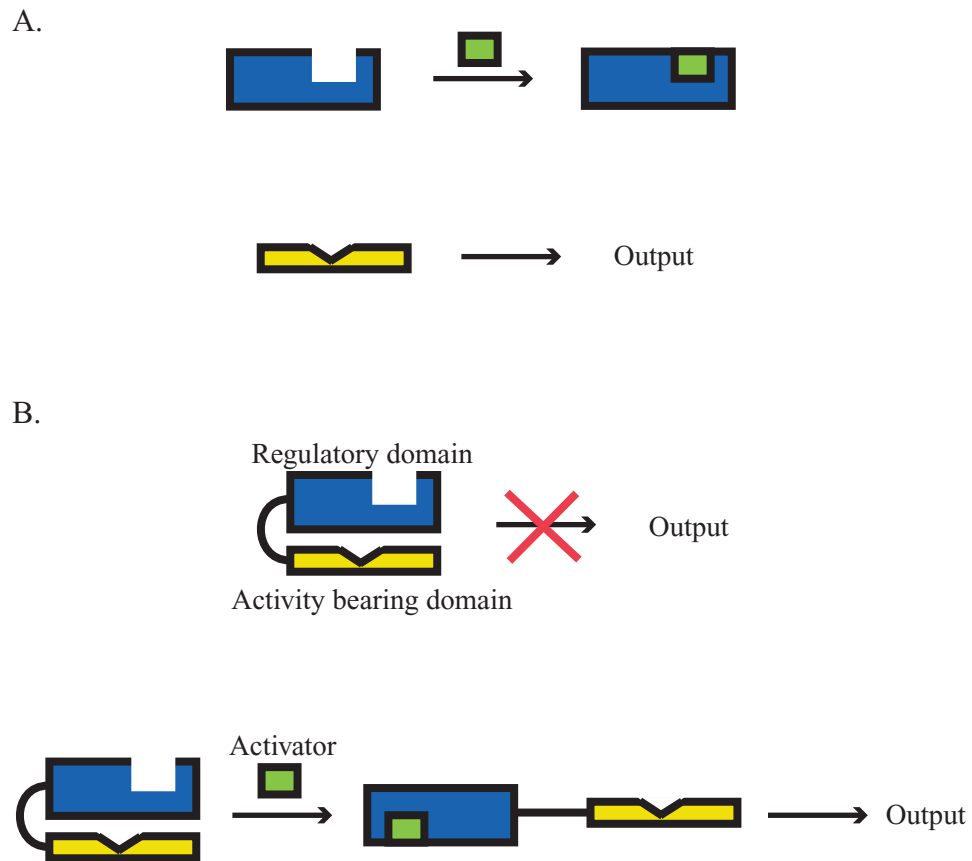


Figure 1-6. Features of autoinhibition. A. Modular proteins are composed of combinations of regulatory (blue) and activity bearing (yellow) modules. *Top*. Protein interaction modules can bind ligand (green) and participate in protein-protein interactions. *Bottom*. Isolated activity bearing modules display constitutive activity. B. *Top*. Intramolecular interactions involving the regulatory domain directly prevents access to the activity bearing domain and inhibits protein function. *Bottom*. Autoinhibition can be relieved upon covalent modification or binding of an activator to enable protein activity.

(Cohen *et al.* 1995; Pawson 1995; Pawson and Nash 2000). For example, the regulatory modules Src homology 2 (SH2) and Src homology 3 (SH3) bind specific motifs encompassing a phosphorylated tyrosine residue and proline-rich sequences, respectively. In addition, catalytic modules, such as kinase or phosphatase domains, display constitutive activity when they are isolated. Structural and thermodynamic coupling of these modular units together into a protein can result in allosteric interactions that link the regulatory domain to the catalytic domain to ultimately regulate the activity of the protein. Many modular proteins are regulated by a subset of allostery called autoinhibition where allosteric interactions at one site of the protein negatively control activity at a distinct site or domain within the same protein (Figure 1-6B). Generally, intramolecular interactions between the regulatory or allosteric site directly prevent access to the active site and inhibit protein function (Kobe and Kemp 1999; Pufall and Graves 2002). Autoinhibition is relieved and the protein activity is restored upon covalent modification, binding of an activating ligand, or proteolysis. Thus, activation involves the disruption of intramolecular interactions and allows for intermolecular interactions. Combination of various regulatory and catalytic domains into different linear arrays produces a biological mechanism through which specificity is configured into the system. The number of regulatory modules within a protein can define the energetic requirements for activation. This regulatory strategy prevents the inappropriate activation of a protein and maintains the fidelity of interactions. The mechanisms by which autoinhibition is achieved can be separated into two general categories: steric occlusion and conformational autoinhibition (Pufall and Graves 2002; Dueber *et al.* 2004).

Autoinhibition through steric occlusion

The activity of a protein can be autoinhibited by sterically blocking access to the active site. The regulatory module is physically situated in a manner that prevents ligand from accessing an otherwise functional active site. Activation occurs by physically displacing the inhibitory element from the active site thus allowing an effector ligand to bind. This type of regulatory mechanism has been observed in many different proteins, including growth factor receptors, adaptor proteins, and guanine nucleotide exchange factors. Both EGF and FGF receptors (EGFR and FGFR, respectively) are predominantly maintained in the autoinhibited state in the absence of growth factors (Schlessinger 2003). Intramolecular interactions between the dimerization module with a C-terminal domain maintains EGFR in a bent conformation that prevents dimerization domain interaction with an adjacent receptor. Binding of EGF ligand causes extension of the dimerization domain allowing intermolecular interactions with the dimerization domain of a nearby receptor (Ferguson *et al.* 2003). Dimerization of receptor tyrosine kinases allows for autophosphorylation and kinase access to substrate sites leading to activation. In the inactivated FGFR, the heparin-binding site is intramolecularly occluded through binding to its own acid box sequence. Binding of both FGF ligand and a heparin cofactor leads to kinase activation. In contrast, the p21 activated kinase (PAK) exists in a dimer that maintains the protein in an autoinhibited state by blocking phosphorylation of the activation loop. Activated Cdc42 or Rac GTPase binding disrupts intramolecular interactions between the N-terminal domain and the C-terminal lobe of the kinase domain (Lei *et al.* 2000), allowing phosphorylation of the kinase activation loop (Buchwald *et al.* 2001). The Rho family guanine nucleotide exchange factor (GEF) Vav

is also regulated by steric occlusion of GTPase-binding active site on the DH domain by an N-terminal helix (Aghazadeh *et al.* 2000). Displacement of this helix through covalent modifications by Src family kinases results in changes in activity through GTPase binding to the active site. Altogether, autoinhibition through steric occlusion forms a subset of allosteric interactions that regulate the function of modular proteins.

Conformational autoinhibition

Conformational autoinhibition is another mechanism through which modular proteins are regulated. In the inactive state, the catalytic module exists in a conformation where the active site is not optimal for ligand binding, reducing protein activity. Intramolecular interactions between the regulatory and catalytic modules distort the conformation of the active site. Binding of a ligand to the regulatory domain, covalent modification, or proteolysis induces conformational changes that regenerate a functional active site, which can subsequently bind to effector proteins. Examples of this form of autoinhibition include the Src and c-Abl kinases, which are composed of multiple regulatory domains that function to inhibit the activity of the kinase domain. Src and c-Abl proteins have similar structures in that they both have a SH3 and SH2 modules N-terminal to the kinase domain catalytic module, which cooperatively autoinhibit the enzyme. In particular, autoinhibition is accomplished through SH3 binding to an internal polyproline sequence and SH2 binding to a singly phosphorylated Tyr527 located at the C-terminus (Sicheri and Kuriyan 1997). In the case of c-Abl, a third regulatory interaction has recently been identified that is required involving intramolecular interactions between the N-terminal myristoyl group into a pocket in the kinase

(Hantschel *et al.* 2003; Nagar *et al.* 2003). Autoinhibition is relieved through binding of external SH2 and SH3 ligands that cause conformational changes (and insertion of the myristoyl group into the membrane for c-Abl) releasing the activation loop to be phosphorylated. Conformational autoinhibition has also been demonstrated in the regulation of the eukaryotic transcription factor-1 (Ets-1) (Pufall and Graves 2002; Lee *et al.* 2005; Pufall *et al.* 2005). Autoinhibition of Ets-1 involves the packing of the inhibitory helices, including the H1 helix, against the ETS domain that binds to DNA. Phosphorylation of multiple serine residues N-terminal to the H1 helix maintains Ets-1 in an autoinhibited conformation through the stabilization of the H1 helix and inhibitory module. DNA binding to the ETS domain causes conformational changes in the ETS domain that is transmitted to the H1 helix, resulting in the unfolding of the H1 helix, the potential association of additional transcription factors, and the activation of Ets-1.

Conclusion

Allostery is an extremely common regulatory mechanism observed in proteins that modulate biological processes. The flexibility and versatility of proteins allow for widespread applications of allosteric effects in governing protein-protein interactions. The function of many large, multimeric proteins can be explained simply through the coupling of conformational changes with the cooperative binding of ligands as described by Monod *et al.* and as observed for hemoglobin and metabolic enzymes like ATCase.

More recently, a host of other proteins have been identified that are regulated by interactions between independently folded modular domains that are generally referred to as autoinhibition. The autoinhibitory interactions observed in many autoinhibited

proteins is considered to be a subset of allostery. Autoinhibition also results from intramolecular interactions involving a regulatory domain that negatively modulates protein activity through changes in conformation. Autoinhibited proteins include transcription factors, adaptor proteins, kinases, apoptotic factors, phosphatases, GEFs, and nuclear localization proteins, all of which are involved in diverse biological processes (Table 1-1). The prevalence and the importance of autoinhibitory proteins are underscored by their representation in a number of signal transduction pathways and the vast number of diseases that are associated with the misregulation of these proteins. For example, there are several proteins in the T-cell receptor pathway that are regulated through autoinhibitory interactions and activated through intermolecular ligand binding. WASP, PAK, mDia, Src and Lck kinases, and Vav are just a few proteins that are allosterically regulated through autoinhibition. Thus, knowledge of the biological function of these proteins requires an understanding of the allosteric mechanisms underlying the regulation of activity, including how specificity and fidelity of signaling is maintained. In order to achieve this, we need to generate quantitative models and perform detailed analyses that can account for the allosteric, autoinhibitory interactions and activities we observe. The work presented in this thesis examines the biochemical and biophysical basis of the allosteric regulation and activation of one such autoinhibited system, WASP, by the Rho GTPase Cdc42, which are involved in the regulation of the actin cytoskeleton. A detailed and quantitative analysis of the biochemical and biophysical properties of WASP and the elements that contribute to its inhibition or activation are described within the framework of classical allostery. The work presented here will provide a structural and thermodynamic rationale for approaching the allosteric

Table 1-1. Examples of proteins regulated by autoinhibition

Protein	Activity Inhibited	Autoinhibitory Mechanism	Reference
NADP malate dehydrogenase	Reduction of oxaloacetate to L-malate	C-terminal disulfide bridge blocks active site	Krimm <i>et al</i> , 1999
SNARE	membrane fusion	SNARE motif with N-terminal domain in syntaxin	Sutton <i>et al</i> , 1998; Chen and Scheller, 2001
EGFR	Receptor dimerization	C-terminal domain with dimerization domain	Ferguson <i>et al</i> , 2003
Abl	Tyr kinase	Myristoyl group, SH2, and SH3 domains to intramolecular substrates	Nagar <i>et al</i> , 2003
Src	Tyr kinase	SH2 and SH3 domains to intramolecular substrates	Xu <i>et al</i> , 1997
PAK	Ser/Thr kinase	Inhibitory switch domain blocks kinase active site	Lei <i>et al</i> , 2000
Twitchin	Ser/Thr kinase	Intramolecular substrate binds to kinase active site	Kobe <i>et al</i> , 1996
SHP2	Phosphatase	N-terminal SH2 binds active site	Hof <i>et al</i> , 1998
Cdc24	Cdc42 GEF	PB1 domain with CH domain	Shimada <i>et al</i> , 2004
Vav	Cdc42/Rac GEF	N-terminal helix with GTPase binding site	Aghazadeh <i>et al</i> , 2000
Dia	actin polymerization	N-terminal region with DAD domain	Xu <i>et al</i> , 2004; Otomo <i>et al</i> , 2005
(N-)WASP	actin polymerization	B region and GBD domain with C-terminal VCA domain	Kim <i>et al</i> , 2000; Prehoda <i>et al</i> , 2000
ERM	membrane and F-actin binding	N-ERMAD with C-ERMAD	Pearson <i>et al</i> , 2000
Vinculin	F-actin binding	N-terminal head region with C-terminal tail region	Bakolitsa <i>et al</i> , 1999
NFAT1	Nuclear localization	Phosphorylation of 13 serine residues	Okamura <i>et al</i> , 2000
Notch	Nuclear localization	Transmembrane domain anchor	Mumm and Kopan, 2000
Ets-1	transcription	Helices HI-1 and HI-2 with ETS domain	Donaldson <i>et al</i> , 1996; Skalicky <i>et al</i> , 1996
NF-kB	transcription	N- with C-terminal domain of p65	Zhong <i>et al</i> , 1998

mechanisms regulating WASP and for understanding its role in the actin cytoskeletal signaling pathway, and which can serve as a general paradigm for the examination of other similarly constructed signaling systems.

References

- Aghazadeh, B., *et al.* (2000). "Structural basis for relief of autoinhibition of the Dbl homology domain of proto-oncogene Vav by tyrosine phosphorylation." Cell **102**(5): 625-33.
- Bakolitsa, C., *et al.* (1999). "Crystal structure of the vinculin tail suggests a pathway for activation." Cell **99**(6): 603-13.
- Biesecker, G., *et al.* (1977). "Sequence and structure of D-glyceraldehyde 3-phosphate dehydrogenase from *Bacillus stearothermophilus*." Nature **266**(5600): 328-33.
- Buchwald, G., *et al.* (2001). "Conformational switch and role of phosphorylation in PAK activation." Mol Cell Biol **21**(15): 5179-89.
- Changeux, J. P. and S. J. Edelstein (1998). "Allosteric receptors after 30 years." Neuron **21**(5): 959-80.
- Changeux, J. P. and S. J. Edelstein (2005). "Allosteric mechanisms of signal transduction." Science **308**(5727): 1424-8.
- Chen, Y. A., *et al.* (2001). "Sequential SNARE assembly underlies priming and triggering of exocytosis." Neuron **30**(1): 161-70.
- Cohen, G. B., *et al.* (1995). "Modular binding domains in signal transduction proteins." Cell **80**(2): 237-48.
- Donaldson, L. W., *et al.* (1996). "Solution structure of the ETS domain from murine Ets-1: a winged helix-turn-helix DNA binding motif." Embo J **15**(1): 125-34.
- Dueber, J. E., *et al.* (2004). "Rewiring cell signaling: the logic and plasticity of eukaryotic protein circuitry." Curr Opin Struct Biol **14**(6): 690-9.

- Eigen, M. (1967). "Kinetics of reaction control information transfer in enzymes and nucleic acids." Nobel Symp. **5**: 333-369.
- Ferguson, K. M., *et al.* (2003). "EGF activates its receptor by removing interactions that autoinhibit ectodomain dimerization." Mol Cell **11**(2): 507-17.
- Gerhart, J. C. and A. B. Pardee (1962). "The enzymology of control by feedback inhibition." J Biol Chem **237**: 891-6.
- Hantschel, O., *et al.* (2003). "A myristoyl/phosphotyrosine switch regulates c-Abl." Cell **112**(6): 845-57.
- Herzfeld, J. and H. E. Stanley (1974). "A general approach to co-operativity and its application to the oxygen equilibrium of hemoglobin and its effectors." J Mol Biol **82**(2): 231-65.
- Hof, P., *et al.* (1998). "Crystal structure of the tyrosine phosphatase SHP-2." Cell **92**(4): 441-50.
- Irwin, M. J., *et al.* (1976). "The crystal structure of tyrosyl-transfer RNA synthetase at 2-7 Å resolution." J Mol Biol **105**(4): 577-86.
- Kobe, B., *et al.* (1996). "Giant protein kinases: domain interactions and structural basis of autoregulation." Embo J **15**(24): 6810-21.
- Kobe, B. and B. E. Kemp (1999). "Active site-directed protein regulation." Nature **402**(6760): 373-6.
- Koshland, D. E., Jr., *et al.* (1966). "Comparison of experimental binding data and theoretical models in proteins containing subunits." Biochemistry **5**(1): 365-85.

- Krimm, I., *et al.* (1999). "Direct NMR observation of the thioredoxin-mediated reduction of the chloroplast NADP-malate dehydrogenase provides a structural basis for the relief of autoinhibition." J Biol Chem **274**(49): 34539-42.
- Lee, G. M., *et al.* (2005). "The structural and dynamic basis of Ets-1 DNA binding autoinhibition." J Biol Chem **280**(8): 7088-99.
- Lei, M., *et al.* (2000). "Structure of PAK1 in an autoinhibited conformation reveals a multistage activation switch." Cell **102**(3): 387-97.
- Lim, W. A. (2002). "The modular logic of signaling proteins: building allosteric switches from simple binding domains." Curr Opin Struct Biol **12**(1): 61-8.
- Monod, J., *et al.* (1963). "Allosteric proteins and cellular control systems." J Mol Biol **6**: 306-29.
- Monod, J., *et al.* (1965). "On the Nature of Allosteric Transitions: a Plausible Model." J Mol Biol **12**: 88-118.
- Mumm, J. S. and R. Kopan (2000). "Notch signaling: from the outside in." Dev Biol **228**(2): 151-65.
- Nagar, B., *et al.* (2003). "Structural basis for the autoinhibition of c-Abl tyrosine kinase." Cell **112**(6): 859-71.
- Okamura, H., *et al.* (2000). "Concerted dephosphorylation of the transcription factor NFAT1 induces a conformational switch that regulates transcriptional activity." Mol Cell **6**(3): 539-50.
- Otomo, T., *et al.* (2005). "Structural basis of actin filament nucleation and processive capping by a formin homology 2 domain." Nature **433**(7025): 488-94.

- Pawson, T. (1995). "Protein modules and signalling networks." Nature **373**(6515): 573-80.
- Pawson, T. and P. Nash (2000). "Protein-protein interactions define specificity in signal transduction." Genes Dev **14**(9): 1027-47.
- Pawson, T. and P. Nash (2003). "Assembly of cell regulatory systems through protein interaction domains." Science **300**(5618): 445-52.
- Perutz, M. F., *et al.* (1964). "Structure of Haemoglobin. an X-Ray Examination of Reduced Horse Haemoglobin." Nature **203**: 687-90.
- Pufall, M. A. and B. J. Graves (2002). "Autoinhibitory domains: modular effectors of cellular regulation." Annu Rev Cell Dev Biol **18**: 421-62.
- Pufall, M. A., *et al.* (2005). "Variable control of Ets-1 DNA binding by multiple phosphates in an unstructured region." Science **309**(5731): 142-5.
- Schlessinger, J. (2003). "Signal transduction. Autoinhibition control." Science **300**(5620): 750-2.
- Shimada, Y., *et al.* (2004). "The nucleotide exchange factor Cdc24p may be regulated by auto-inhibition." Embo J **23**(5): 1051-62.
- Sicheri, F. and J. Kuriyan (1997). "Structures of Src-family tyrosine kinases." Curr Opin Struct Biol **7**(6): 777-85.
- Skalicky, J. J., *et al.* (1996). "Structural coupling of the inhibitory regions flanking the ETS domain of murine Ets-1." Protein Sci **5**(2): 296-309.
- Sutton, R. B., *et al.* (1998). "Crystal structure of a SNARE complex involved in synaptic exocytosis at 2.4 Å resolution." Nature **395**(6700): 347-53.

- Weber, G. (1972). "Ligand binding and internal equilibria in proteins." Biochemistry **11**(5): 864-78.
- Weber, G. (1975). "Energetics of ligand binding to proteins." Adv Protein Chem **29**: 1-83.
- Xu, W., *et al.* (1997). "Three-dimensional structure of the tyrosine kinase c-Src." Nature **385**(6617): 595-602.
- Xu, Y., *et al.* (2004). "Crystal structures of a Formin Homology-2 domain reveal a tethered dimer architecture." Cell **116**(5): 711-23.
- Zhong, H., *et al.* (1998). "Phosphorylation of NF-kappa B p65 by PKA stimulates transcriptional activity by promoting a novel bivalent interaction with the coactivator CBP/p300." Mol Cell **1**(5): 661-71.

Chapter 2 Regulation of the cellular actin cytoskeleton

Introduction

The actin cytoskeleton is a dynamic cellular framework that is central to functioning of many biological processes and provides a unique organization to generate highly specialized cellular structures through which specific signals are received from the vast extracellular milieu. These signals in turn are internalized and transmitted along spatially and temporally defined pathways to trigger the activation of downstream cellular processes, including those affecting cellular morphogenesis, migration, polarization, and differentiation. Therefore, deciphering the mechanisms regulating components of the cytoskeleton, including actin and regulators of actin, becomes crucial for understanding the organization of the cytoskeleton and its role in maintaining normal cellular function.

Actin dynamics in the cell

Actin cytoskeletal dynamics dominate a number of cellular processes underlying cellular morphology, division, and motility. These processes depend on the cell's ability to extend, retract, or stabilize the cellular membrane in a well-defined and organized manner. One of the best characterized examples of where actin cytoskeletal dynamics play a critical role is cell motility. Movement of a cell requires the protusion of its leading edge followed by the contraction and retraction of the cellular body. The leading edge of cells is comprised of a dense actin meshwork, which organizes the production of

lamellipodia or membrane ruffles such as those observed in keratocytes, and bundles of actin, which are involved in the formation of filopodia or finger-like protrusions such as those observed in fibroblast or dendritic cells (Hall 1998; Etienne-Manneville and Hall 2002; Pollard and Borisy 2003). Focal adhesions in the cellular body provide anchor points for actin stress fibers required for contractile movement (Etienne-Manneville 2004). Although there are many other components and additional complexity involved in the behavior of motile cells, including microtubule dynamics and vesicular transport, the actin cytoskeleton provides a major driving force that directs cellular motility in response to extracellular cues.

In order to create these specialized, dynamic actin structures, the actin filaments comprising these structures must be assembled, disassembled, or rearranged. The cellular pool of ATP-actin, the form of actin incorporated into filaments, is typically maintained as monomers that are sequestered through binding with actin binding proteins, such as thymosin- β 4 and profilin. Whereas the thymosin- β 4-actin heterodimeric complex remains sequestered from addition into growing filaments, the profilin-actin complex can be incorporated into the barbed ends of pre-existing actin filaments upon release from profilin. Actin polymerization proceeds spontaneously above the critical concentration, which is defined as the concentration at which polymerization of actin monomers (also referred to as G-actin) into filaments (F-actin) occur. The critical concentration for the barbed end is 0.12 μ M and for the pointed end is 0.6 μ M (Pollard 1986). Elongation proceeds at both the pointed and barbed ends of filaments, but largely at the barbed ends where the polymerization rate for ATP-actin is higher ($k_+ = 11.6 \mu\text{M}^{-1} \text{s}^{-1}$) than at the pointed ends ($k_+ = 1.3 \mu\text{M}^{-1} \text{s}^{-1}$) (Pollard 1986). Therefore, at steady state when the

concentration of ATP-actin is greater than the critical concentration for barbed end and less than that for the pointed end, continuous polymerization occurs primarily at the barbed end and depolymerization takes place at the pointed end, resulting in treadmilling.

Upon initial nucleation, barbed end elongation at the leading edge of the cell occurs in a branched network and filament polymerization drives membrane protrusion, pushing the membrane forward. The current and most widely accepted mechanistic description defining this process is outlined by the dendritic nucleation/array treadmilling model (Mullins *et al.* 1998; Pollard *et al.* 2000; Pollard and Borisy 2003) (Figure 2-1). Barbed end elongation is promoted by factors, including the Ena/VASP proteins and formins, which bind to filament barbed ends and protect them from the activity of capping proteins (Bear *et al.* 2002; Pruyne *et al.* 2002). Capping protein, including CapZ and gelsolin, binds to the barbed end and prevent elongation (Carlier *et al.* 1997). The debranching or severing of filaments by ADF/cofilin or uncapping of filaments produces free barbed ends for elongation to occur (Carlier *et al.* 1997). Once incorporated into the growing filament, ATP-actin is hydrolyzed to ADP-actin and inorganic phosphate is released (Carlier and Pantaloni 1986; Pollard 1986). ADP-actin depolymerized from the pointed end is bound by profilin, a nucleotide exchange factor that catalyzes the exchange of ADP for ATP, generating ATP-actin for another round of polymerization. In summary, polymerization at the barbed ends causes the growth of filaments directed toward the cellular membrane while the pointed ends are either capped or retracting through depolymerization. The entire array of actin and associated proteins treadmills at the leading edge of the cell and provides the mechanism for moving the membrane forward.

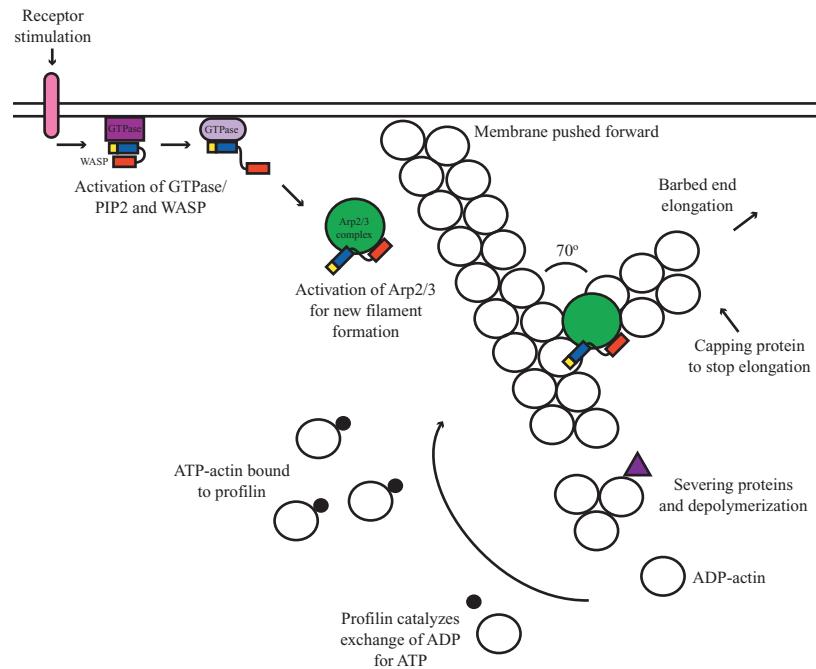


Figure 2-1. Dendritic nucleation/array treadmilling model for actin polymerization at the leading edge of motile cells (adapted from Pollard *et al*, 2000). Upon receptor stimulation, GTPase is activated resulting in WASP activation. WASP in turn activates Arp2/3 complex, which nucleates branched filament formation from the side of pre-existing filaments. Growing filaments are capped or severed. Profilin catalyzes the exchange of ADP for ATP of depolymerized actin monomers. ATP-actin can be incorporated into new barbed ends.

Although actin polymerization proceeds favorably in the presence of free barbed ends (i.e. with a pre-existing nucleus), the *de novo* generation of actin filaments is energetically and kinetically unfavorable and is an inherently slow process. Thus, the requirement for nucleation generally results in an initial lag phase in the actin polymerization that precedes filament elongation. In principle, the formation of a functional actin nucleus requires the initial dimerization of two actin monomers followed by the addition of a third monomer to form a trimer. Generation of either the dimer or trimer is energetically unfavorable and produces unstable, transient actin complexes. However, upon formation of the trimer, the kinetic rate constants of further monomer addition are similar to those for observed for polymerization (Sept and McCammon 2001). In other words, it becomes more likely that a monomer will be added to form a tetramer than for the dissociation of a monomer to reform a dimer to occur. Consequently, the trimer functions as the actin nucleus from which polymerization can proceed.

Nucleators of actin polymerization

Because the rate limiting step for actin polymerization is *de novo* nucleation of new filaments, the rapid generation of cellular actin structures depends on the activation of cellular actin nucleation machinery that can stabilize actin dimer and trimer formation and promote actin polymerization. Several cellular factors that facilitate actin polymerization have been identified, including formins, Spire, and Arp2/3 complex.

The formin family are multidomain proteins characterized by the presence of formin homology (FH) domains. In particular, the FH2 domain dimerizes, forming a ring

that serves as the minimal functional unit. The formin dimer nucleates new barbed end filament growth by first stabilizing actin dimer formation and capping the barbed end (Romero *et al.* 2004; Xu *et al.* 2004; Otomo *et al.* 2005). This allows for the catalysis of *de novo* actin filament formation, which form long, unbranched actin bundles required for cytokinesis, cellular polarization, and stress fiber formation (Ridley 1999; Pruyne *et al.* 2002; Zigmond 2004). In addition, the FH2 dimer moves processively with the growing filament to accelerate actin nucleation and to prevent barbed end capping by capping proteins (Higgs 2005; Otomo *et al.* 2005).

The recently identified actin nucleator Spire is also a multidomain protein that contains four WASP homology 2 (WH2) domains, which are known to bind to actin monomers (Quinlan *et al.* 2005). Spire caps the pointed end of new filaments and catalyzes the formation of a single-stranded actin tetramer through interactions with the WH2 domains. This arrangement between actin and the WH2 domains is proposed to serve as a template to recruit additional actin monomers that can then form a double strand necessary for actin filament formation. Generation of this actin nucleus by Spire allows for the subsequent rapid barbed end elongation, which is required to establish polarity in *Drosophila* oocytes and embryos, although much of the mechanism through which this occurs remains to be determined.

The best characterized and understood actin nucleator is the highly conserved actin-related protein (Arp) 2/3 complex. Arp2/3 complex (~230 kDa) is a multisubunit organization composed of seven subunits, including Arp3, Arp2, p41 (ARPC1), p34 (ARPC2), p21 (ARPC3), p20 (ARPC4), and p16 (ARPC5). The Arp2 and Arp3 subunits have folds that are highly homologous to the actin monomer (Robinson *et al.* 2001).

Thus, Arp2 and Arp3 are hypothesized to provide the first two subunits, a pseudo-actin dimer, for a nucleus from which actin filaments can grow (Mullins *et al.* 1998; Volkmann *et al.* 2001; Egile *et al.* 2005). However, Arp2/3 complex by itself is a poor nucleator. Examination of the crystal structure of Arp2/3 complex reveals that Arp2 and Arp3 are separated by a large cleft in the crystal structure. Arp2 and Arp3 also occupy an orientation that is not compatible with the formation of a pseudo-actin dimer or nucleation of a new actin filament, suggesting that this crystallized complex is inactive (Robinson *et al.* 2001). Activation of Arp2/3 complex requires conformational changes that can result in the closure of this cleft, which is thought to be accomplished through nucleotide hydrolysis of the Arp subunits and binding to nucleation promoting factors (NPFs), such as those from the WASP family of proteins, which provide the third actin monomer required to complete a functional nucleus. Recent EM analyses suggest that Arp2/3 complex exists in different conformational states (Rodal *et al.* 2005). Binding of existing actin filaments coordinately with the binding of WASP proteins stabilizes the activated structure of Arp2/3 complex by promoting the closure of the cleft between Arp2 and Arp3 and actin nucleation (Rodal *et al.* 2005). This is further corroborated by NMR and crosslinking data showing that the central and acidic regions (CA) of N-WASP contacts Arp2, Arp3, p21, and p40 subunits (Kreishman-Deitrick *et al.* 2005), indicating that N-WASP helps to bridge the cleft between Arp2 and Arp3 in order to activate the Arp2/3 complex. In addition, Arp2/3 complex provides a cap for the pointed ends to ensure that actin filament elongation occurs at the barbed ends. Binding of Arp2/3 complex to the sides of pre-existing actin filaments generates new 70° branch networks

from which new filaments can grow toward the leading edges of motile cells (Figure 2-1) (Mullins *et al.* 1998; Pollard and Borisy 2003).

Given the complexity of the actin cytoskeleton and its importance in mediating critical biological functions, including cell motility, it is not surprising that the components involved in actin dynamics are tightly regulated. The organization and rearrangement of actin in response to specific extracellular signals are linked through the functions of a large number of cellular signaling factors. Two important classes of proteins that mediate these interactions are the Rho family of GTPases and their effectors.

Regulation of the actin cytoskeleton by Rho GTPases and their effectors

Members of the Ras-homologous (Rho) family of small GTPases (20-30 kDa) are considered to behave as molecular switches that control signal transduction pathways, cycling from an inactive, GDP bound state and an active, GTP bound state (Figure 2-2) (Bourne 1995; Hoffman and Cerione 2000; Vetter and Wittinghofer 2001; Dvorsky and Ahmadian 2004). There are three known types of regulatory proteins that control the nucleotide cycling of Rho GTPases between inactive and active states: guanine nucleotide exchange factors (GEFs), guanine nucleotide activating proteins (GAPs), and guanine nucleotide dissociation inhibitors (GDIs). GEFs accelerate slow nucleotide exchange by facilitating the release of GDP from GTPase, which allows the protein to bind GTP that is present in high concentrations in the cytosol (Erickson and Cerione 2004). GAPs increase the intrinsically slow rate of nucleotide hydrolysis, leading to GTPase inactivation and termination of signaling (Moon and Zheng 2003). GDIs are

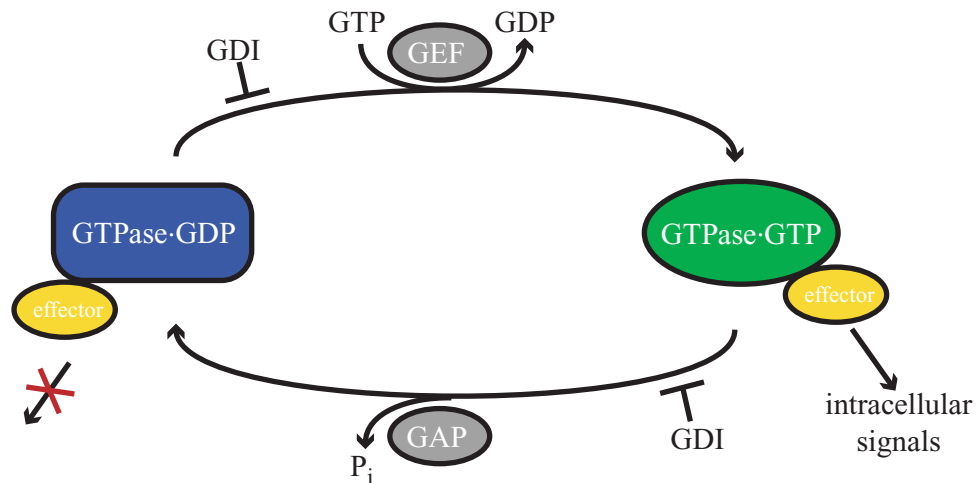


Figure 2-2. GTPase cycle. GTPases cycle between an inactive, GDP-bound state and an active, GTP-bound state. GTP-bound GTPases can bind to effectors to transmit signals to downstream components of the signaling pathway. Binding of GEF to GTPase-GDP facilitates nucleotide exchange and activates the GTPase. Binding of GAP accelerates nucleotide hydrolysis, causing the GTPase to return to an inactive state. GDI binds to the GDP- and GTP-bound states and sequesters the GTPase from signaling.

regulatory proteins that are thought to bind to both the inactive, GDP bound state and active, GTP bound state and sequester the Rho GTPases from the membrane and signaling (DerMardirossian and Bokoch 2005; Dransart *et al.* 2005).

The Rho family of GTPases regulates the activity of many signal transduction pathways implicated in controlling cellular behavior. They are involved in the regulation of cell polarity, cell cycle progression, gene transcription, enzyme activation, vesicular transport pathways, and microtubule dynamics (Etienne-Manneville and Hall 2002; Jaffe and Hall 2005). In addition, the Rho family of GTPases is best known as key regulators of the actin cytoskeleton involved in the assembly, disassembly, and organization of actin. They provide an important link between cell surface receptors and components regulating the actin cytoskeleton. In response to upstream signals, Rho GTPases interact with the membrane through a post-translational lipid modification, which adds a geranylgeranyl group to the C-terminal cysteine (located in the CAAX box). Localization of the Rho GTPase to the membrane followed by its concomitant activation by GEFs allow for the spatial regulation and activation of downstream signaling components that control actin cytoskeletal rearrangements, although the exact mechanisms through which this occurs are not entirely understood.

Among the Rho family of GTPases, Cdc42, Rac, and Rho are the three most well-characterized. Studies in many different cell types have shown that Cdc42 and Rac regulate the formation of filopodial and lamellipodial actin-based structures, respectively, whereas Rho promotes the assembly of actin-myosin filaments, stress fibers, and focal adhesions. Cdc42, Rac, and Rho GTPases mediate their effects on the actin cytoskeleton through interactions with a large number of effector proteins. These effectors, which

include kinases, lipases, and scaffolding proteins, are modulated by their own sets of regulatory interactions that direct the rearrangements of the actin cytoskeleton. For example, Cdc42 and Rac regulate Arp2/3 complex mediated actin polymerization through interactions with the WASP family of proteins and indirectly through the Scar/WAVE family of proteins, respectively. Cdc42 and Rac are also known bind to and activate PAK and IRSp53 to stimulate changes in the actin cytoskeleton (Miki *et al.* 2000; Ridley 2001). Rho GTPases also regulate actin polymerization through direct interactions with the formin protein mDia and actin-myosin filament formation through interactions that include ROCK (Figure 2-3).

The regulatory interactions mediated through the Rho GTPase signaling network are far more complex than the few described above and undoubtedly includes those accomplished through crosstalk, cooperativity, as well as positive and negative feedback behaviors. However, it is not entirely clear how Rho GTPases can specifically target one effector from a large pool of available proteins. In order to appreciate how specificity and fidelity of Rho GTPase signaling can be generated and maintained in these pathways, a detailed understanding of an individual Rho GTPase/effector interaction pair is required. The remainder of this thesis will focus primarily on one Rho GTPase/effector pair, Cdc42 and WASP, and examine how the biochemical and biophysical properties of these proteins can result in a highly specific interaction that function to ultimately regulate changes in the actin cytoskeletal architecture.

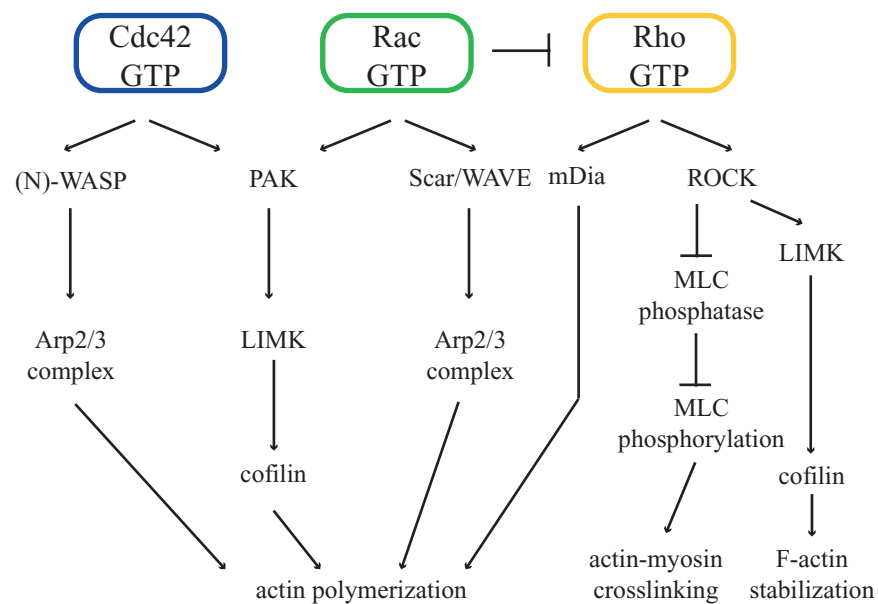


Figure 2-3. Actin cytoskeletal signaling pathways regulated by the Rho GTPases Cdc42, Rac, and Rho. Both Cdc42 and Rac regulate actin polymerization through the WASP/Scar family of proteins and through PAK. Rho also stimulates actin polymerization through mDia and the organization of actin myosin filaments through ROCK.

WASP is an effector of the Rho GTPase Cdc42

Physiological importance of WASP

The Wiskott-Aldrich syndrome protein (WASP) family includes hematopoietic WASP, the ubiquitously expressed neuronal WASP (N-WASP), suppressor of cyclic AMP receptor/WASP family verprolin homologous (Scar/WAVE1-3), and the yeast homolog Bee1p/Las17p (Figure 2-4). WASP was initially identified in individuals with mutations in the WAS gene located on Xp11.22-Xp11.23. Mutations within WASP proteins, including frameshift, missense, and nonsense, deplete WASP levels, typically leading to the pediatric X-linked immunodeficiency disorder Wiskott-Aldrich Syndrome (WAS). WAS is diagnosed by clinical manifestations of thrombocytopenia, bloody diarrhea, eczema, and recurrent infections (Wiskott 1936; Aldrich *et al.* 1954; Derry *et al.* 1994; Snapper and Rosen 1999). A milder form of WAS also exists and is manifested in the form of X-linked thrombocytopenia (XLT) (Canales and Mauer 1967). Both diseases are characterized by severe cytoskeletal defects with increased abnormalities in platelets. Stimulated T cells isolated from individuals affected by WAS display atypical morphology characterized by increased heterogeneity, aberrant forms, and the lack of dense populations of microvillar projections, which depend on actin filaments for their structure (Kenney *et al.* 1986; Gallego *et al.* 1997). More recently, EM analyses of unstimulated T cells reveal that WASP deficiency does not cause any changes in microvillar length or density (Majstoravich *et al.* 2004). The difference in cytoskeletal morphology observed in these studies may be attributed to a difference in T cell activation states and may suggest that WASP only plays a role in actin rearrangements upon stimulation of T cells. Alternatively, WASP deficiency may be compensated by the

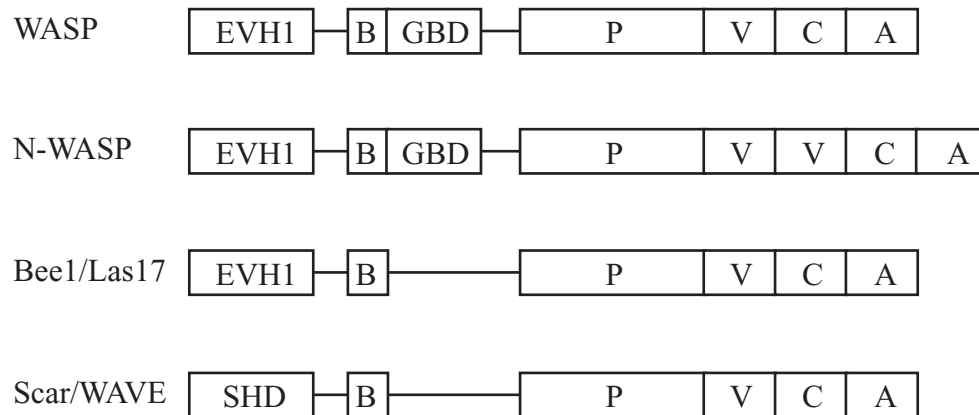


Figure 2-4. Domain organization of the WASP family of proteins. Members of the WASP family contain a basic region (B), a proline rich region (P) followed by a characteristic set of C-terminal domains containing a verprolin homology domain (V), a central domain (C), and an acidic region (A), collectively termed VCA. WASP homologues contain an Ena/VASP homology 1 (EVH1) domain at the N-terminus whereas Scar/WAVE homologues have a Scar homology domain (SHD). WASP and N-WASP each also contain a GTPase binding domain (GBD).

functional redundancy of other proteins present that are involved in actin assembly, such as N-WASP and formins (Majstoravich *et al.* 2004). In addition, two additional missense mutations identified in WASP, L270P and I294T, were shown to give rise to X-linked neutropenia (XLN), a disease with a phenotype distinct from WAS or XLT probably due to the presence of a defective WASP protein (Devriendt *et al.* 2001; Burns *et al.* 2004; Westerberg *et al.* 2005). Patients diagnosed with XLN are characterized with severe neutropenia, monocytopenia, and recurrent bacterial infections (Devriendt *et al.* 2001; Burns *et al.* 2004; Westerberg *et al.* 2005). Work in mouse models further substantiates the critical role of WASP in the development and function of hematopoietic cells. WASP knockout mice have defective T cell function incapable of forming functional immunological synapses, which require the rearrangement or polymerization of actin filaments to organize the clustering of T cell receptors and adhesion molecules (Snapper *et al.* 1998). Embryos deficient of the neuronal WASP homolog, N-WASP, initially survive but ultimately die due to developmental delays and defects in neuronal and cardiac development (Snapper *et al.* 2001). Further analyses of fibroblast cells isolated from N-WASP knockout mice reveal that the protrusion of filopodia is decreased markedly compared to fibroblasts containing functional N-WASP (Snapper *et al.* 2001). Altogether, the disease phenotypes observed in both affected humans and in mouse models emphasize the importance of WASP and its regulation in hematopoietic development and function.

Domain organization of WASP

WASP is a modular protein that contains multiple domains through which WASP function is regulated and mediated (Figure 2-5). WASP is characterized by an N-

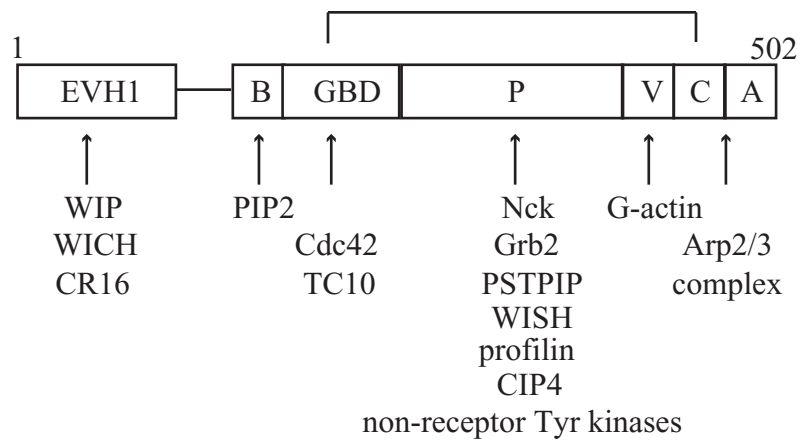


Figure 2-5. Examples of proteins that interact with WASP domains. EVH1, Ena/VASP homology 1; B, basic region; GBD, GTPase binding domain; P, proline rich region; V, verprolin homology region; C, central region; A, acidic region.

terminal Ena/VASP homology 1 (EVH1) domain that is followed by a basic (B) region and a GTPase binding domain (GBD). These domains are connected by a proline-rich (P) sequence to the C-terminal activity bearing domain, collectively referred to as the VCA domain, which corresponds to a verprolin (V) homology region, central (C) region, and acidic (A) region.

The EVH1 domain (WASP residues 39-149), also referred to as the WASP homology 1 (WH1) domain, is related to similar domains identified in the cytoskeletal regulatory proteins Enabled and VASP, which participate as adaptors for protein targeting (Ramesh *et al.* 1997). The importance of this domain for WASP function is reflected by the finding that a majority of missense mutations (>85%) that cause WAS can be localized to the EVH1 domain (Ochs and Notarangelo 2005). Interactions between the N-WASP EVH1 domain were initially confirmed using GST-pull down, coimmunoprecipitation, and yeast two hybrid assays (Ramesh *et al.* 1997; Martinez-Quiles *et al.* 2001). Further studies of the EVH1 domain reveal that WASP directly binds to the C-terminal portion of the ubiquitously expressed WASP interacting protein (WIP) and that mutations in the EVH1 domain disrupt the binding interface between WIP and WASP, potentially leading to the mislocalization, destabilization, and increased degradation of WASP (Anton *et al.* 2002; Sasahara *et al.* 2002; Volkman *et al.* 2002). Studies using vaccinia virus further indicated that N-WASP and WIP are recruited together as a complex to promote actin-based motility (Moreau *et al.* 2000). More recent results suggest that a majority of N-WASP and WIP exist as a complex in T cells and are recruited to lipid rafts through the association with an adaptor protein, CrkL, which binds to the ZAP-70 kinase (Sasahara *et al.* 2002). The CrkL/WIP/N-WASP complex provides

a mechanism through which N-WASP is maintained in an inactive state but can be recruited to the immunological synapse. Phosphorylation of WIP by PKC θ results in the dissociation of WIP from N-WASP, thereby releasing N-WASP from WIP inhibition (Sasahara *et al.* 2002). Other proteins that have been shown to bind to the (N-)WASP EVH1 domain include verprolin homologues CR16 (a glucocorticoid enhanced gene-product) and WIRE/WICH (WIP related/WIP- and CR16-homologous protein) (Ho *et al.* 2001; Kato *et al.* 2002). N-WASP and CR-16 have been found to be colocalized in embryonic hippocampal neurons and in growth cone filopodia *in vivo* but do not appear to affect actin polymerization mediated by N-WASP and Arp2/3 complex *in vitro* (Ho *et al.* 2001). Similarly, WICH binds tightly to N-WASP (more weakly to WASP) and is involved in microspike formation in COS7 cells (Kato *et al.* 2002).

The basic (B) region (WASP residues 224-237) follows the EVH1 domain and consists of a stretch of ~13 amino acids containing six lysine residues. This basic stretch of amino acids has been shown to serve as an important regulatory motif N-WASP homolog that interacts with acidic phospholipids, primarily that of phosphatidylinositol (4,5)-bisphosphate (PIP2) (Ma *et al.* 1998; Prehoda *et al.* 2000). The B region has been implicated to play a role in the inhibition of N-WASP activity through potential electrostatic interactions with the C-terminal acidic region of the VCA domain (Miki *et al.* 1998) and through direct interactions with Arp2/3 complex (Prehoda *et al.* 2000), although some of these interactions have not been fully substantiated.

As in the case for many other effectors of the Rho family of GTPases, WASP contains a GTPase binding domain (GBD) (residues 238-310) that includes a conserved sixteen residue sequence, called the Cdc42/Rac interacting binding (CRIB) motif, plus

additional sequences (Burbelo *et al.* 1995). In WASP, the CRIB motif encompasses residues 238-251 and contain a consensus sequence of I-S-X-P-(X)₂₋₄-F-X-H-X-X-H-V-G containing eight core residues characteristic of CRIB motifs identified in various Cdc42 and Rac effectors. Mutation of a CRIB motif residue (H208D in N-WASP) prevents activation of WASP *in vitro* and formation of filopodia in cells, establishing its requirement for GTPase binding (Miki *et al.* 1998; Rohatgi *et al.* 1999). Although the WASP CRIB motif has been found to be necessary for Cdc42 binding, the motif alone is not sufficient for binding to Cdc42 in a nucleotide dependent manner (Rudolph *et al.* 1998). The isolated WASP CRIB fragment minimally binds to Cdc42-GTP with moderate affinity ($K_D = 470\text{-}490$ nM), but the affinity increases with additional sequences surrounding the CRIB motif ($K_D = 20\text{-}77$ nM) (Rudolph *et al.* 1998; Abdul-Manan *et al.* 1999). More recently, it was shown that two critically conserved tyrosine residues located in the GBD, Y253 and Y291, can serve as substrates for non-receptor Src-family kinases, which may provide an additional mechanism for the regulation of WASP (Cory *et al.* 2002; Suetsugu *et al.* 2002; Cory *et al.* 2003; Torres and Rosen 2003; Torres and Rosen 2005).

A long poly-proline rich region (P; residues 311-419) following the GBD has been shown to interact with SH3 domain containing proteins involved in cytoskeletal regulation. Adapter proteins such as Nck, Grb2, PSTPIP, and WISH typically contain a combination of SH2 and/or SH3 domains that are used to recruit WASP to the membrane or serve as scaffolding upon which additional proteins critical for integrating signaling pathways involved in actin cytoskeletal dynamics are recruited (Rivero-Lezcano *et al.* 1995; She *et al.* 1997; Anton *et al.* 1998; Wu *et al.* 1998; Fukuoka *et al.* 2001). Src-like

non-receptor tyrosine kinases, including Fgr, Fyn, Lck, Btk, and Itk, also contain SH3 domains that engage the WASP P region and SH2 domains that can bind to phosphorylated tyrosine substrates in WASP (Cory *et al.* 2002; Torres and Rosen 2003; Badour *et al.* 2004; Torres and Rosen 2005). The protein kinase C-related kinase homology region 1 (HR1) domain protein CIP4 contains an SH3 domain that binds to the P region of WASP in order to recruit WASP to microtubules in COS7 cells (Tian *et al.* 2000). Profilin, an actin binding nucleotide exchange factor, interacts with WASP through its P region (Suetsugu *et al.* 1998; Yasar *et al.* 2002). Although the exact role of profilin binding is not clear, the profilin-actin interaction may provide a mechanism through which actin monomers are recruited to the WASP verprolin homology domain and/or WASP activation is enhanced.

The C-terminus of WASP is composed of three smaller regions collectively termed VCA domain (residues 420-502) corresponding to a verprolin (V) homology region, a central (C) hydrophobic region, and an acidic (A) region (Machesky and Insall, 1998). Biochemical studies have shown that the isolated VCA domain is sufficient to fully activate Arp2/3 complex (Machesky and Insall 1998; Higgs and Pollard 1999). The verprolin homology segment binds to monomeric (G-)actin and is postulated to be responsible for recruiting G-actin to complete the nucleus initiated by Arp2/3 complex (Marchand *et al.* 2001). The hydrophobic central region contains the conserved sequence $\Phi\text{XXX}\Phi\text{XXX}\Phi\text{XXRXXX}\Phi$ and forms an amphipathic helix crucial to the regulation of WASP activity and the subsequent stimulation of Arp2/3 complex (Rohatgi *et al.* 1999; Rohatgi *et al.* 2000; Marchand *et al.* 2001; Panchal *et al.* 2003; Kreishman-Deitrick *et al.* 2005). Additional mutational analyses of the C region at residues Leu470, Met474,

Arg477, and Ile481 were also found to disrupt interactions between the VCA domain and Arp2/3 complex and prevent the subsequent activation of Arp2/3 complex and actin polymerization (Marchand *et al.* 2001; Panchal *et al.* 2003). The highly acidic C-terminal tail imparts the binding affinity of WASP for Arp2/3 complex, probably through interactions with the conserved W500 residue. A W500S mutation eliminates binding of WASP to Arp2/3 complex (Marchand *et al.* 2001). The isolated VCA domain is sufficient for the constitutive activation of Arp2/3 complex. More recent investigations revealed that S483 and S484 are casein kinase 2 (CK2) substrates and that phosphorylation of these serines contributes to enhanced VCA domain activity toward Arp2/3 complex *in vitro* and in mammalian COS7 cells (Cory *et al.* 2003).

Regulation of WASP: autoinhibition and activation

In the absence of activators, WASP exists in an autoinhibited conformation where intramolecular interactions between the N-terminal GBD and the C-terminal VCA module inhibit WASP activation. Initial biochemical studies showed that the GBD binds specifically to the VCA domain in a GST pull-down assay and that the GBD can block VCA domain activity toward Arp2/3 complex (Machesky and Insall 1998; Miki *et al.* 1998; Higgs and Pollard 1999; Kim *et al.* 2000). NMR studies showed that the GBD fragment is disordered in solution and only upon the addition of 2,2,2-trifluoroethanol (TFE), a solvent known to induce alpha helical structure, or the addition of saturating VCA peptides does the GBD adopt discrete structure (Rudolph *et al.* 1998; Abdul-Manan *et al.* 1999; Rohatgi *et al.* 1999; Kim *et al.* 2000). Subsequent truncation and pull-down studies demonstrated that the core sequence minimally required for WASP autoinhibition

is composed of a fragment of the GBD, lacking a portion of the CRIB motif (residues 242-310), connected by a GGSGGS linker to the C region (residues 461-492), where the measured K_D is $\sim 1 \mu\text{M}$ (Kim *et al.* 2000). The NMR solution structure of a minimal WASP construct, GBD-C, revealed that WASP adopts a compact folded structure (Kim *et al.* 2000). Examination of the autoinhibited WASP structure suggests that the WASP structure can be considered in three layers as shown in Figure 2-6. The first layer is comprised of the beta hairpin and alpha 1 helix of the GBD and has been shown to bind to Cdc42 (Figure 2-6, yellow layer). The second layer consists of alpha helices 2-4 of the GBD (Figure 2-6, cyan layer). The structural elements of the GBD from the first two layers are linked by an artificial linker of GGSGGS residues to the C-terminal C region of the VCA domain, which adopts a helical structure when packed against the GBD and forms the third layer (Figure 2-6, red layer). Addition of the B region and CRIB motif residues did not significantly affect binding to the VCA domain, thereby suggesting that the truncated GBD sequence used in the NMR structure is necessary and sufficient to bind to the C region and together forms the minimal construct required for WASP autoinhibition.

Three models have been proposed to explain how interactions between the GBD and the VCA domain result in the autoinhibition of WASP and N-WASP. In the first model, which was proposed by our lab, the interactions between the GBD and VCA sequester the regions required for binding and activation of Arp2/3 complex. Previous biochemical and NMR studies showed that the C and A regions of WASP bind to Arp2/3 complex (Higgs and Pollard 1999; Rohatgi *et al.* 1999; Panchal *et al.* 2003). Examination of the autoinhibited structure of WASP revealed that the hydrophobic

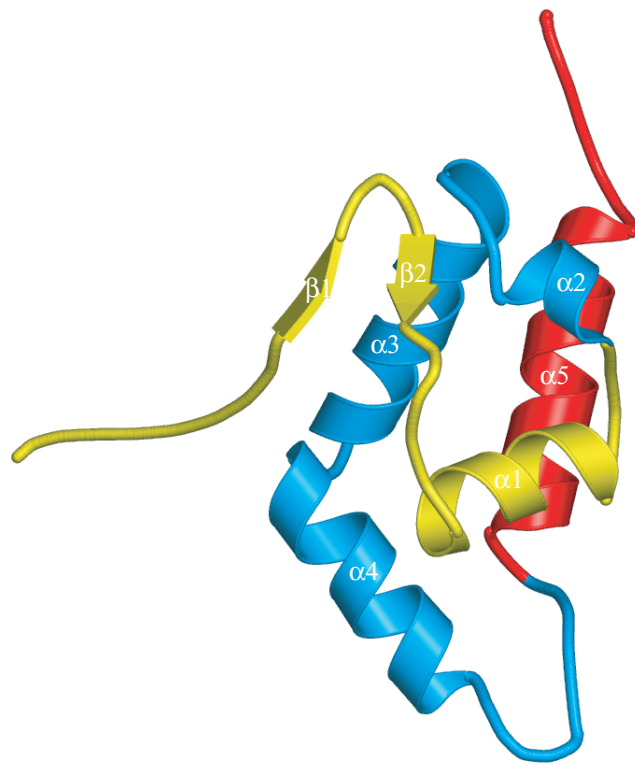


Figure 2-6. Structure of autoinhibited WASP (Protein Data Bank ID code 1EJ5) (Kim *et al*, 2000). The structure can be considered in three layers, which are indicated in different colors. The first two layers (yellow and cyan) containing the beta hairpin and alpha helices 1-4 corresponds to the GBD (residues 242-310). The third layer (red) consisting of alpha helix 5 corresponds to the central (C) helix of the VCA domain (residues 461- 492) that is connected to the GBD by a GGSGGS linker. Elements of the GBD that contact Cdc42 directly in the Cdc42-GBD structure (Abdul-Manan *et al*, 1999) are yellow.

residues of the C region, including L466, V467, L470, and M474, are buried in the hydrophobic core of WASP (Kim *et al.* 2000). Sequence analysis predicted that the C region forms a conserved amphipathic helix where many of the residues required for activation of Arp2/3 complex are completely buried in the autoinhibited core through interactions with the GBD (Panchal *et al.* 2003). Subsequent mutation of key residues in the C region (namely L466, L470, M474, R477, and I481) of VCA peptides demonstrated that the activation of Arp2/3 complex in actin polymerization assays is impaired (Panchal *et al.* 2003). Furthermore, structural and biochemical analysis of the WASP L270P mutation, which gives rise to the XLN disease phenotype, revealed that destabilization of the autoinhibited core causes constitutive WASP activity toward Arp2/3 complex through increased exposure of the C region (Devriendt *et al.* 2001). Altogether, these results strongly indicate that the hydrophobic packing of secondary structural elements in the autoinhibited WASP structure masks the binding site for Arp2/3 complex. Therefore, autoinhibition of WASP involves the sequestration of VCA by preventing the activation of downstream machinery required to stimulate actin polymerization.

In the second model, proposed by Lim and colleagues, the residues encompassed in the basic region N-terminal to the GBD are suggested to play a critical role in the autoinhibition of N-WASP (Prehoda *et al.* 2000). Here, the interactions between the GBD and the VCA domain are necessary for autoinhibition but are not sufficient to repress WASP activity toward Arp2/3 complex. Instead, residues in the B region act cooperatively with the GBD to bind to the VCA domain and directly to Arp2/3 complex. This combination of regulatory interactions maintains WASP in an inactive state

potentially by causing a conformational change in the VCA domain and/or Arp2/3 complex. Evidence supporting this direct interaction includes a pull-down assay between N-WASP GST-BGBD in the presence of VCA and Arp2/3 complex and enhanced activation of N-WASP in the presence of PIP2, which binds to the B region (Prehoda *et al.* 2000). However, this direct autoinhibitory interaction between the B region and Arp2/3 complex has not been fully substantiated by our lab or others (Egile *et al.* 1999; Rohatgi *et al.* 1999; Rohatgi *et al.* 2000). In addition, deletion of the B region does not significantly affect the affinity between the GBD and VCA (Rohatgi *et al.* 2000) suggesting that the B region enhances WASP autoinhibition but is not the primary mechanism for repression. Instead, the data presented by Prehoda *et al.* is consistent with the basic region modulating the conformational equilibrium of Arp2/3 complex and the stability of WASP while the GBD sequesters the VCA residues required for Arp2/3 complex activation. Components from the second model may prove to work in concert with our first model to enhance repression of WASP activity and further stabilize the autoinhibited conformation of WASP, thereby preventing Arp2/3 complex access to the VCA domain.

More recently, a third model has been proposed to explain WASP autoinhibition. Ho *et al.* have suggested that N-WASP may be involved in a larger multi-component complex of adaptor and scaffold proteins that regulates WASP inhibition (Ho *et al.* 2004). Toca-1 (transducer of Cdc42-dependent actin assembly), a component isolated from *Xenopus* extracts, was shown to bind to both Cdc42-GTP and N-WASP. However, the addition of Toca-1 to actin polymerization assays resulted only in a small increase in N-WASP activity in the presence of Cdc42-GTP. Addition of WIP to the same assay

caused a dramatic increase in polymerization activity that was absent in an assay only containing Cdc42-GTP, N-WASP, and Toca-1. This observation coupled to the fact that N-WASP always copurifies as a complex with WIP in *Xenopus* extracts led the authors to propose that the association of WIP to N-WASP is required to maintain WASP in an autoinhibited conformation and that interactions with Toca-1 is required to counteract WIP activity and stimulate N-WASP activation (Ho *et al.* 2004). However, this model is not consistent with many studies that show that intramolecular interactions between GBD (or BGBD) with VCA are sufficient to repress WASP activity (Higgs and Pollard 1999; Rohatgi *et al.* 1999; Kim *et al.* 2000). Rather, the function of WIP may serve to enhance the autoinhibitory interactions of N-WASP by further stabilizing the N-WASP inhibited conformation and occluding the binding site for Arp2/3 complex, which is consistent with the first model. Addition of Toca-1 then modulates the conformational equilibrium of N-WASP by potentially inhibiting WIP or binding to Cdc42-GTP and N-WASP. Thus, while both the second and third models propose alternative mechanisms to explain WASP autoinhibition, the data presented in each study are also compatible with our first model, such that both the basic region and WIP function to ensure high-levels of (N-) WASP activity by modulating the conformational equilibrium of (N-)WASP and sequestering residues in the C region of VCA from binding Arp2/3 complex. Destabilization of the autoinhibitory core of WASP, through interactions with Cdc42, PIP2, or Toca-1, results in the stabilization of the activated WASP state and causes the exposure of the VCA domain, thereby allowing Arp2/3 complex to bind.

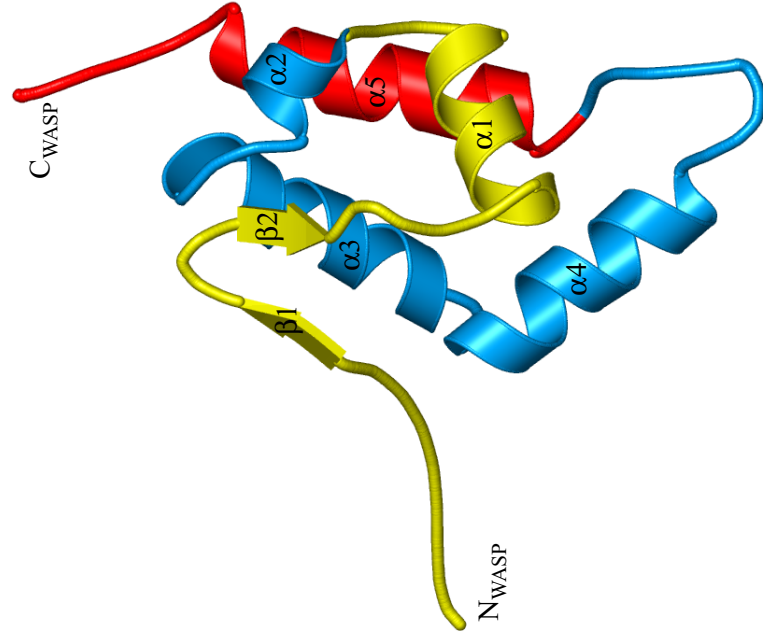
Activation of WASP requires that the VCA residues sequestered from binding Arp2/3 complex become physically separated from autoinhibitory interactions with the

GBD. The best characterized activator of WASP to date is the Rho family GTPase Cdc42. Initial studies isolated WASP as a component in *Xenopus* oocyte extracts (named MCAP2) that was required for Arp2/3-mediated actin polymerization stimulated by Cdc42 (Ma *et al.* 1998). Subsequent attempts to isolate and identify MCAP2 isolated WASP as a downstream effector of activated Cdc42 through sequence homology to the CRIB motif found in p21 activated kinase (PAK), a downstream effector of Rac GTPase. Binding to WASP GBD is Cdc42 specific, with binding to Rac observed to a much lesser extent in GST-pull down assays. A constitutively active Cdc42 mutant, G12VCdc42, stimulates WASP activity *in vitro* whereas the dominant negative Cdc42 mutant, T17NCdc42 does not (Kolluri *et al.* 1996; Symons *et al.* 1996; Ma *et al.* 1998; Miki *et al.* 1998). Similar experiments with analogous Rac mutants are not affected thereby confirming GTPase specificity. Consequently, Cdc42 was specifically shown to bind to the WASP GBD isolated from human neutrophils (Symons *et al.* 1996) and B cell lysates (Kolluri *et al.* 1996) in a nucleotide dependent manner. Additional experiments demonstrated that a GST-tagged GBD can specifically pull down GTP-bound Cdc42 and that the GBD domain is necessary and sufficient to mediate binding (Kolluri *et al.* 1996; Symons *et al.* 1996). Furthermore, addition of Cdc42-GTP is required for (N-)WASP stimulated Arp2/3-mediated actin polymerization in *Xenopus* oocyte extracts and in a purified component system (Higgs and Pollard 1999; Rohatgi *et al.* 1999; Rohatgi *et al.* 2000). Thus, the presence of Cdc42 can significantly accelerate WASP mediated actin polymerization.

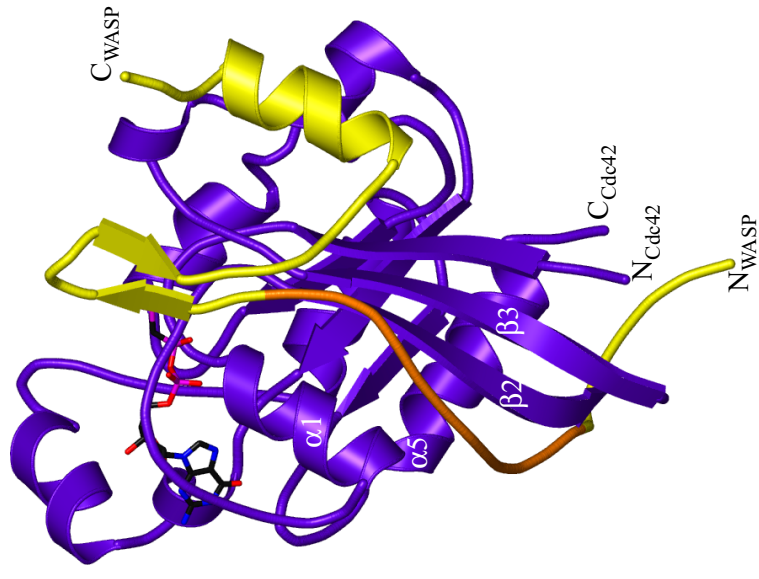
Examination of the structure of WASP and Cdc42 suggests that the specificity of the interaction is likely due to contacts between the WASP CRIB motif and the switch I

Figure 2-7. Autoinhibition and activation of WASP. A. WASP GBD (yellow and cyan) bound to the C domain helix (red) (Kim *et al*, 2000). B. WASP GBD (yellow and orange) bound to Cdc42-GMPPCP (purple) (Abdul-Manan *et al*, 1999). CRIB motif residues not present in A. are highlighted in orange.

A.



B.



and alpha 5 helix of GTP-bound Cdc42 (Figure 2-7b) (Abdul-Manan *et al.* 1999). In the presence of Cdc42 bound to a GTP analog, GMPPCP, the beta hairpin and alpha 1 helix of the WASP GBD is organized such that the N-terminal portion of the GBD interacts with switch I and II of Cdc42-GMPPCP. The CRIB motif, which is unstructured in isolation, forms a linear strand that binds to Cdc42-GMPPCP in an extended conformation and parallels the beta 2 and beta 3 strands. Interactions between the CRIB motif and the beta 2 strand are postulated to stabilize the intermolecular interactions between WASP and Cdc42-GMPPCP, providing the driving force for binding. This is in contrast to the structure of the C region bound to the GBD in the WASP autoinhibited structure (Figure 2-7a). In the context of the autoinhibited structure of GBD-C, the relative orientations of the beta hairpin and the alpha 1 helix of the first layer comprising the GBD are different and these secondary structural elements are packed against the second layer, generating many of the hydrophobic contacts. The CRIB motif residues remain largely unstructured and are not present in the autoinhibited WASP structure (Kim *et al.* 2000). Comparison of the overall Cdc42-GBD structure against the autoinhibited fold of GBD-C reveals that the two complexes are structurally distinct and incompatible with one another. This structural incompatibility provides a mechanism for WASP activation by Cdc42. It is likely that the binding of the first structural layer of WASP to Cdc42-GTP causes its physical separation from the second layer and the subsequent destabilization of the autoinhibitory core. This can result in the cooperative unfolding of WASP and the release and exposure of the C region of VCA for binding to Arp2/3 complex. Consistent with this, NMR analyses revealed that the addition of Cdc42-GMPPCP to a sample containing ¹⁵N-GBD-C resulted in chemical shifts changes

and significant line broadening of many WASP resonances (Buck *et al.* 2001; Buck *et al.* 2004). Binding of Cdc42 to the CRIB motif is reflected by the appearance of four downfield-shifted amide proton peaks at ~9 ppm corresponding to residues S234, K235, G239, and S242. The previously structured C region in the autoinhibited WASP structure is unfolded in the presence of Cdc42-GMPPCP as amide peaks in the HSQC spectrum representing the folded WASP core are severely broadened, collectively clustered toward the center of the spectrum, and show a lack of peak dispersion. Thus, the NMR data is consistent with a mechanism where Cdc42-GTP binding results in the physical displacement of VCA from the GBD.

In order to examine how binding of Cdc42 contributes to the destabilization of WASP, a recent study by Buck *et al.* used NMR spectroscopy and the rate of deuterium exchange of amide protons to measure changes in WASP folding, stability, and dynamics (Buck *et al.* 2001). Results from studies with the truncated autoinhibited WASP, ¹⁵N-BGBD-C (containing the residues from basic region, GBD, and C region), indicate that a majority of amides located in the alpha helices are highly protected from exchange with deuterium, which is reflected by the relatively high magnitude of calculated protection factors (averaging 6×10^4). In contrast, amides located in the beta hairpin are rapidly exchanged due to local fluctuations and protection factors were not measurable. Prior analysis of the Cdc42-WASP interaction indicates that the binding affinity of Cdc42 for autoinhibited BGBD-C ($K_D = 3.5 \mu\text{M}$) compared to the affinity for the GBD alone ($K_D \sim 100 \text{ nM}$) is reduced substantially, ~100-fold, a phenomenon that has been similarly observed for p21 activated kinase, PAK (600 nM for the full length protein vs. 18 nM for the regulatory domain only) (Buchwald *et al.* 2001). These differences in the binding

affinity for Cdc42 of the isolated GBD and GBD-C constructs allowed for monitoring of hydrogen exchange in WASP by ligand displacement (Buck *et al.* 2001). Briefly, Cdc42 is added to a sample containing ^{15}N -GBD-C to permit exchange, followed by quenching, which is facilitated by the addition of unlabeled GBD to displace the lower binding affinity interaction between ^{15}N -GBD-C and Cdc42. The results display a uniform increase in the hydrogen exchange rates of the amide protons across the entire molecule that are normally protected by the autoinhibited fold, suggesting that Cdc42 binding contributes to a global destabilization of WASP. Exchange rates of the most protected amides in the hydrophobic core of WASP, including residues in alpha helix 3, are affected the most by Cdc42 binding. This suggests that the same residues that are critical for WASP autoinhibition provide important contacts in the Cdc42 bound structure. Altogether, these results substantiate our hypothesis that the binding of Cdc42 to WASP GBD results in the cooperative, physical displacement of the VCA domain from the GBD, thereby allowing Arp2/3 complex access to bind to the VCA domain.

The energetic contribution from Cdc42 binding alone is likely to be insufficient to induce complete WASP destabilization and activation (under non-saturating conditions). A majority of amides in both the GBD and the C region remain protected from hydrogen exchange even upon binding to Cdc42 (Buck *et al.* 2001). This finding is consistent with numerous observations, from our lab and others, that show only partial activation of a highly stabilized WASP construct with non-saturating concentrations of Cdc42. Preliminary results from *in vitro* polymerization data also demonstrate that at lower concentrations Cdc42 can only partially activate WASP and may require the synergy provided by the addition of other activators to achieve a level of activation comparable to

that observed for the VCA peptide (Higgs and Pollard 1999; Prehoda *et al.* 2000; Rohatgi *et al.* 2000). Furthermore, similar studies with the PAK protein also support these observations. Cdc42 binding to PAK provides limited destabilization of the PAK autoinhibited dimer, but it is sufficient to allow autophosphorylation (Buchwald *et al.* 2001). The subsequent autophosphorylation of PAK causes the dimer to dissociate into a monomeric form, resulting in a pathway to PAK activation that is GTPase independent. Thus, the binding energy contributed by Cdc42 association may not provide enough energy to trigger complete disruption of the autoinhibited folds of both WASP and PAK.

Several lines of evidence suggest that the basic region may play an important role in the cooperative regulation and activation of WASP. Initial studies showed that PIP2 reconstituted in synthetic liposomes can pull down truncated WASP constructs containing the B region and the GBD (Higgs and Pollard 1999; Prehoda *et al.* 2000; Rohatgi *et al.* 2000). Furthermore, addition of PIP2 liposomes stimulated N-WASP activated Arp2/3-mediated actin polymerization in reconstituted *in vitro* assays and in *Xenopus* oocyte extracts (Rohatgi *et al.* 1999; Rohatgi *et al.* 2000). Overexpression of PI5K, an enzyme that produces PIP2, also results in the formation of N-WASP mediated motile actin comet tails (Rozelle *et al.* 2000; Benesch *et al.* 2002). More recent studies have demonstrated that PIP2 binding to the B region can activate N-WASP in a multivalent manner (Papayannopoulos *et al.* 2005). These studies also show that binding and activation of N-WASP is sensitive to the spatial density of PIP2, resulting in a sharp, cooperative activation curve that suggests binding of one PIP2 molecule enhances the binding of the next molecule. Furthermore, in N-WASP, the sensitivity to PIP2 can be tuned with the number of lysine residues present in the B region, where increasing the

number of basic residues increases PIP2 multivalency and reduces the N-WASP activation threshold. However, the addition of Cdc42-GMPPNP can significantly decrease the threshold requirement for activation by PIP2 and cause potent N-WASP activation (Papayannopoulos *et al.* 2005). These observations are consistent with many other studies, which show that lower concentrations of PIP2 alone can only stimulate weak activation of N-WASP and requires the presence of Cdc42-GTP to fully activate N-WASP. Thus, the activation of N-WASP can be modeled using a thermodynamic framework proposed by Prehoda *et al.* where interactions among the B-GBD module, VCA, and Arp2/3 complex collectively repress N-WASP activity and activation of N-WASP requires the input of both Cdc42 and PIP2 (Prehoda *et al.* 2000). According to this model, the addition of one input enhances the binding of the second input by disrupting autoinhibitory interactions and stabilizing the activated state of N-WASP. The degree to which binding of one input affects the binding affinity of the second input is encompassed by the cooperativity factor c . Therefore, highly cooperative WASP activation and potent signal integration can be achieved by PIP2 and the concomitant binding of another activator to an adjacent WASP domain, such as Cdc42 to the GBD (Higgs and Pollard 1999; Prehoda *et al.* 2000; Rohatgi *et al.* 2000; Rohatgi *et al.* 2001). However, implicit in this model is the assumption that Cdc42, PIP2, and Cdc42 plus PIP2 together can stimulate equivalent levels of N-WASP activation. This assumption may hold at saturating concentrations of Cdc42 and PIP2 but not necessarily at non-saturating concentrations. Under conditions where lower concentrations of input are present, the conformational equilibrium of WASP must also be considered.

A number of other proteins that bind to WASP have also been identified, although much of the mechanisms through which they regulate WASP activity are poorly understood. Interactions between the P region of WASP and the SH3 domains of several proteins may provide for the recruitment of components necessary for actin polymerization and for activation independent of Cdc42 (Moreau *et al.* 2000). For example, the adapter proteins Nck and Grb2 contain multiple SH3 domains that can bind to the P region. All three SH3 domains of Nck are required for effective WASP activation and binding of Nck is required for N-WASP mediated motility of vaccinia virus (Rivero-Lezcano *et al.* 1995; Rohatgi *et al.* 2001; Scaplehorn *et al.* 2002). Either SH3 domain in Grb2 stimulates WASP activity in *in vitro* polymerization assays whereas mutations in Grb2 SH3 abolishes association with WASP (Carlier *et al.* 2000; Rohatgi *et al.* 2001; Benesch *et al.* 2002). Nck and Grb2 also contain SH2 domains that associate directly with activated tyrosine kinase receptors through phosphotyrosine motifs, thereby providing a link between WASP and the membrane. Cdc42 interacting protein 4 (CIP4) is a Cdc42 effector protein that also interacts with WASP through a C-terminal SH3 domain. The CIP4 SH3 domain binds to the P region of WASP in pull down assays and mediates WASP localization to microtubules in COS-7 cells (Tian *et al.* 2000). However, the role of Cdc42 binding is not understood entirely as WASP binds CIP4 and is localized to sites of microtubules independently of Cdc42. In the majority of cases involving SH3 domain containing proteins and WASP, potent stimulation of WASP activity *in vitro* requires the synergistic cooperation of proteins added concomitantly, usually with either Cdc42 or PIP2. The combinations of PIP2/Nck, Cdc42/Grb2, PIP2/Nck/Grb2, and Nck/Grb2, can all result in the potent stimulation of (N-)WASP

mediated actin polymerization and vesicle motility, enhanced to similar levels achieved by a constitutively active WASP.

The data from all of these studies combined are consistent with a model where WASP autoinhibition is achieved through the stabilization of the inhibited state and the sequestration of critical C region residues of the VCA domain from binding to Arp2/3 complex. Stabilization of the autoinhibited state of WASP is predicted to occur through regulatory interactions of the basic region coupled to the GBD and/or the presence of WIP. Activation of WASP then follows as a result of interactions that destabilize the hydrophobic core of WASP, including binding of Cdc42-GTP, PIP2, and SH3 containing proteins, and stabilize the activated state of WASP. These interactions lead to the release and exposure of the VCA domain to bind to Arp2/3 complex and stimulate actin polymerization.

Conclusion

The actin cytoskeleton provides a critical framework underlying many complex cellular structures that drive a number of fundamental biological processes. Actin provides the building block for many of these dynamic cytoskeletal structures. However, actin alone cannot achieve these functions. Recent investigations have uncovered a multitude of accessory proteins that are required to regulate the function of actin and the formation of actin into complex networks. An understanding of the individual components involved in this organization and their regulation and interaction with other cellular factors are required to fully understand the biological function of the cytoskeletal machinery.

Recent work has highlighted the critical role of WASP in regulating the reorganization of the actin cytoskeletal architecture in response to extracellular signals. Much progress, gained through extensive cellular and biochemical studies, has been made towards elucidating the regulatory mechanism of WASP and its binding partners in order to gain insight into the biological function of WASP. However, little is known about the structural and biophysical basis of WASP activation or how the binding of an activator is coupled to WASP activation. An understanding of the molecular mechanism through which WASP cooperatively integrates and responds specifically to multiple signals requires a quantitative analysis of the protein's biochemical properties and the elements that contribute to its inhibition or activation. The work presented in this thesis aims to address these issues by describing an expanded thermodynamic framework that is developed to understand how binding of Cdc42 is coupled to WASP activation through the parameterization of our model and its validation. Understanding of the biochemical and biophysical properties of WASP will be used to reveal novel features that challenge the accepted notions of the established concept in the field of GTPases. Additionally, these properties can be used to understand the regulatory interactions of WASP with other proteins through the development of newly engineered biological modules.

References

- Abdul-Manan, N., *et al.* (1999). "Structure of Cdc42 in complex with the GTPase-binding domain of the 'Wiskott-Aldrich syndrome' protein." Nature **399**(6734): 379-83.
- Aldrich, R. A., *et al.* (1954). "Pedigree demonstrating a sex-linked recessive condition characterized by draining ears, eczematoid dermatitis and bloody diarrhea." Pediatrics **13**(133-39).
- Anton, I. M., *et al.* (2002). "WIP deficiency reveals a differential role for WIP and the actin cytoskeleton in T and B cell activation." Immunity **16**(2): 193-204.
- Anton, I. M., *et al.* (1998). "The Wiskott-Aldrich syndrome protein-interacting protein (WIP) binds to the adaptor protein Nck." J Biol Chem **273**(33): 20992-5.
- Badour, K., *et al.* (2004). "Fyn and PTP-PEST-mediated regulation of Wiskott-Aldrich syndrome protein (WASp) tyrosine phosphorylation is required for coupling T cell antigen receptor engagement to WASp effector function and T cell activation." J Exp Med **199**(1): 99-112.
- Bear, J. E., *et al.* (2002). "Antagonism between Ena/VASP proteins and actin filament capping regulates fibroblast motility." Cell **109**(4): 509-21.
- Benesch, S., *et al.* (2002). "Phosphatidylinositol 4,5-bisphosphate (PIP₂)-induced vesicle movement depends on N-WASP and involves Nck, WIP, and Grb2." J Biol Chem **277**(40): 37771-6.
- Bourne, H. R. (1995). "GTPases: a family of molecular switches and clocks." Philos Trans R Soc Lond B Biol Sci **349**(1329): 283-9.

- Buchwald, G., *et al.* (2001). "Conformational switch and role of phosphorylation in PAK activation." Mol Cell Biol **21**(15): 5179-89.
- Buck, M., *et al.* (2001). "Global disruption of the WASP autoinhibited structure on Cdc42 binding. Ligand displacement as a novel method for monitoring amide hydrogen exchange." Biochemistry **40**(47): 14115-22.
- Buck, M., *et al.* (2004). "A two-state allosteric model for autoinhibition rationalizes WASP signal integration and targeting." J Mol Biol **338**(2): 271-85.
- Burbelo, P. D., *et al.* (1995). "A conserved binding motif defines numerous candidate target proteins for both Cdc42 and Rac GTPases." J Biol Chem **270**(49): 29071-4.
- Burns, S., *et al.* (2004). "Mechanisms of WASp-mediated hematologic and immunologic disease." Blood **104**(12): 3454-62.
- Canales, M. L. and A. M. Mauer (1967). "Sex-linked hereditary thrombocytopenia as a variant of Wiskott-Aldrich syndrome." N Engl J Med **277**(17): 899-901.
- Carlier, M. F., *et al.* (1997). "Actin depolymerizing factor (ADF/cofilin) enhances the rate of filament turnover: implication in actin-based motility." J Cell Biol **136**(6): 1307-22.
- Carlier, M. F., *et al.* (2000). "GRB2 links signaling to actin assembly by enhancing interaction of neural Wiskott-Aldrich syndrome protein (N-WASp) with actin-related protein (ARP2/3) complex." J Biol Chem **275**(29): 21946-52.
- Carlier, M. F. and D. Pantaloni (1986). "Direct evidence for ADP-Pi-F-actin as the major intermediate in ATP-actin polymerization. Rate of dissociation of Pi from actin filaments." Biochemistry **25**(24): 7789-92.

- Cory, G. O., *et al.* (2003). "Phosphorylation of the WASP-VCA domain increases its affinity for the Arp2/3 complex and enhances actin polymerization by WASP." Mol Cell **11**(5): 1229-39.
- Cory, G. O., *et al.* (2002). "Phosphorylation of tyrosine 291 enhances the ability of WASp to stimulate actin polymerization and filopodium formation. Wiskott-Aldrich Syndrome protein." J Biol Chem **277**(47): 45115-21.
- DerMardirossian, C. and G. M. Bokoch (2005). "GDIs: central regulatory molecules in Rho GTPase activation." Trends Cell Biol **15**(7): 356-63.
- Derry, J. M., *et al.* (1994). "Isolation of a novel gene mutated in Wiskott-Aldrich syndrome." Cell **78**(4): 635-44.
- Devriendt, K., *et al.* (2001). "Constitutively activating mutation in WASP causes X-linked severe congenital neutropenia." Nat Genet **27**(3): 313-7.
- Dransart, E., *et al.* (2005). "RhoGDIs revisited: novel roles in Rho regulation." Traffic **6**(11): 957-66.
- Dvorsky, R. and M. R. Ahmadian (2004). "Always look on the bright side of Rho: structural implications for a conserved intermolecular interface." EMBO Rep **5**(12): 1130-6.
- Egile, C., *et al.* (1999). "Activation of the CDC42 effector N-WASP by the Shigella flexneri IcsA protein promotes actin nucleation by Arp2/3 complex and bacterial actin-based motility." J Cell Biol **146**(6): 1319-32.
- Egile, C., *et al.* (2005). "Mechanism of filament nucleation and branch stability revealed by the structure of the arp2/3 complex at actin branch junctions." PLoS Biol **3**(11): e383.

- Erickson, J. W. and R. A. Cerione (2004). "Structural elements, mechanism, and evolutionary convergence of Rho protein-guanine nucleotide exchange factor complexes." Biochemistry **43**(4): 837-42.
- Etienne-Manneville, S. (2004). "Actin and microtubules in cell motility: which one is in control?" Traffic **5**(7): 470-7.
- Etienne-Manneville, S. and A. Hall (2002). "Rho GTPases in cell biology." Nature **420**(6916): 629-35.
- Fukuoka, M., *et al.* (2001). "A novel neural Wiskott-Aldrich syndrome protein (N-WASP) binding protein, WISH, induces Arp2/3 complex activation independent of Cdc42." J Cell Biol **152**(3): 471-82.
- Gallego, M. D., *et al.* (1997). "Defective actin reorganization and polymerization of Wiskott-Aldrich T cells in response to CD3-mediated stimulation." Blood **90**(8): 3089-97.
- Hall, A. (1998). "Rho GTPases and the actin cytoskeleton." Science **279**(5350): 509-14.
- Higgs, H. N. (2005). "Formin proteins: a domain-based approach." Trends Biochem Sci **30**(6): 342-53.
- Higgs, H. N. and T. D. Pollard (1999). "Regulation of actin polymerization by Arp2/3 complex and WASp/Scar proteins." J Biol Chem **274**(46): 32531-4.
- Ho, H. Y., *et al.* (2004). "Toca-1 mediates Cdc42-dependent actin nucleation by activating the N-WASP-WIP complex." Cell **118**(2): 203-16.
- Ho, H. Y., *et al.* (2001). "CR16 forms a complex with N-WASP in brain and is a novel member of a conserved proline-rich actin-binding protein family." Proc Natl Acad Sci U S A **98**(20): 11306-11.

- Hoffman, G. R. and R. A. Cerione (2000). "Flipping the switch: the structural basis for signaling through the CRIB motif." Cell **102**(4): 403-6.
- Jaffe, A. B. and A. Hall (2005). "RHO GTPases: Biochemistry and Biology." Annu Rev Cell Dev Biol.
- Kato, M., *et al.* (2002). "WICH, a novel verprolin homology domain-containing protein that functions cooperatively with N-WASP in actin-microspike formation." Biochem Biophys Res Commun **291**(1): 41-7.
- Kenney, D., *et al.* (1986). "Morphological abnormalities in the lymphocytes of patients with the Wiskott-Aldrich syndrome." Blood **68**(6): 1329-32.
- Kim, A. S., *et al.* (2000). "Autoinhibition and activation mechanisms of the Wiskott-Aldrich syndrome protein." Nature **404**(6774): 151-8.
- Kolluri, R., *et al.* (1996). "Direct interaction of the Wiskott-Aldrich syndrome protein with the GTPase Cdc42." Proc Natl Acad Sci U S A **93**(11): 5615-8.
- Kreishman-Deitrick, M., *et al.* (2005). "NMR analyses of the activation of the Arp2/3 complex by neuronal Wiskott-Aldrich syndrome protein." Biochemistry.
- Ma, L., *et al.* (1998). "Corequirement of specific phosphoinositides and small GTP-binding protein Cdc42 in inducing actin assembly in *Xenopus* egg extracts." J Cell Biol **140**(5): 1125-36.
- Ma, L., *et al.* (1998). "The Arp2/3 complex mediates actin polymerization induced by the small GTP-binding protein Cdc42." Proc Natl Acad Sci U S A **95**(26): 15362-7.
- Machesky, L. M. and R. H. Insall (1998). "Scar1 and the related Wiskott-Aldrich syndrome protein, WASP, regulate the actin cytoskeleton through the Arp2/3 complex." Curr Biol **8**(25): 1347-56.

- Majstoravich, S., *et al.* (2004). "Lymphocyte microvilli are dynamic, actin-dependent structures that do not require Wiskott-Aldrich syndrome protein (WASp) for their morphology." Blood **104**(5): 1396-403.
- Marchand, J. B., *et al.* (2001). "Interaction of WASP/Scar proteins with actin and vertebrate Arp2/3 complex." Nat Cell Biol **3**(1): 76-82.
- Martinez-Quiles, N., *et al.* (2001). "WIP regulates N-WASP-mediated actin polymerization and filopodium formation." Nat Cell Biol **3**(5): 484-91.
- Miki, H., *et al.* (1998). "Induction of filopodium formation by a WASP-related actin-depolymerizing protein N-WASP." Nature **391**(6662): 93-6.
- Miki, H., *et al.* (2000). "IRSp53 is an essential intermediate between Rac and WAVE in the regulation of membrane ruffling." Nature **408**(6813): 732-5.
- Moon, S. Y. and Y. Zheng (2003). "Rho GTPase-activating proteins in cell regulation." Trends Cell Biol **13**(1): 13-22.
- Moreau, V., *et al.* (2000). "A complex of N-WASP and WIP integrates signalling cascades that lead to actin polymerization." Nat Cell Biol **2**(7): 441-8.
- Mullins, R. D., *et al.* (1998). "The interaction of Arp2/3 complex with actin: nucleation, high affinity pointed end capping, and formation of branching networks of filaments." Proc Natl Acad Sci U S A **95**(11): 6181-6.
- Ochs, H. D. and L. D. Notarangelo (2005). "Structure and function of the Wiskott-Aldrich syndrome protein." Curr Opin Hematol **12**(4): 284-91.
- Otomo, T., *et al.* (2005). "Structural basis of actin filament nucleation and processive capping by a formin homology 2 domain." Nature **433**(7025): 488-94.

- Panchal, S. C., *et al.* (2003). "A conserved amphipathic helix in WASP/Scar proteins is essential for activation of Arp2/3 complex." Nat Struct Biol **10**(8): 591-8.
- Papayannopoulos, V., *et al.* (2005). "A polybasic motif allows N-WASP to act as a sensor of PIP(2) density." Mol Cell **17**(2): 181-91.
- Pollard, T. D. (1986). "Rate constants for the reactions of ATP- and ADP-actin with the ends of actin filaments." J Cell Biol **103**(6 Pt 2): 2747-54.
- Pollard, T. D., *et al.* (2000). "Molecular mechanisms controlling actin filament dynamics in nonmuscle cells." Annu Rev Biophys Biomol Struct **29**: 545-76.
- Pollard, T. D. and G. G. Borisy (2003). "Cellular motility driven by assembly and disassembly of actin filaments." Cell **112**(4): 453-65.
- Prehoda, K. E., *et al.* (2000). "Integration of multiple signals through cooperative regulation of the N-WASP-Arp2/3 complex." Science **290**(5492): 801-6.
- Pruyne, D., *et al.* (2002). "Role of formins in actin assembly: nucleation and barbed-end association." Science **297**(5581): 612-5.
- Quinlan, M. E., *et al.* (2005). "Drosophila Spire is an actin nucleation factor." Nature **433**(7024): 382-8.
- Ramesh, N., *et al.* (1997). "WIP, a protein associated with wiskott-aldrich syndrome protein, induces actin polymerization and redistribution in lymphoid cells." Proc Natl Acad Sci U S A **94**(26): 14671-6.
- Ridley, A. J. (1999). "Stress fibres take shape." Nat Cell Biol **1**(3): E64-6.
- Ridley, A. J. (2001). "Rho family proteins: coordinating cell responses." Trends Cell Biol **11**(12): 471-7.

- Rivero-Lezcano, O. M., *et al.* (1995). "Wiskott-Aldrich syndrome protein physically associates with Nck through Src homology 3 domains." Mol Cell Biol **15**(10): 5725-31.
- Robinson, R. C., *et al.* (2001). "Crystal structure of Arp2/3 complex." Science **294**(5547): 1679-84.
- Rodal, A. A., *et al.* (2005). "Conformational changes in the Arp2/3 complex leading to actin nucleation." Nat Struct Mol Biol **12**(1): 26-31.
- Rohatgi, R., *et al.* (2000). "Mechanism of N-WASP activation by CDC42 and phosphatidylinositol 4, 5-bisphosphate." J Cell Biol **150**(6): 1299-310.
- Rohatgi, R., *et al.* (1999). "The interaction between N-WASP and the Arp2/3 complex links Cdc42-dependent signals to actin assembly." Cell **97**(2): 221-31.
- Rohatgi, R., *et al.* (2001). "Nck and phosphatidylinositol 4,5-bisphosphate synergistically activate actin polymerization through the N-WASP-Arp2/3 pathway." J Biol Chem **276**(28): 26448-52.
- Romero, S., *et al.* (2004). "Formin is a processive motor that requires profilin to accelerate actin assembly and associated ATP hydrolysis." Cell **119**(3): 419-29.
- Rozelle, A. L., *et al.* (2000). "Phosphatidylinositol 4,5-bisphosphate induces actin-based movement of raft-enriched vesicles through WASP-Arp2/3." Curr Biol **10**(6): 311-20.
- Rudolph, M. G., *et al.* (1998). "The Cdc42/Rac interactive binding region motif of the Wiskott Aldrich syndrome protein (WASP) is necessary but not sufficient for tight binding to Cdc42 and structure formation." J Biol Chem **273**(29): 18067-76.

- Sasahara, Y., *et al.* (2002). "Mechanism of recruitment of WASP to the immunological synapse and of its activation following TCR ligation." Mol Cell **10**(6): 1269-81.
- Scaplehorn, N., *et al.* (2002). "Grb2 and Nck act cooperatively to promote actin-based motility of vaccinia virus." Curr Biol **12**(9): 740-5.
- Sept, D. and J. A. McCammon (2001). "Thermodynamics and kinetics of actin filament nucleation." Biophys J **81**(2): 667-74.
- She, H. Y., *et al.* (1997). "Wiskott-Aldrich syndrome protein is associated with the adapter protein Grb2 and the epidermal growth factor receptor in living cells." Mol Biol Cell **8**(9): 1709-21.
- Snapper, S. B. and F. S. Rosen (1999). "The Wiskott-Aldrich syndrome protein (WASP): roles in signaling and cytoskeletal organization." Annu Rev Immunol **17**: 905-29.
- Snapper, S. B., *et al.* (1998). "Wiskott-Aldrich syndrome protein-deficient mice reveal a role for WASP in T but not B cell activation." Immunity **9**(1): 81-91.
- Snapper, S. B., *et al.* (2001). "N-WASP deficiency reveals distinct pathways for cell surface projections and microbial actin-based motility." Nat Cell Biol **3**(10): 897-904.
- Suetsugu, S., *et al.* (2002). "Sustained activation of N-WASP through phosphorylation is essential for neurite extension." Dev Cell **3**(5): 645-58.
- Suetsugu, S., *et al.* (1998). "The essential role of profilin in the assembly of actin for microspike formation." Embo J **17**(22): 6516-26.
- Symons, M., *et al.* (1996). "Wiskott-Aldrich syndrome protein, a novel effector for the GTPase CDC42Hs, is implicated in actin polymerization." Cell **84**(5): 723-34.

- Tian, L., *et al.* (2000). "Cdc42-interacting protein 4 mediates binding of the Wiskott-Aldrich syndrome protein to microtubules." J Biol Chem **275**(11): 7854-61.
- Torres, E. and M. K. Rosen (2003). "Contingent phosphorylation/dephosphorylation provides a mechanism of molecular memory in WASP." Mol Cell **11**(5): 1215-27.
- Torres, E. and M. K. Rosen (2005). "Protein tyrosine kinase and GTPase signals cooperate to phosphorylate and activate WASP/N-WASP." J Biol Chem.
- Vetter, I. R. and A. Wittinghofer (2001). "The guanine nucleotide-binding switch in three dimensions." Science **294**(5545): 1299-304.
- Volkman, B. F., *et al.* (2002). "Structure of the N-WASP EVH1 domain-WIP complex: insight into the molecular basis of Wiskott-Aldrich Syndrome." Cell **111**(4): 565-76.
- Volkman, N., *et al.* (2001). "Structure of Arp2/3 complex in its activated state and in actin filament branch junctions." Science **293**(5539): 2456-9.
- Westerberg, L., *et al.* (2005). "Wiskott-Aldrich syndrome protein deficiency leads to reduced B-cell adhesion, migration, and homing, and a delayed humoral immune response." Blood **105**(3): 1144-52.
- Wiskott, A. (1936). "Familiarer, angeborener Morbus Werlhoffi?" Monatsschr. Kinderheil **68**: 212-16.
- Wu, Y., *et al.* (1998). "Tyrosine phosphorylation regulates the SH3-mediated binding of the Wiskott-Aldrich syndrome protein to PSTPIP, a cytoskeletal-associated protein." J Biol Chem **273**(10): 5765-70.
- Xu, Y., *et al.* (2004). "Crystal structures of a Formin Homology-2 domain reveal a tethered dimer architecture." Cell **116**(5): 711-23.

Yarar, D., *et al.* (2002). "Motility determinants in WASP family proteins." Mol Biol Cell **13**(11): 4045-59.

Zigmond, S. H. (2004). "Formin-induced nucleation of actin filaments." Curr Opin Cell Biol **16**(1): 99-105.

Chapter 3 Development of a two-state model describing the allosteric regulation and activation of WASP

(Adapted from Leung and Rosen 2005)

Introduction

Many signaling proteins are regulated by allosteric interactions where autoinhibitory contacts prevent access to an activity bearing region by maintaining the protein in an inactive state. Activation of the protein requires the replacement of intramolecular interactions with intermolecular interactions allowing the protein to shift to the active state. The interconversion of signaling proteins between inactive and active states is established by a conformational equilibrium that is likely to control the function of the protein and subsequent signal transduction as a result of activation. Ligand binding events or covalent modifications can shift the conformational equilibrium or the stability of the protein towards the active conformation. While many of the interactions involved in regulating autoinhibitory systems have been identified and qualitatively characterized, the thermodynamic properties of such systems remain to be examined in detail. The work presented in this chapter will describe the thermodynamic and structural analyses of the allosteric regulation and activation of the autoinhibited signaling protein WASP by the Rho GTPase Cdc42.

Formulation of the WASP two-state model

We have developed a simple two-state model based upon the classical framework of allostery outlined by Wyman, Monod, and Changeaux (Monod *et al.* 1965).

Analagous to the classical allosteric enzymes that can shift between two states (the T and R states), WASP exists in an equilibrium between an inactive, closed conformation ($WASP_i$) and an activated, predominantly open conformation ($WASP_a$) (Figure 3-1). K_{eq} is the equilibrium constant that describes the transition between the two states and is equal to the ratio of the concentrations of inactive to active states of WASP ($K_{eq} = [WASP_i]/[WASP_a]$). An activator, such as Cdc42, can bind to both states of WASP with affinities $K_{D,i}$ for the inactive WASP conformation and $K_{D,a}$ for the active WASP conformation, but has a higher binding affinity for the active WASP conformation. The parameter C represents the allosteric constant, which is equal to the ratio of affinities of Cdc42 for the active and inactive states of WASP ($K_{D,a}/K_{D,i}$). The thermodynamic box, shown in Figure 3-1, thus dictates that the WASP conformational equilibrium in the presence of the activator Cdc42 is equal to the product of the equilibrium constant and the allosteric constant ($K_{eq} * C$), such that the binding of Cdc42 is coupled to the activation of WASP. Thus, binding of Cdc42 shifts the WASP conformational equilibrium by the magnitude of C, where a small value of C effectively biases the WASP equilibrium and provides the driving force for WASP activation and stimulation of Arp2/3 complex mediated actin polymerization. Therefore, the allosteric regulation and activation of WASP by Cdc42 can be described using three parameters: K_{eq} , C, and [A] (concentration of activator) (Buck *et al.* 2004; Leung and Rosen 2005).

In developing this model, we make the following assumptions:

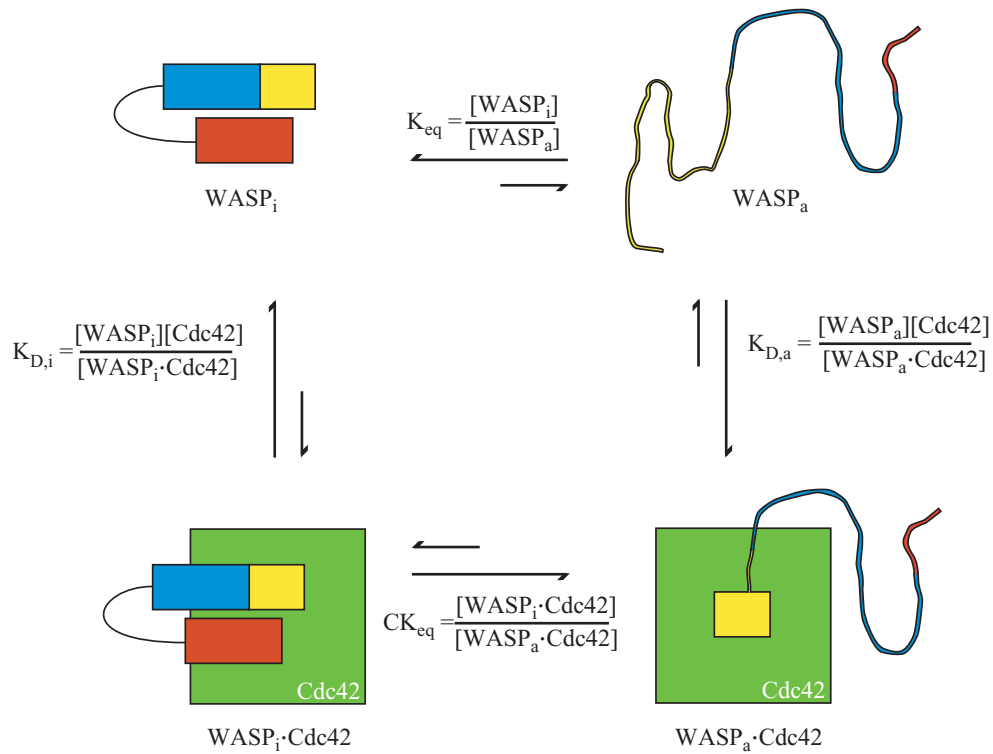


Figure 3-1. Allosteric regulation and activation of WASP by Cdc42. WASP exists in equilibrium between an inactive, folded autoinhibited state (WASP_i) and an active, predominantly unfolded state (WASP_a). Cdc42 biases this equilibrium toward activation because of its higher affinity for the active WASP state. WASP_i and WASP_a represent inactive and active states of WASP, respectively.

First, we presuppose that the allosteric equilibrium of WASP can be quantitatively represented by the folding equilibrium of WASP. Structural and biophysical data have previously shown that the GBD of WASP adopts two structurally distinct conformations (Figure 2-6) (Abdul-Manan *et al.* 1999; Kim *et al.* 2000; Buck *et al.* 2001). In the absence of activated Cdc42, the GBD of WASP exists in a folded conformation packed against VCA. The presence of Cdc42 causes the reorganization of the secondary structural elements comprising the GBD such that the beta hairpin and the alpha 1 helix are abstracted from interactions with the C-terminal VCA domain and repacked against structural elements in Cdc42 (namely the alpha 1 and 5 helices and the beta 2 strand). Consequently, the remaining portion of WASP, primarily the VCA domain, melts and becomes largely unfolded. Thus, by associating the two-state equilibrium of WASP with its folding equilibrium, we can relate the allosteric equilibrium (K_{eq}) to the free energy of unfolding (ΔG) where $\Delta G = -RT \ln K_{eq}$. According to this assumption, the fraction of WASP proteins in the active state is described quantitatively by:

$$f_{\text{active}} = (1 + X) / [K_{eq} (1 + C_{\text{Cdc42}} X) + (1 + X)] \quad (\text{Eqn. 3-1})$$

where

$$X = [A] / K_{D,a} \quad (\text{Eqn. 3-2})$$

and

$$K_{eq} = [WASP_{i,0}] / [WASP_{a,0}] = \exp(\Delta G_{eq} / RT) . \quad (\text{Eqn. 3-3})$$

$[A]$ is the concentration of activator, Cdc42; $[WASP_{i,0}]$ and $[WASP_{a,0}]$ are the concentrations of inactive WASP and active WASP, respectively, in the absence of

Cdc42; $K_{D,a}$ is the binding affinity of WASP_a for Cdc42; ΔG_{eq} is the difference in free energy between the inactive and active states of WASP; and R and T are the ideal gas constant and temperature (See Appendix I for the derivation of equations).

Second, we assume that the parameter C can be determined by measuring the binding affinities of Cdc42 for WASP proteins that mimic the highly stabilized, inhibited conformation of WASP ($K_{D,i}$) and significantly destabilized, fully activated conformation of WASP ($K_{D,a}$) compared to wildtype WASP. Thus,

$$C_{Cdc42} = K_{D,a} / K_{D,i} \quad (\text{Eqn. 3-4})$$

where $K_{D,i}$ is the binding affinity of WASP_i for Cdc42. The measured binding affinities are actually those of equilibrium mixtures of inactive WASP and active WASP that is described by the following equation:

$$\begin{aligned} K_D &= [\text{total free WASP}][\text{free Cdc42}] / [\text{total complex}] \\ &= (K_{D,a} (1 + K_{eq})) / (1 + K_{eq} C_{Cdc42}) \end{aligned} \quad (\text{Eqn. 3-5})$$

Therefore, by measuring the binding affinities of Cdc42 for the two states of WASP, we can calculate a value for the C parameter (Equation 3-4) and determine the efficiency of WASP activation upon Cdc42 binding.

The minimum and maximum amounts of WASP in the activated state can be determined from Equation 3-1 in the extreme conditions where there are no activator or

where there are saturating concentrations of activator. In the absence of any activator, Equation 3-1 further simplifies to:

$$f_{\text{active}(0)} = 1 / (1 + K_{\text{eq}}) \quad (\text{Eqn. 3-6})$$

where $f_{\text{active}(0)}$ represents the minimum fraction of WASP in the active state. In the presence of an infinite amount of activator, the maximum fraction of WASP in the active state is described by:

$$f_{\text{active}(\infty)} = 1 / (1 + C_{\text{Cdc42}} K_{\text{eq}}). \quad (\text{Eqn. 3-7})$$

Previous work in our lab demonstrated that the two-state model can predict the hydrogen exchange behavior and binding affinity of Cdc42-GTP for different WASP proteins with a range of folding stabilities (Buck *et al.* 2004). A series of WASP proteins with different stabilities was generated by varying the linker lengths between the GBD and the C domain. A highly stabilized WASP construct, B.GBD-C ($\Delta G = -6.1 \text{ kcal mol}^{-1}$), which is used to approximate the inactive conformation of WASP, had a measured binding affinity for Cdc42-GMPPNP of 6.7 μM . NMR characterization of this WASP construct in complex with Cdc42-GMPPNP revealed that binding of Cdc42-GMPPNP to ^{15}N -labeled B.GBD-C caused significant broadening of WASP resonances, suggesting that Cdc42 binding results in the destabilization of the autoinhibitory fold of B.GBD-C. This is corroborated by NMR hydrogen exchange data that show an increase in hydrogen exchange of the most protected amides upon binding to Cdc42 leading to the global destabilization of WASP. However, further examination of the NMR data also revealed that many resonances remain in similar positions in both the free and bound

complex, suggesting that the B.GBD-C protein retains properties characteristic of the autoinhibited state and that Cdc42 binding does not induce complete unfolding. These observations are in contrast to a GBD-only construct that binds to Cdc42 with high affinity (23 nM), and which is assumed to approximate the active conformation of WASP. Based upon the measured binding affinities, the behavior of WASP proteins in free and bound complexes with Cdc42 can be predicted according to the two-state model in order to determine how WASP stability, hydrogen exchange behavior, and affinity for Cdc42 are related. Measured hydrogen exchange rates of different WASP constructs with varying linker lengths, in the absence or presence of Cdc42, vary according to the stabilities of the constructs and the two-state equilibrium that in a manner that can be predicted by the model. The binding affinities of additional WASP constructs (in the presence of low concentrations of denaturant) for Cdc42 are also related to differences in stability, conforming to predictions from the two-state model. Therefore, these tests of the two-state model are borne out experimentally and validate the applicability of the two-state allosteric model to provide an energetic description of the WASP system.

In these studies, the various stabilities of the WASP proteins were generated by either increasing the linker length between the GBD and C domains or by introducing small amounts of chemical denaturant to destabilize the autoinhibited fold. More importantly, the WASP constructs used did not contain a functional binding domain for Arp2/3 complex with which we could measure WASP activity or quantitate the coupling of Cdc42 binding with WASP activation. Consequently, we were interested in further developing our WASP two-state model by expanding the range of WASP stabilities and by using more physiologically relevant constructs that would serve to mimic the inhibited

and activated states of WASP. These constructs would then allow us to directly examine the relationship between Cdc42 binding and WASP activation toward Arp2/3 complex mediated actin polymerization.

Generation of mutations in WASP GBD-C

Analysis of two particular GBD mutations suggest that the introduction of different single missense mutations, both physiological and non-physiological, can potentially generate a series of WASP proteins of various stabilities. Mutational analysis of the WAS gene in individuals affected with X-linked neutropenia (XLN) revealed a single amino acid substitution of the conserved leucine 270 residue with proline (L270P) (Devriendt *et al.* 2001). Examination of the WASP structure revealed that L270 is centrally located in the hydrophobic core of WASP; specifically, L270 resides in the alpha 1 helix of the GBD and forms interactions with residues in the alpha 3 helix, the alpha 4 helix, and the VCA domain (Devriendt *et al.* 2001). Mutation to L270P results in the complete destabilization of the hydrophobic core of WASP and consequently, loss of autoinhibition. These effects cause the constitutive activation of WASP, giving rise to a disease phenotype that is contrary to other known WASP mutations that cause the loss of WASP expression and function, giving rise to classical WAS or XLT (Figure 3-2) (Gallego *et al.* 1997; Devriendt *et al.* 2001). Biochemical studies of the WASP L270P demonstrate that the mutant is highly prone to limited proteolysis by subtilisin and has a significantly reduced melting temperature as measured by CD spectroscopy when compared to wildtype (Devriendt *et al.* 2001). L270P also show increased affinity for Cdc42 but is constitutively activated towards Arp2/3 complex in the absence of Cdc42 in reconstituted pyrene-actin polymerization assays. Structural studies reveal that the

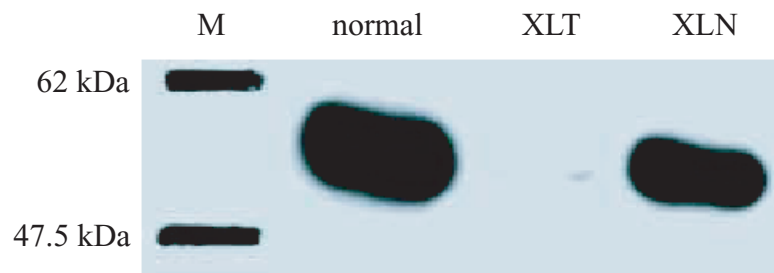


Figure 3-2. Western blot of WASP expression. EBV-transformed B cell lysates from normal, XLT, and XLN male individuals (adapted from Devreindt *et al*, 2001).

L270P mutant is unfolded as the corresponding $^1\text{H}/^{15}\text{N}$ -HSQC spectrum lacks the hallmarks characteristic of folding, including wide amide chemical shift dispersion and narrow, uniform line widths that are observed for wildtype WASP (Devriendt *et al.* 2001). More recently, another novel mutation in WASP isolated from an individual suffering from severe XLN, I294T, has been found to be similarly located in the GBD on the alpha 3 helix (Burns *et al.* 2004; Westerberg *et al.* 2005). I294 is positioned near Y291, which is a critical phosphorylation site (Cory *et al.* 2002; Torres and Rosen 2003), that faces the hydrophobic core of WASP. Substitution of I294 with a threonine residue is also predicted to disrupt the autoinhibitory fold of WASP leading to the constitutive activation of WASP.

To identify residues that when mutated can potentially result in the destabilization of WASP, the structure of the minimally autoinhibited WASP construct, GBD-C, was examined in order to identify residues in the hydrophobic core that make several contacts with other regions in the core. Residues that were focused on were primarily located on the outside of the Cdc42 binding interface and in the second layer (blue) of the GBD-C structure that forms interactions with both the first layer (yellow) of the GBD and the third layer (red) of the C region (Figure 3-3). In addition to the two disease-associated residues L270 and I294, residues L281, I290, and M307 were identified. L281 is located on the alpha 2 helix and is in close proximity to the alpha 3 and 5 helices. I290 is situated on the alpha 3 helix and contacts both alpha 2 and 5 helices. M307 is located on the C-terminal portion of the alpha 4 helix, also contacting both alpha 2 and 5 helices. In order to rapidly screen for mutations that differentially destabilize WASP, various single amino acid substitutions, or in combination, were introduced at positions 270, 281, 290,

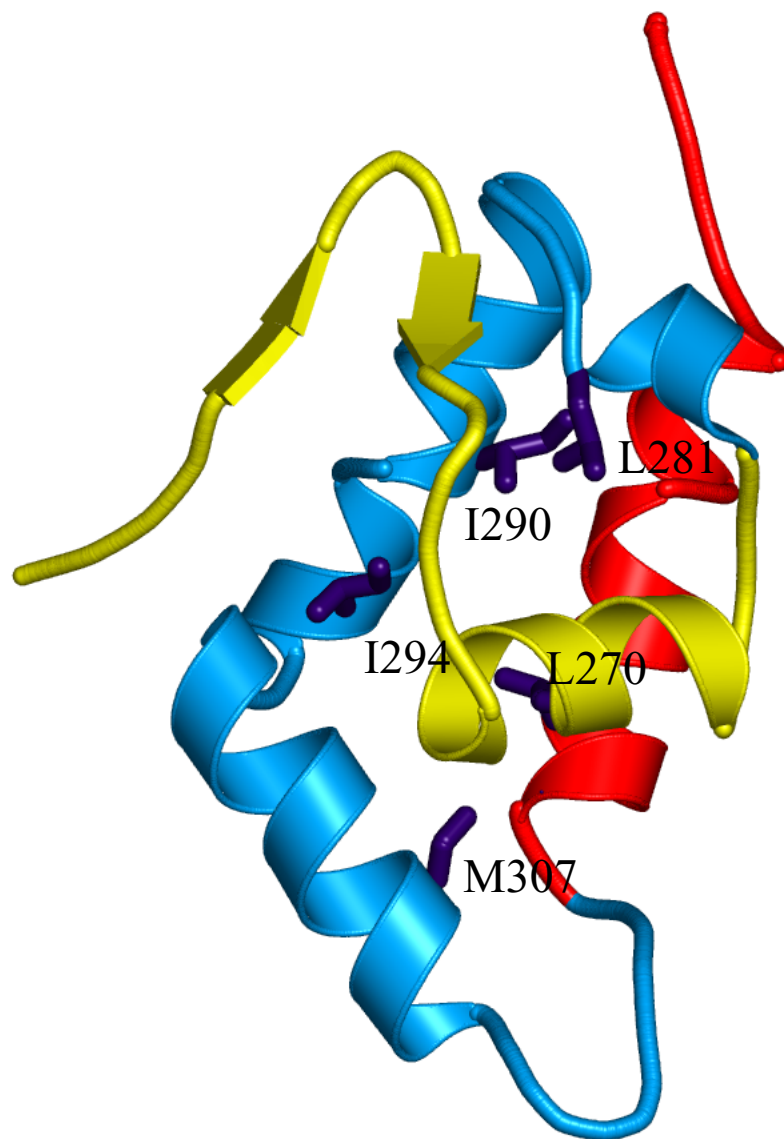


Figure 3-3. WASP residues that were mutated in this study. Side chains of residues mutated in the background of the GBD-C and (B)GBD-VCA constructs are purple and are located in the GBD outside of the Cdc42 binding interface.

294, and 307 in the GBD-C construct (WASP residues 242-310, GGSGGS, 461-492) (Figure 3-4), which has been shown to be well-behaved and whose properties are well-characterized. The biochemical properties of thirteen GBD-C proteins were characterized using CD spectroscopy, limited proteolysis, and 1-D NMR spectroscopy.

Biochemical characterization of WASP GBD-C mutants

CD measurements monitoring the change in molar ellipticity of each mutant ($\lambda = 222$ nm) as a function of temperature from 4 to 90°C displayed a wide range of melting temperatures (Table 3-1). Wildtype GBD-C has a melting temperature of 80°C and is highly stabilized, as expected. In contrast, M307A and M307K have melting temperatures of 76 and 68°C, respectively, reflecting slight destabilization relative to wildtype. An alanine substitution at position 290 or 294 results in more significant destabilization with a melting temperature of 64°C and 56°C, respectively. A glutamine substitution at position 290 caused a dramatic decrease in melting temperature to 38°C, suggesting that the I290Q mutant is highly destabilized and predominantly unfolded. The slight decrease in ellipticity observed for I290Q is probably due to the melting of residual secondary structural elements. The disease mutations, I294T and L270P, in the background of the GBD-C constructs have melting temperatures of 54 and 35°C (Devriendt *et al.* 2001), respectively, indicating that these proteins are severely destabilized and are largely unfolded. The longer full-length WASP protein is presumably less stable and introduction of these two mutations would result in the unfolding of WASP, consistent with the characteristics of the disease phenotype

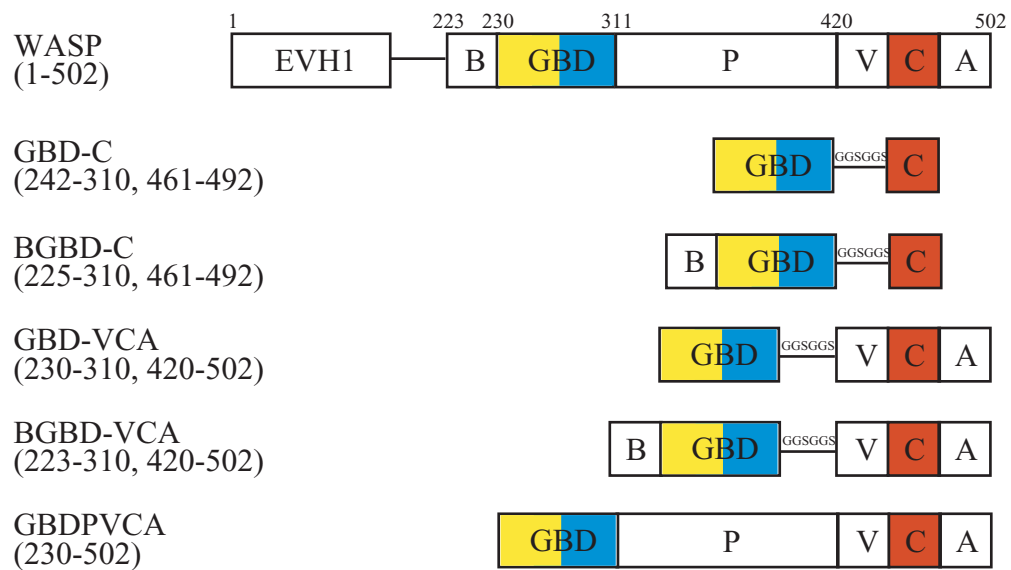


Figure 3-4. Domain organization of WASP constructs. EVH1, Ena/Vasp homology 1; B, basic region; P, proline-rich region; V, verprolin homology region; C, central hydrophobic domain; A, acidic region; GGSGGS, linker. Color coding matches that of the autoinhibited WASP structure in Figure 2-9.

Table 3-1. Temperature denaturation of GBD-C constructs as determined by CD spectroscopy.

GBD-C construct	T _m (°C)
WT	80
I290W	79
L270A	77
M307A	76
M307K	68
L281A	66
I290A	64
L281P	57
I294A	56
I294T	54
I290A/L281A	45
I290A/L270A	43
I290Q	38
L270P*	35

* Kim, *et al.* (2000) *Nature* 404:151-8.

(Devriendt *et al.* 2001). The temperature denaturation curves were all reversible for wildtype and mutant GBD-C constructs.

The wide range of melting temperatures generated by the introduction of mutations in the hydrophobic core of GBD-C suggests that each mutation has a different capacity to destabilize the autoinhibitory core of WASP, resulting in different degrees of unfolding. Limited proteolysis experiments of these constructs using subtilisin, a non-specific serine protease, were performed to qualitatively probe the stability of each mutant. Results from the proteolytic time courses indicate that the wildtype GBD-C protein can be cleaved into two products after a five-minute incubation with subtilisin and further degraded to lower molecular weight products after a two hour incubation (Figure 3-5). The limited proteolysis of the mutant GBD-C constructs also show similar patterns of degradation but with gradually increasing rates of proteolysis that are consistent with the corresponding decrease in melting temperature observed in the series of constructs listed in Table 3-1. For example, the proteolysis of L281 proceeds more rapidly compared to the wildtype GBD-C, producing two clear products after five minutes and is predominantly a single species after a ninety-minute incubation. Mutant proteins with melting temperatures below 50 °C, such as I290A/L281A, I290A/L270A, and I290Q, show accelerated proteolysis that is completed after one hour incubation. These results are consistent with those obtained from temperature denaturation, which indicate that as the melting temperature of the GBD-C construct decreases, the protein becomes destabilized, unfolded, and susceptible to proteolytic degradation.

¹H-NMR spectra acquired for some GBD-C mutants further corroborates these findings (Figure 3-6). The wildtype GBD-C show all the hallmarks that are characteristic

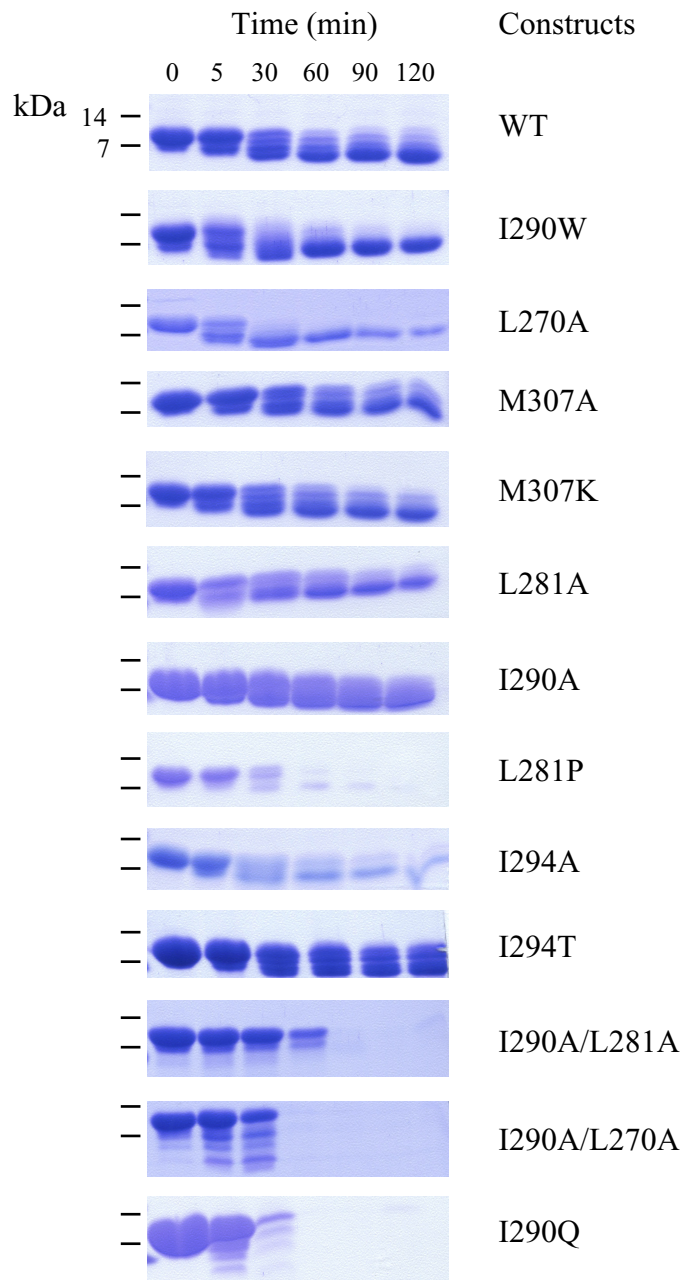


Figure 3-5. Limited proteolysis of GBD-C wildtype and mutant proteins. 200 μ M of proteins were incubated with 40 μ g/ml of subtilisin on a cold metal block on ice and samples were taken at time points indicated above and across (minutes), run on SDS-PAGE, and stained with Coomassie Brilliant Blue.

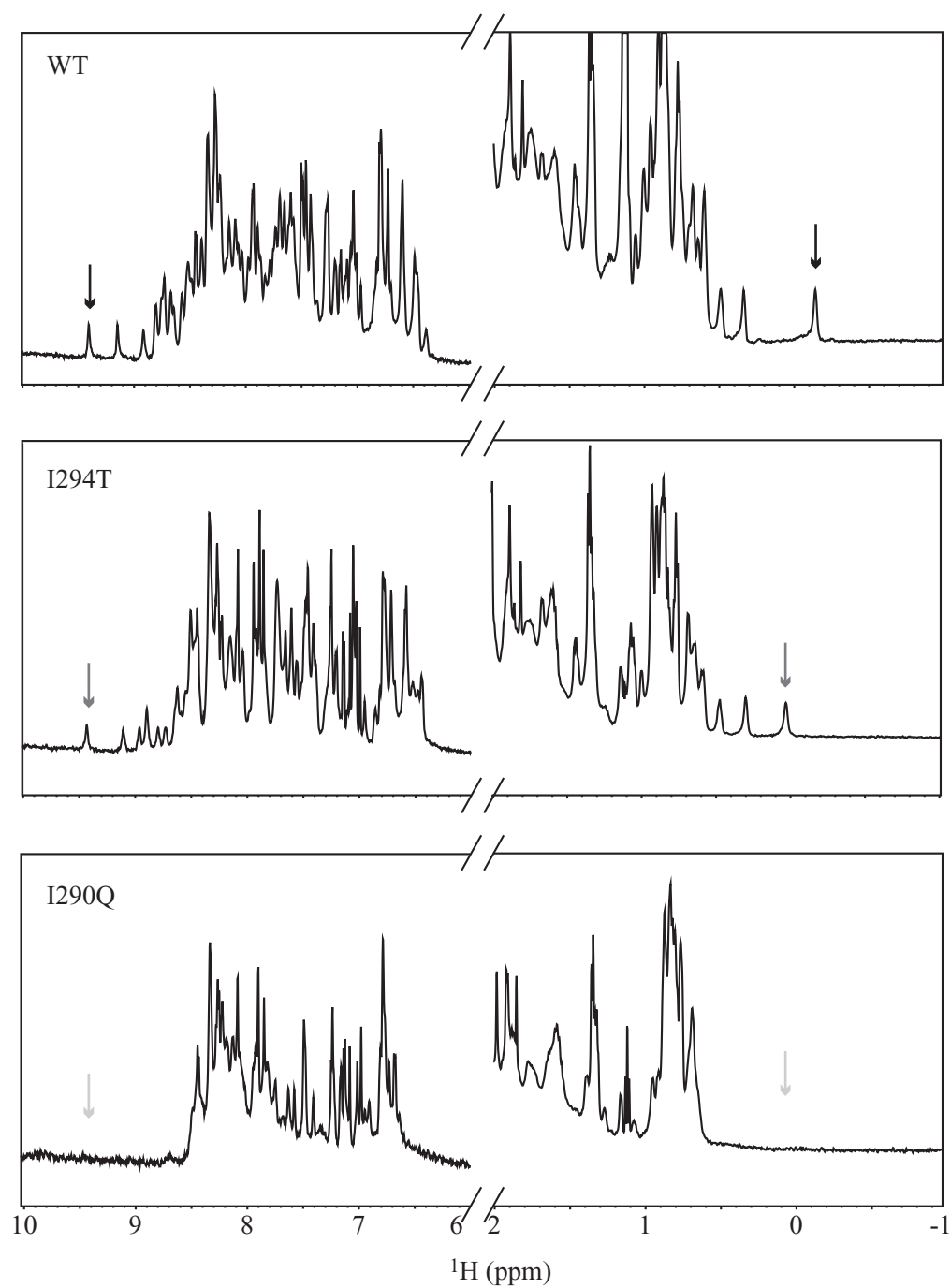


Figure 3-6. ^1H NMR spectra of GBD-C wildtype and mutant proteins. *Left panels.* Amide region. Arrow indicates the W252 aromatic peak that becomes progressively downfield shifted and broadened as GBD-C unfolds. *Right panels.* Methyl region. Arrow indicates the L281 upfield shifted methyl peak that becomes progressively downfield shifted or broadened.

of a folded protein. The methyl region of the wildtype spectrum reveals three distinctive methyl resonances that are upfield shifted. One of these peaks, located at -0.1 ppm, has been identified as a methyl proton from residue L281 (Annette Kim, unpublished result), which is located on the alpha 2 helix. GBD-C also contains a single tryptophan residue, W252, located in the beta hairpin of the GBD. In the folded protein, the chemical shift of the W252 sidechain amide is upfield shifted from >10 ppm to 9.4 ppm. Introduction of an I294T mutation into the hydrophobic core results in a change in the peak position of L281 and broadening of the W252 peaks. This suggests that the I294T mutant disrupts the autoinhibitory interactions in the core of WASP and is destabilized compared to wildtype. Introduction of an I290Q mutation results in the complete unfolding of the protein. The three methyl and tryptophan peaks disappear from their chemical shifts in the wildtype spectrum, either through peak broadening or chemical shift change. These findings altogether are consistent with those obtained from CD and limited proteolysis.

Collectively, these results show that a series of WASP mutant proteins with a range of stabilities can be generated through the introduction of single mutations into the GBD. The biochemical data obtained from CD spectroscopy, limited proteolysis, and NMR spectroscopy indicate that the WASP mutants are differentially stabilized suggesting that these mutations can be applied to a larger, more physiologically relevant WASP construct with potentially similar results.

Parameterization of the two-state model using WASP GBD-VCA mutant proteins

To generate a range of differentially stabilized WASP proteins in a more physiologically relevant construct, a selected set of mutations that were examined in the GBD-C construct were translated into the longer GBD-VCA construct (residues 230-310, GGSGGS, 420-502), which contains functional binding sites for both Cdc42 and Arp2/3 complex. The difference between the GBD-VCA and GBD-C constructs includes the addition of N-terminal GBD residues, an extension of the artificial GGSGGS linker between the GBD and C domains with the insertion of the verprolin homology (V) domain, and the addition of the C-terminal acidic region. The effects of mutations on GBD-VCA stability were initially measured using thermal denaturation and monitored by CD spectroscopy, similar to those previously described for the GBD-C constructs (Figure 3-7). The results obtained demonstrate that the melting temperatures of GBD-VCA mutants follow a similar trend as the GBD-C mutants. For example, wildtype GBD-VCA has the highest melting temperature of 71°C whereas GBD-VCA M307K has a more intermediate melting temperature of 53°C. These are similar to wildtype GBD-C and GBD-C M307K where the melting temperatures are higher (80 and 76°C, respectively; Table 3-1) because the GBD-C is a shorter construct and presumably more stable. The melting temperature of the most destabilized GBD-VCA mutant I290Q can only be approximated to be less than 20°C since I290Q is predominantly unfolded. This is similar to the low melting temperature observed for the GBD-C I290Q mutant (38°C), which was one of the most destabilized proteins measured in that series. Table 3-2 lists a summary of the CD results for all GBD-VCA mutant proteins. Further examination of

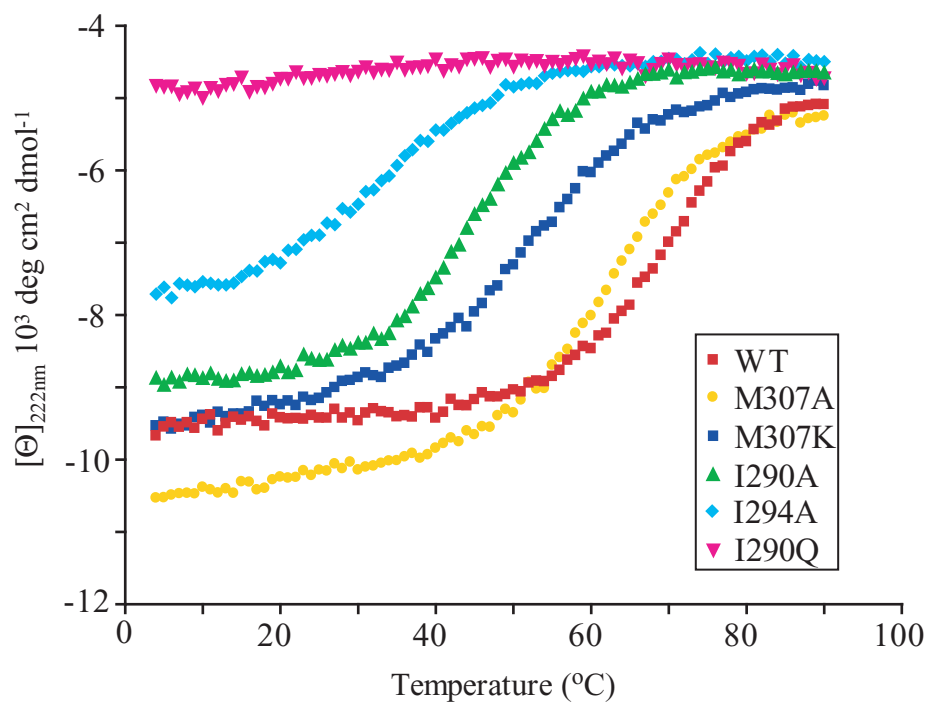


Figure 3-7. Thermal denaturation of GBD-VCA wildtype and mutant proteins using CD spectroscopy. The change in absorbance at 222 nm of 10 μ M samples were monitored from 4 to 90 $^{\circ}$ C.

Table 3-2. Temperature denaturation of GBD-VCA constructs as determined by CD spectroscopy.

GBD-VCA construct	T _m (°C)
WT	71
M307A	64
M307K	53
I290A	46
I294A	35
I290Q	<20

the I290Q construct in the background of the GBD-VCA construct revealed accelerated limited proteolysis with subtilisin when compared to the wildtype GBD-VCA construct (Figure 3-8A). The 1-D NMR spectrum of the GBD-VCA I290Q construct also supports this observation as the indole resonance of W252 and W500 are both downfield shifted to >10 ppm in the proton dimension (Figure 3-8B). Overall, the melting temperatures of GBD-VCA mutants range from 10 to 20 degrees less than the corresponding GBD-C mutants. These results are consistent with findings from other studies that have shown that increasing the length of a loop is related to an entropic penalty for folding and is inversely correlated to a decrease in stability (Ladurner and Fersht 1997; Nagi and Regan 1997). Thus, a series of biologically functional WASP constructs were generated with a range of melting temperatures and subsequently used to parameterize and test the allosteric model of WASP.

The folding stabilities of the GBD-VCA series of mutants were measured by titration of urea and monitored by CD spectroscopy at 222 nm (Figure 3-9). Results from urea denaturation experiments were consistent with those obtained from temperature denaturation experiments as the more stabilized constructs, such as GBD-VCA and M307A, have higher, negative free energies of folding ($\Delta G = -4.2$ and -3.4 kcal mol⁻¹, respectively) compared to constructs of intermediate stabilities, such as M307K and I290A ($\Delta G = -2.4$ and -1.5 kcal mol⁻¹, respectively) (Table 3-3). The ΔG of a highly destabilized construct, I294A, can only be approximated (~ 0.4 kcal mol⁻¹) because a pre-transition (lower) baseline could not be obtained at low concentrations of urea, which affects the accuracy of the ΔG value extracted that is based upon curve fitting. Similarly, a post-transition (upper) baseline from the urea melt of GBD-VCA could not be obtained

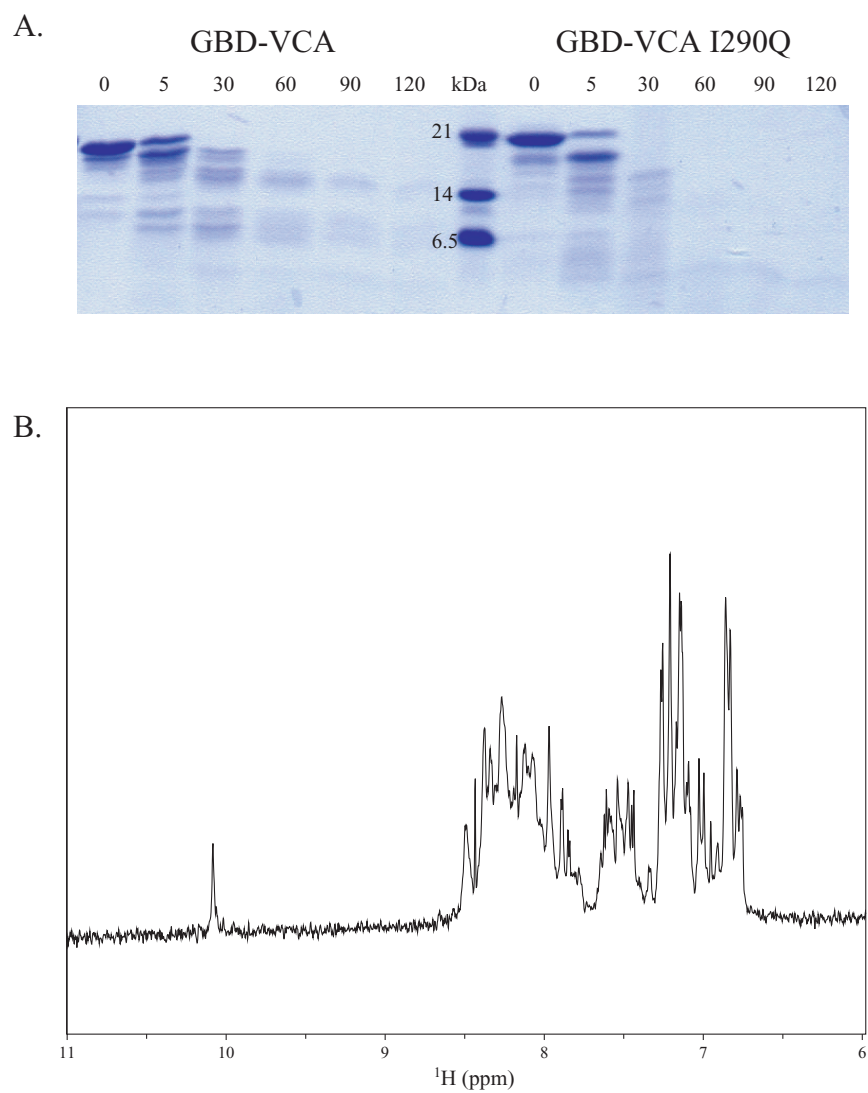


Figure 3-8. Biochemical characterization of GBD-VCA and GBD-VCA I290Q. A. Time course of limited proteolysis of GBD-VCA (left) and GBD-VCA I290Q (right). B. ^1H NMR spectrum of GBD-VCA I290Q. The indole resonances of W252 and W500 are both downfield shifted to >10 ppm, which is indicative of protein unfolding.

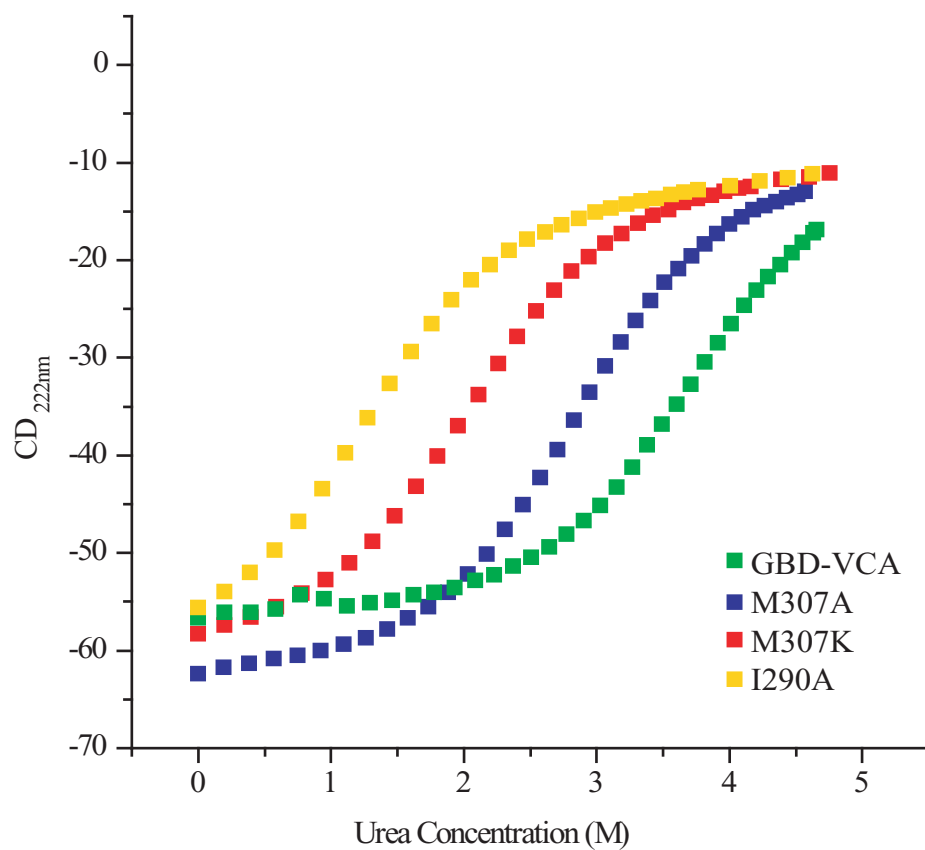


Figure 3-9. Urea denaturation of GBD-VCA proteins. Increasing concentrations of urea was titrated into 10 μ M GBD-VCA samples. CD absorbance was monitored at 222 nm and at 25°C.

Table 3-3. Measured Values of ΔG , K_{eq} , and K_D

WASP	ΔG , kcal·mol ⁻¹	K_{eq}	K_D , μM
BGBD-C	-5.5	11,000	98 \pm 13
GBD-VCA	-4.2	1,200	114 \pm 8
M307A (GBD-VCA)	-3.4	310	71 \pm 5
GBDPVCA	-3.3**	260	n.d.
M307K (GBD-VCA)	-2.4	58	13 \pm 1
I290A (GBD-VCA)	-1.5	13	4.0 \pm 0.1
I294A (GBD-VCA)	-0.4*	2	0.50 \pm 0.05
I290Q (GBD-VCA)	n.d.	n.d.	0.20 \pm 0.04
M307A (BGBD-VCA)	-3.9	730	n.d.
M307K (BGBD-VCA)	-2.8	110	n.d.
I290A (BGBD-VCA)	-2.5	68	n.d.
I294A (BGBD-VCA)	-0.9*	5	n.d.

n.d., not determined

*This measurement is only approximate and may not represent unfolding of tertiary structure.

**Buck *et al*, 2004.

because GBD-VCA is highly stabilized and melts at very high denaturant concentrations, beyond the limits of denaturant solubility. Using guanidine hydrochloride (GdnHCl) as a denaturant instead, similar titrations were performed and the absorbance at 225 nm was monitored (GdnHCl absorbs at 222 nm; (Buck *et al.* 2004)). A melting curve with both pre- and post-transition baselines was obtained. The ΔG values obtained from both GdnHCl ($\Delta G = -4.0 \pm 0.1 \text{ kcal mol}^{-1}$) and urea ($\Delta G = -4.2 \pm 0.1 \text{ kcal mol}^{-1}$) titrations were near identical, suggesting that the ΔG value from the urea titration can be used confidently to compare against the ΔG values of GBD-VCA mutant proteins also calculated from urea titrations. Furthermore, the chemical denaturation of the minimal construct required for WASP autoinhibition, BGBD-C, was also examined. BGBD-C has a measured ΔG value of $-5.5 \text{ kcal mol}^{-1}$ and is significantly more stable than the representative full length WASP construct, GBDPVCA ($\Delta G = -3.3 \text{ kcal mol}^{-1}$; (Buck *et al.* 2004)). Therefore, a series of WASP constructs were generated, including those that are more stabilized (e.g. BGBD-C and GBD-VCA) or less stabilized (e.g. I294A and I290Q) against unfolding compared to wildtype GBD-VCA. Another mutant construct, M307A, was also created, which has a folding stability comparable to GBDPVCA.

Because we make the assumption that the allosteric equilibrium can be quantitatively represented by the folding equilibrium of WASP, values for K_{eq} were calculated based upon Equation 3-3 (Table 3-3). Proteins in this series have equilibrium constants ranging from 11,000 to less than 13. These results suggest that highly stabilized constructs ($K_{eq} > 1000$), such as BGBD-C and GBD-VCA, exist in a predominantly inactive, folded conformation whereas less stabilized constructs ($K_{eq} < 100$), such as I294A and I290Q, exist in a largely active, unfolded conformation.

Based upon this analysis, we make the assumption that the most stable BGBD-C construct ($K_{eq} \approx 11,000$) closely approximates the fully inactive, closed state of WASP and that the least stable GBD-VCA I290Q construct ($K_{eq} < 2$) closely approximates the active, open state of WASP.

In order to establish a value for C_{Cdc42} required for the complete parameterization of the two-state model, the binding affinities of each WASP construct for active Cdc42 were determined. The apparent binding affinities of WASP for Cdc42 were measured by monitoring the fluorescence quenching of Cdc42 loaded with a fluorescent GTP analog, mantGMPPNP, in a titration (Table 3-3). The measured binding affinities for Cdc42-mantGMPPNP displayed an inverse correlation with WASP protein folding stabilities. For example, BGBD-C has a binding affinity of $98 \pm 13 \mu\text{M}$ for activated Cdc42. This binding affinity is ~ 1.4 -fold lower than the full-length WASP equivalent GBD-VCA M307A ($K_D = 71 \pm 5 \mu\text{M}$; Figure 3-10) and ~ 500 -fold lower than the least stable protein GBD-VCA I290Q ($K_D = 0.20 \pm 0.04 \mu\text{M}$). WASP mutants in the middle of the series have more intermediate binding affinities ranging from 13 to $0.5 \mu\text{M}$. Using the measured values of $K_{D,a}$ (GBD-VCA I290Q) and $K_{D,i}$ (BGBD-C) to estimate $C_{Cdc42,GTP}$ according to Equation 3-4 produces:

$$C_{Cdc42,GTP} = K_{D,a} / K_{D,i} = 1.73 \times 10^{-3}$$

Comparison of the binding affinity as a function of protein folding stability reveal a correlation such that the binding affinity for active Cdc42 increases as the protein folding stability decreases. In addition, the greatest changes in K_D occur in the transition region,

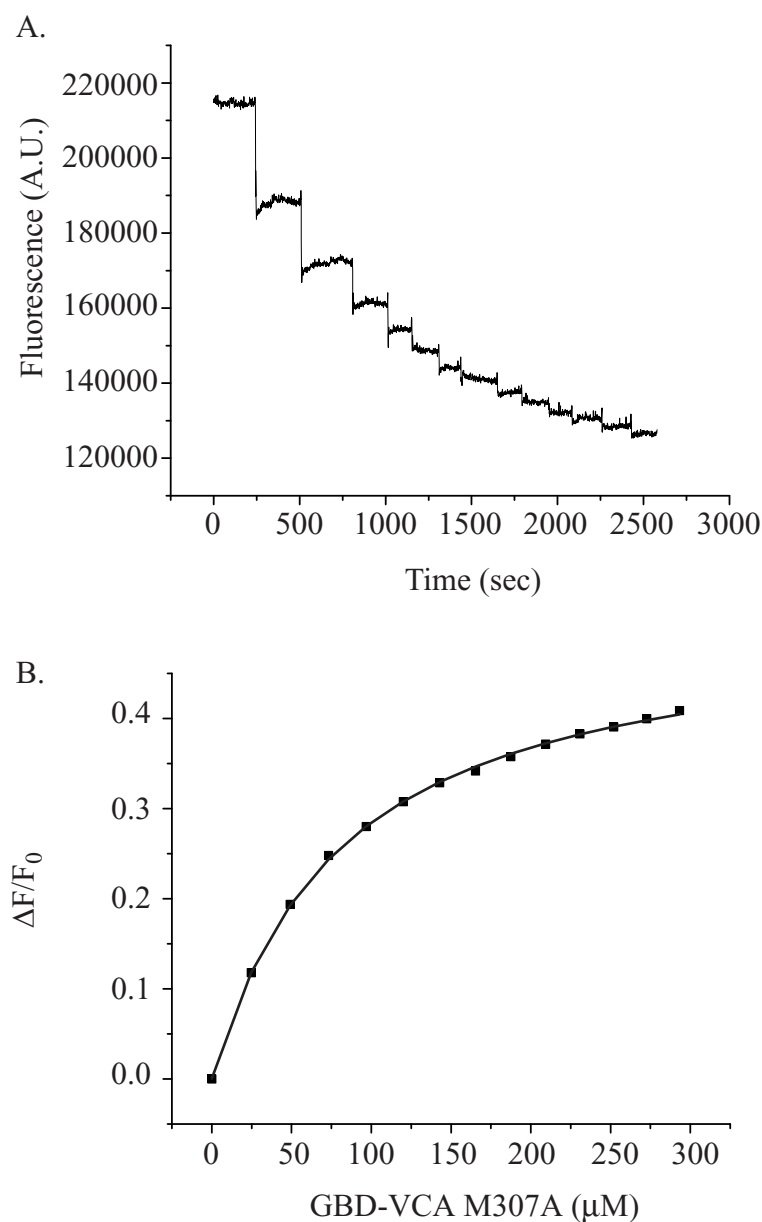


Figure 3-10. Binding affinity of GBD-VCA M307A for Cdc42-mantGMPPNP. A. Binding was followed by monitoring the quenching of mant fluorescence at 432 nm ($\lambda_{\text{ex}}=350$ nm) upon addition of GBD-VCA M307A. B. Equilibrium dissociation constant (K_D) was obtained by fitting the data to a quadratic equation for a single-site binding isotherm.

between folding stabilities of -4 and -1 kcal mol⁻¹ (Figure 3-11). Further analysis show that the experimental data fit well ($r^2 = 0.97$) to the predictions of the two-state model relating K_D to ΔG . The $C_{Cdc42,GTP}$ value obtained from the fit of all the data according to Equation 5 in Figure 3-11, 2.35×10^{-3} , is similar to the value determined from the two endpoints alone, 1.73×10^{-3} . The $C_{Cdc42,GTP}$ values obtained in this study are also similar to one measured previously, 3.4×10^{-3} , under slightly different conditions and using the binding affinity of a GBD only construct to approximate $K_{D,a}$ (Buck *et al.* 2004).

Once the parameters for the model, K_{eq} and $C_{Cdc42,GTP}$, were determined, WASP activity toward Arp2/3 complex was examined as a function of the allosteric equilibrium. WASP activity toward Arp2/3 complex is measured in a reconstituted pyrene-actin polymerization assay using highly purified components. Incorporation of pyrene-labeled actin monomers into a growing filament corresponds to a simultaneous increase in observed fluorescence. Therefore, WASP activity can be monitored by measuring the change in pyrene-actin fluorescence in the presence of Arp2/3 complex. GBD-VCA mutants display a range of activities toward Arp2/3 complex that correlates inversely to the corresponding folding stabilities (Figure 3-12 and 3-13A, black circles). For example, highly destabilized proteins, such as I290Q and I294A ($\Delta G = -0.4$ kcal mol⁻¹), display a rapid increase in fluorescence corresponding to higher levels of activity (fractional activity >0.5, relative to VCA). The activation levels of these mutants are almost comparable to the levels achieved by the constitutively activated VCA peptide. More stable proteins, such as M307A and wildtype GBD-VCA ($\Delta G = -3.4$ and -4.2 kcal mol⁻¹, respectively), are significantly less active (fractional activity <0.1) where the

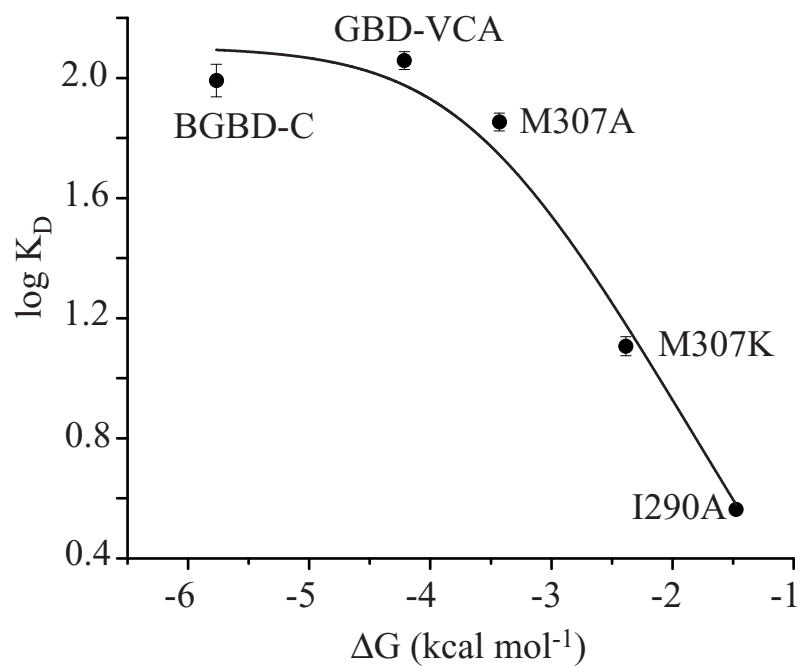


Figure 3-11. Affinity of WASP proteins for Cdc42-GMPPNP as a function of stability. K_D values for Cdc42-GMPPNP are shown as black circles. The black line indicates the log fit of the data to Equation 3-5.

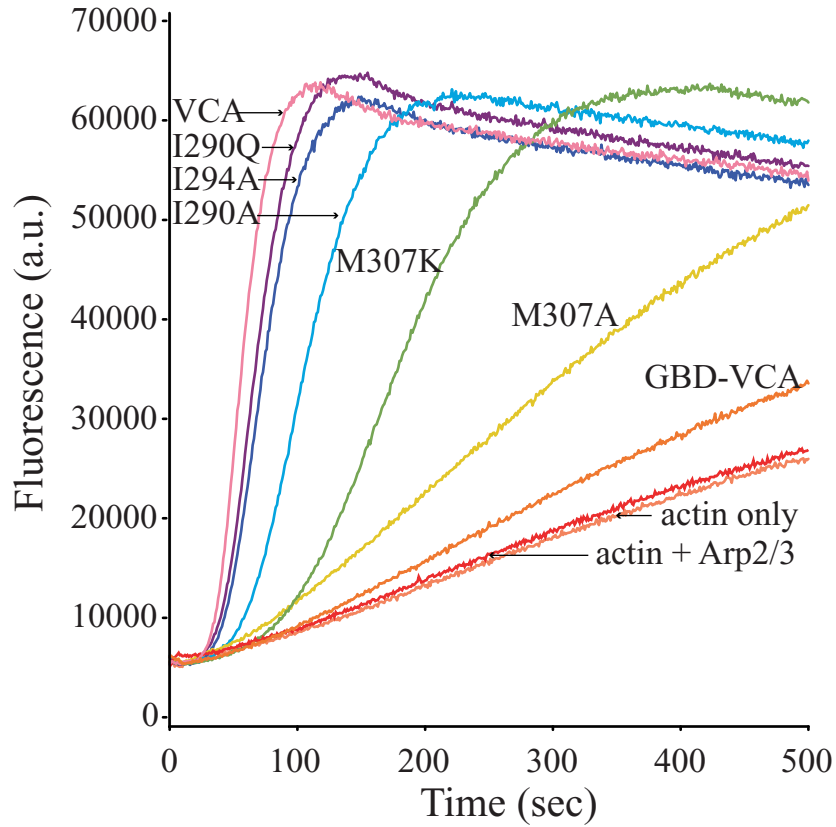
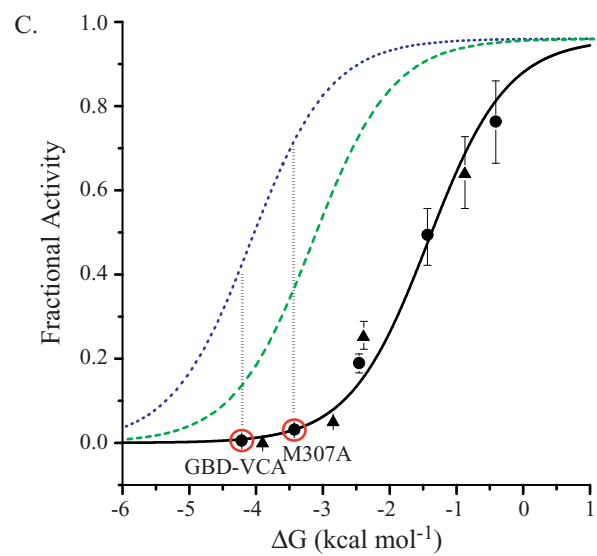
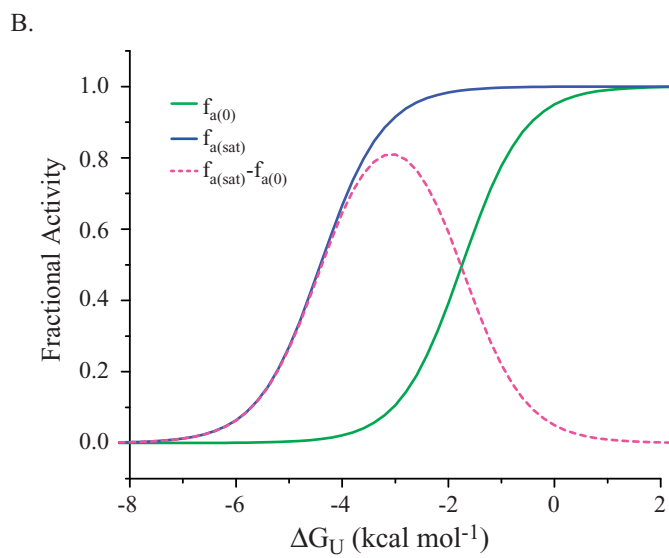
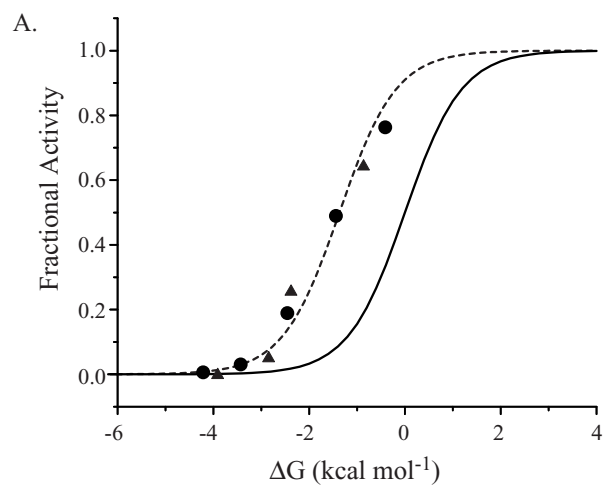


Figure 3-12. Activity of WASP proteins using the Arp2/3 complex mediated pyrene-actin polymerization assay. Pyrene actin polymerization assays of 500 nM WASP proteins in the presence of 10 nM Arp2/3 complex (except "actin only curve") and 4 μ M actin (6% pyrene-labeled).

Figure 3-13. Activity of WASP proteins as a function of stability. Fractional activity (relative to VCA) of WASP proteins in the pyrene-actin polymerization assay. GBD-VCA and BGBD-VCA (wildtype and mutant proteins) are indicated by circles and triangles, respectively. A. Comparison of experimental data (circles) with that predicted by the model (solid line). Fitting of experimental data is offset by ~ 1.7 kcal mol⁻¹ (dashed line). B. Predicted activation of WASP by Cdc42-GTP after adjusting for $C_{\text{Arp2/3}}$ (pink dotted line). WASP alone (green line) and in the presence of Cdc42-GTP (blue line). C. The fractional activities predicted by the model in the absence of activator after adjusting for $C_{\text{Arp2/3}}$ (Equation 8), in the presence of Cdc42-GDP (Equation 9), and in the presence of Cdc42-GTP are shown as black solid, green dashed, and blue dotted lines, respectively. The C values used for Cdc42 GMPPNP and Cdc42-GDP are 1.1×10^{-2} and 5.4×10^{-2} , respectively.



activity levels are more gradual and are just above that of the controls, actin only and actin with Arp2/3 complex.

A sequence of basic amino acids N-terminal to the GBD has been shown to be a factor in autoinhibitory interactions in the neuronal WASP homolog, N-WASP (Prehoda *et al.* 2000; Rohatgi *et al.* 2000). To evaluate the contribution of this stretch of residues towards WASP autoinhibition, a second series of mutant WASP constructs were generated containing the basic region N-terminal to GBD-VCA (BGBD-VCA). This series of mutants was also characterized using chemical denaturation with urea and pyrene-actin polymerization assays to obtain folding stabilities and activities toward Arp2/3 complex. Addition of the basic region increased the overall stabilities of BGBD-VCA proteins by $\sim 0.6 \text{ kcal mol}^{-1}$ ($\Delta\Delta G$) (Table 3-3) when compared to the corresponding mutant constructs in the background of GBD-VCA. For example, BGBD-VCA M307A has a ΔG value of $-3.9 \text{ kcal mol}^{-1}$ that is $0.5 \text{ kcal mol}^{-1}$ greater than that of GBD-VCA M307A. Examination of the activities of the BGBD-VCA constructs toward Arp2/3 complex reveal that an increase in folding stability results in the simultaneous decrease in the activity towards Arp2/3 complex in the pyrene-actin polymerization assays, similar to the GBD-VCA constructs (Figure 3-14). Comparison of the activities of the BGBD-VCA proteins with the GBD-VCA proteins shows that the experimental data similarly fall along the same curve (Figure 3-13A, black triangles). These results suggest that the basic region modulates the interaction between GBD and VCA by increasing the stability of those intramolecular interactions, consistent with the model of WASP autoinhibition through sequestration of the VCA domain. If the basic region were acting through an independent mechanism involving direct interactions with Arp2/3

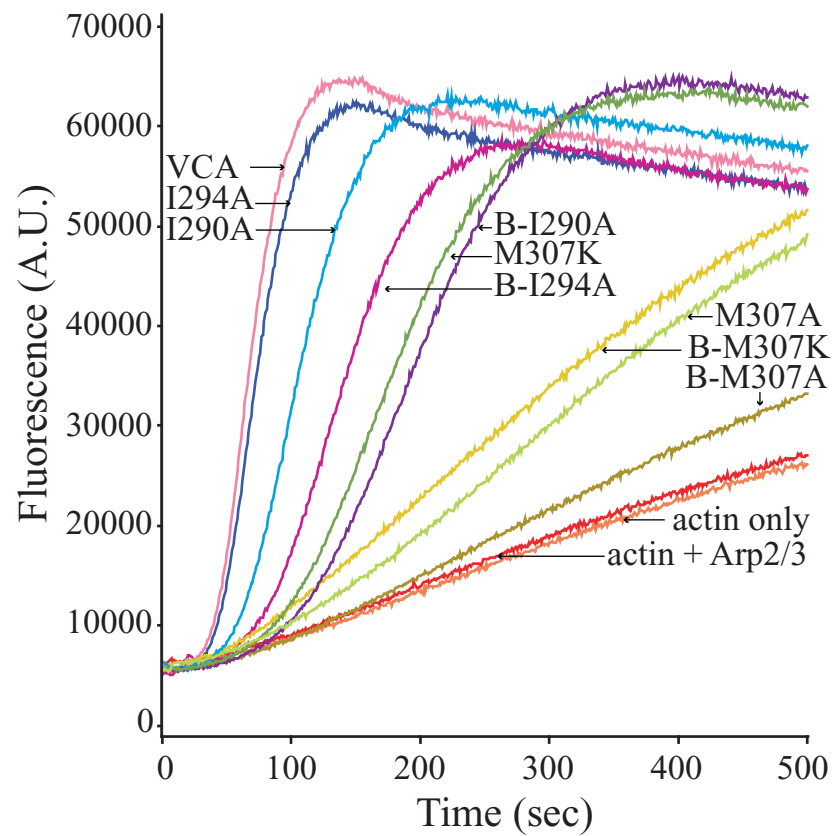


Figure 3-14. Effect of the basic region on the activity of WASP. Pyrene-actin polymerization assays comparing GBD-VCA wildtype and mutant proteins with BGBD-VCA wildtype and mutant proteins (indicated by a B-prefix).

complex (Prehoda *et al.* 2000), then the biochemical properties of BGBD-VCA proteins are expected to fall on a curve separate from the GBD-VCA proteins (see Chapter 4). Consequently, WASP activity toward Arp2/3 complex is limited by the folding stability of autoinhibited domain and reflects a shifting in the equilibrium between inactive and active states.

Having established the parameters, we wanted to evaluate how well the experimental data compares to predictions made from the two-state model. In the fitting of the experimental data to Equation 6, we noticed that the collective data (including GBD-VCA and BGBD-VCA constructs) fall on the same curve but are systematically shifted ($\sim 1.7 \text{ kcal mol}^{-1}$) from the curve that is predicted by the model (Figure 3-13A). Whereas the fluorescence binding assays measures the direct interaction between Cdc42 and WASP, functionality of the polymerization assays requires the addition of both Arp2/3 complex and actin. Arp2/3 complex and actin are both known to bind to WASP and therefore additional equilibria must also be considered. For this reason, we wanted to test if the Arp2/3 complex and actin could bias the WASP allosteric equilibrium such that $C_{\text{Arp2/3}} \neq 1$. The binding affinity of Arp2/3 complex for WASP constructs were measured using a rhodamine anisotropy fluorescence assay (Figure 3-15). Binding of Arp2/3 complex to WASP constructs was performed in the presence of $4 \mu\text{M}$ actin-latrunculin to approximate the conditions of the polymerization assay and was monitored by the increase of rhodamine fluorescence anisotropy upon addition of Arp2/3 complex. The measured binding affinities of GBD-VCA I290Q and BGBD-VCA for Arp2/3 complex were 25 nM and 474 nM , respectively. The measured value of GBD-VCA I290Q for Arp2/3 complex is similar to that obtained in a titration of VCA activity toward Arp2/3

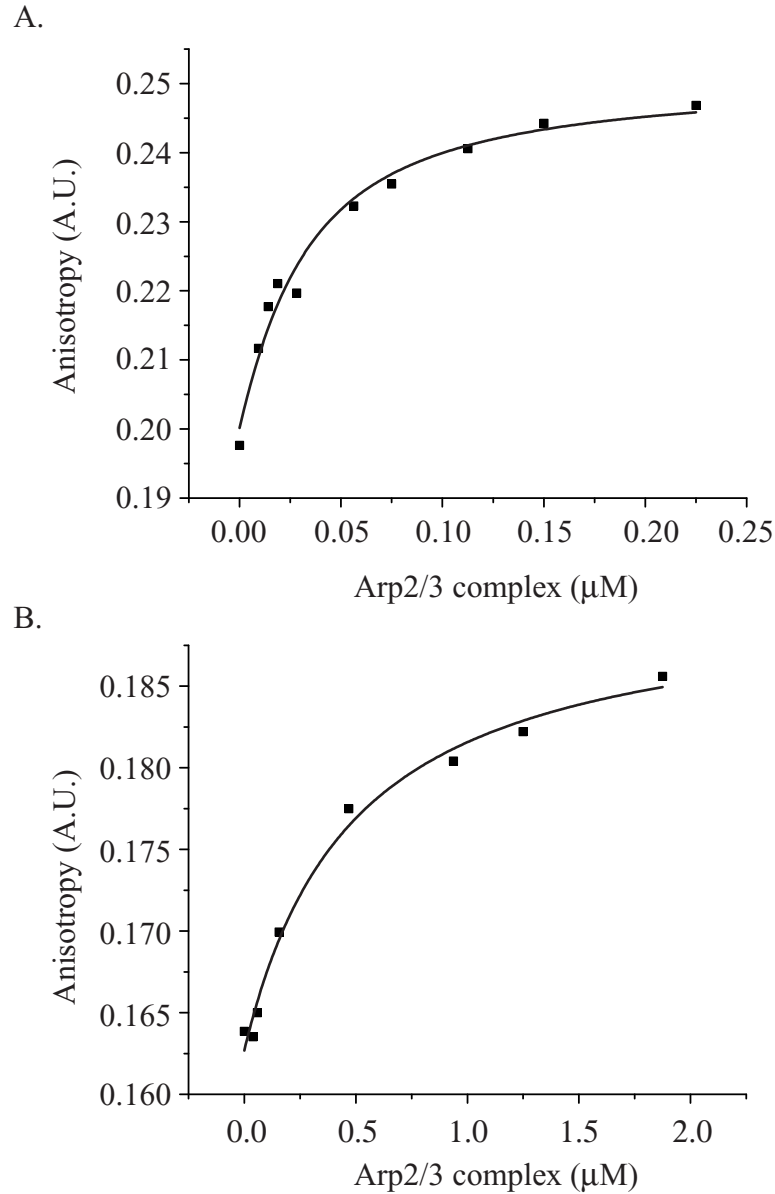
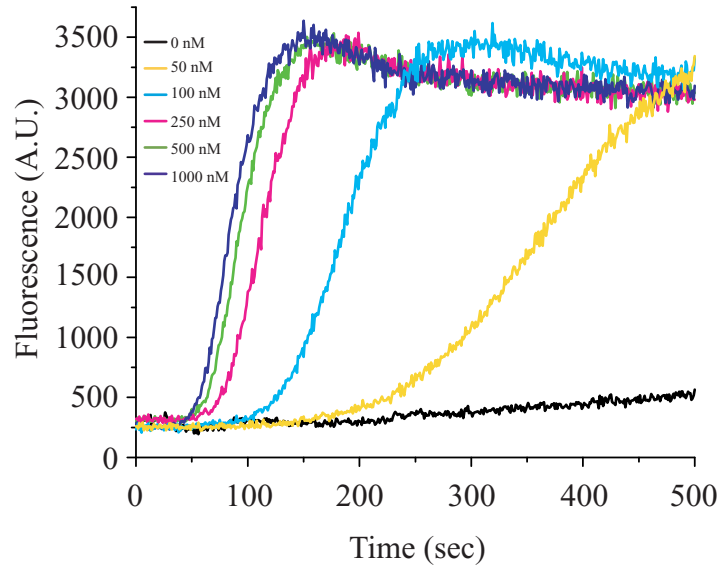


Figure 3-15. Binding affinities of BGBD-VCA and BGBD-VCA I290Q for the Arp2/3 complex. Binding affinities were measured using a rhodamine fluorescence anisotropy assay. WASP constructs contained a C-terminal cysteine residue and labeled with tetramethylrhodamine 5'-maleimide. Rhodamine fluorescence was monitored at 574 nm ($\lambda_{\text{ex}}=552$ nm). Experiments were performed with 15 nM WASP construct, 4 μM of latrunculin-actin, and increasing concentrations of the Arp2/3 complex. A. BGBD-VCA I290Q. B. BGBD-VCA.

A.



B.

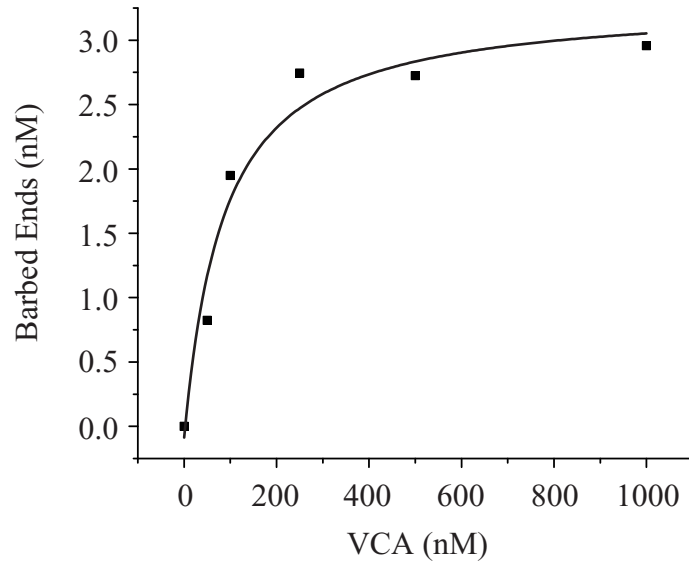


Figure 3-16. Pyrene-actin polymerization curves of VCA titration. A. VCA activated Arp2/3 mediated actin polymerization at different concentrations. B. Binding curve from VCA titration data.

complex ($K_{d(\text{Arp2/3}),a} = 85 \text{ nM}$) (Figure 3-16). These results indicate that Arp2/3 complex and actin combined shift the WASP allosteric equilibrium by a value of:

$$C_{\text{Arp2/3}} = K_{d(\text{Arp2/3}),a} / K_{d(\text{Arp2/3}),i} = 0.053$$

according to Equation 3-4. In the conditions of the polymerization assay, the concentration of Arp2/3 complex is very small relative to WASP, such that the fraction of active WASP can be described by (See Appendix for the complete derivation of equations):

$$f_{\text{Arp2/3},a} = 1 / (((K_{d(\text{Arp2/3}),a} (1 + K_{\text{eq}})) / [\text{WASP}_{\text{total}}] + C_{\text{Arp2/3}} * K_{\text{eq}} + 1) \quad (\text{Eqn.3-8})$$

The data in the polymerization assay fit well ($r^2 = 0.97$) to the above equation describing the fraction of activated Arp2/3 complex and actin bound to active WASP (Figure 3-13B). The $K_{D(\text{Arp2/3}),a}$ (21 nM) obtained from the fitting of the data is similar to that measured in a titration of VCA activity toward Arp2/3 complex (85 nM). Therefore, these results collectively demonstrate that the two-state model reasonably describes WASP affinity for Cdc42, activation by Cdc42, and activity toward Arp2/3 complex as functions of the allosteric equilibrium of WASP.

Development of a conformation specific antibody for the activated state of WASP

The following work described in this section was done in collaboration with Janis Burkhardt, Christine Labno, and Daoqi You (Labno *et al.* 2003).

The spatial and temporal regulation of WASP activity is important for the fidelity and precise activation of signaling components controlling the actin cytoskeleton, including those at the immunological synapse (Cannon *et al.* 2001; Cannon and Burkhardt 2002; Badour *et al.* 2003; Badour *et al.* 2004; Cannon and Burkhardt 2004). Therefore, determining where WASP is localized and when WASP is activated are critical towards understanding and establishing causality to signaling events. A common method used to detect WASP *in vivo* is labeling with polyclonal antibodies that are commercially available. However, polyclonal antibodies are non-discriminatory against different WASP conformations as described in this study and therefore reflect the total population of WASP. Thus, it is difficult to examine the function of WASP in mediating these processes. However, the biochemical properties of WASP presented in the previous section are such that we can take advantage of the fact that WASP transitions between the two-states, from an inactive state to an active state. Toward this purpose, we have developed a monoclonal antibody that behaves as a specific sensor for the active conformation of WASP and therefore can directly monitor changes in the conformational equilibrium and activation state of WASP.

Development of the WASP 26E6 monoclonal antibody

Mouse monoclonal antibodies for the inactive or active state of WASP were developed by immunizing mice with WASP peptides. Peptides encompassing different regions of WASP were selected with the objective of producing monoclonal antibodies that recognize epitopes that are only accessible when WASP is in the active state (Figure 3-17). Peptides for the active state of WASP, active (S277-Q310), include residues from the GBD C-terminal to the CRIB motif and outside of the binding interface of Cdc42. Monoclonal antibodies raised against the active peptide should consequently recognize and bind only to active WASP, when the epitope is exposed through interactions with activators like Cdc42 or by mutation in the hydrophobic core of WASP.

Antibodies from hybridomas generated and obtained from the Memorial Sloan Kettering Cancer Center Monoclonal Antibody Core Facility (New York, NY) were screened for conformation specific binding to WASP using enzyme-linked immunosorbent assay (ELISA) and subjected to multiple rounds of subcloning in order to isolate monoclonal antibodies with high specificities to a single active WASP conformation. To screen the generated antibodies using ELISA, GST-tagged peptides of the GBD, GBD-C, or GBD-C L270P WASP proteins were purified and used to bind to α -GST coated plates. Supernatants from hybridomas were applied to the coated plates prior to labeling with a second antibody conjugated to horseradish peroxidase and exposure to enzyme substrate. Results from these screens produced a single monoclonal antibody, 26E6, which preferentially recognizes the open, active conformation of WASP (Figure 3-18). To test the specificity of 26E6, different conditions were generated that bias the WASP two-state equilibrium and cause WASP to occupy either the inactive or active state. Application of 26E6 shows that this antibody binds specifically to the GST-GBD

A.



B.

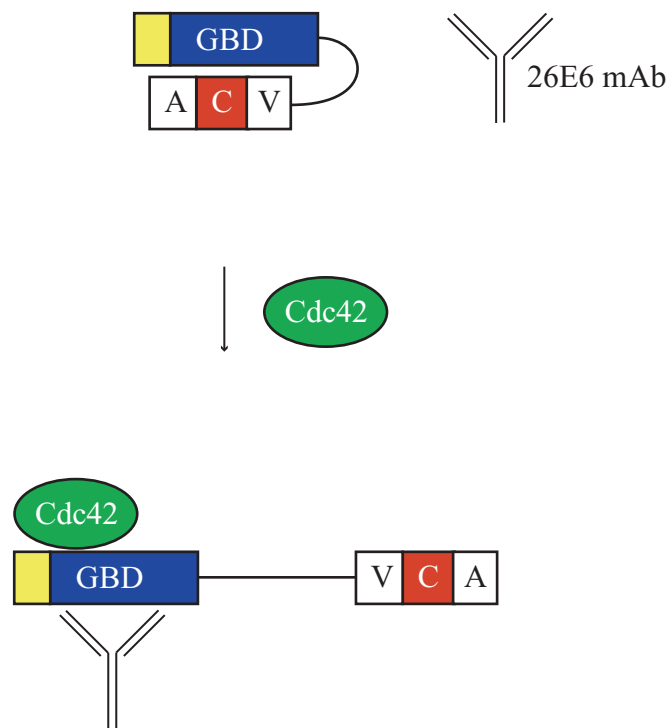


Figure 3-17. Development of a monoclonal antibody that preferentially binds to active WASP. A. Mice were injected with the active peptide which contains sequences from the GBD outside of the CRIB motif. B. 26E6 mAb only binds to WASP in the active state.

A.

	GST-active	GST-GBD-C L270P	GST-GBD	GST-GBD-VC	GST-GBD-C	GST only	blank
26E6	0.886	0.815	0.762	0.050	0.044	0.051	0.038
30A5	1.657	0.840	1.966	0.107	0.051	0.062	0.049
blank	0.062	0.071	0.051	0.060	0.059	0.051	0.045
terminal sera active	2.428	0.804	2.196	0.135	0.124	0.137	0.049
terminal sera inhibited	1.005	> 2.300	1.919	1.783	1.882	0.138	0.048
terminal sera mixed	2.207	2.004	2.022	1.038	1.155	0.122	0.049
blank	0.058	0.068	0.070	0.053	0.065	0.072	0.059
polyclonal antibody	0.098	0.205	0.981	0.831	0.057	0.057	0.054

B.

GST-GBD + 300 μ M Cdc42	GST-GBD-C + 300 μ M Cdc42	empty	GST-GBD-VC + 10 μ M Cdc42	GST-GBD-VC + 50 μ M Cdc42	GST-GBD-VC + 150 μ M Cdc42	GST-GBD-VC + 300 μ M Cdc42	GST-GBD-VC + 500 μ M Cdc42
0.933	0.059	0.069	0.074	0.083	0.095	0.117	0.115

Figure 3-18. ELISA results indicate that 26E6 binds specifically to activated WASP. A. ELISA plate coated with 10 ng of GST or GST-WASP proteins (columns). Wells were incubated with antibodies (rows) 26E6 (1:300 dilution of 10 mg/ul), 30A5 (1:300 dilution of 10 mg/ml), terminal sera from mice injected with active peptide (1:1000 dilution), terminal sera from mice injected with inhibited peptide (1:1000 dilution), mixed terminal sera (1:1000), or a control polyclonal antibody from Upstate. B. ELISA wells coated with GST-WASP proteins and different concentrations of Cdc42-GMPPNP. Wells were incubated with 26E6 antibody (1:300 dilution of 10 mg/ml).

with a high OD₄₅₀ of 0.762. GST-GBD-C L270P, a construct which represents a constitutively active state of the WASP protein, similarly has a high OD₄₅₀ of 0.815. In addition, 26E6 recognized WASP proteins that are activated by incubation with Cdc42-GMPPNP (Figure 3-18b). Addition of increasing concentrations of Cdc42-GMPPNP results in an increase in OD₄₅₀. However, the maximum OD₄₅₀ observed in the presence of 300 μ M Cdc42-GMPPNP (OD₄₅₀ = 0.117) is significantly less than that observed for GST-GBD (OD₄₅₀ = 0.933). These results are consistent with the observation that GST-GBD-VC construct is a significantly stabilized WASP protein and that addition of Cdc42-GMPPNP results only in the partial destabilization of the protein. However, we cannot rule out the possibility that binding of Cdc42-GMPPNP sterically hinders 26E6 binding because the binding interface for 26E6 on WASP or GST-GBD-VC is unknown. In contrast, 26E6 clearly does not bind to either of the autoinhibited WASP proteins, GST-GBD-VC and GST-GBD-C, with OD₄₅₀ < 0.050. These results confirm that 26E6 is a conformation specific monoclonal antibody for the active state of WASP that can discriminate between the two states of WASP.

Regulation of actin polymerization at the immunological synapse by Itk

Formation of the immunological synapse requires signal coordination and integration from components regulating the actin cytoskeletal machinery. Cdc42 and WASP have both been previously identified as components of the immunological synapse where recruitment of WASP to the contact interface between APC and T cell occurs independently of Cdc42 activation (Cannon *et al.* 2001). Localization of autoinhibited WASP to the synapse involves interactions with the proline rich binding

domain of WASP. WASP activation requires Cdc42-GTP, which concentrates at the immunological synapse upon T cell engagement with antigen on the APC surface and activation of Lck and Zap-70. However, T cells isolated from knockout mice deficient in Itk and Rlk display defective signaling and development, suggesting a role for Tec family kinases in the regulation of the immunological synapse. To investigate the role of Itk in actin polymerization at the immunological synapse and to test the specificity of the 26E6 monoclonal antibody, 26E6 was used to probe the state of WASP at the T cell:APC interface during different stages of T cell activation (Labno *et al.* 2003). Labeling with 26E6 revealed an enrichment of activated WASP at the synapse in conjugates formed in the presence of antigen, but which is lacking in conjugates with Itk^{-/-} T cells (Figure 3-19). Activation of Cdc42 by Itk (through Vav) causes the colocalization of Cdc42-GTP and activated WASP at the synapse (Figure 3-20). Therefore, Itk is an essential component of the actin cytoskeleton that is required for the localization of Cdc42 to the immunological synapse and the subsequent activation of WASP by Cdc42-GTP. These results suggest that the development of a conformation specific monoclonal antibody can be used effectively as a direct sensor to probe the activation state of WASP. The approach is a general method that can be adapted and applied to other proteins where activation is regulated by distinct conformational states.

Conclusion

The allosteric regulation of WASP can be described accurately and quantitatively using the two-state mathematical formalism introduced by Monod, Wyman, and Changeux (Monod *et al.* 1965). WASP exists in an allosteric equilibrium between an

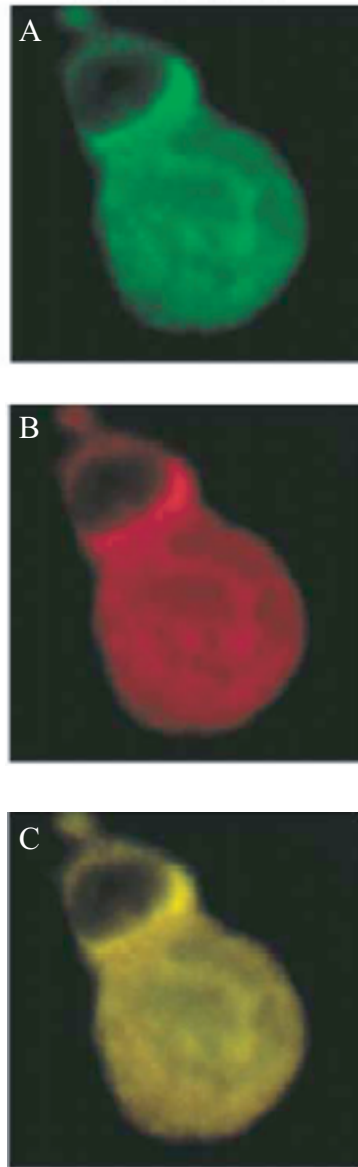


Figure 3-19. Activated Cdc42-GTP and WASP are colocalized at the immunological synapse (adapted from Labno *et al*, 2003). A. Activated Cdc42-GTP as detected by GFP-WASP-GBD. B. Activated WASP labeled with 26E6 mAb. C. Overlay of A. and B.

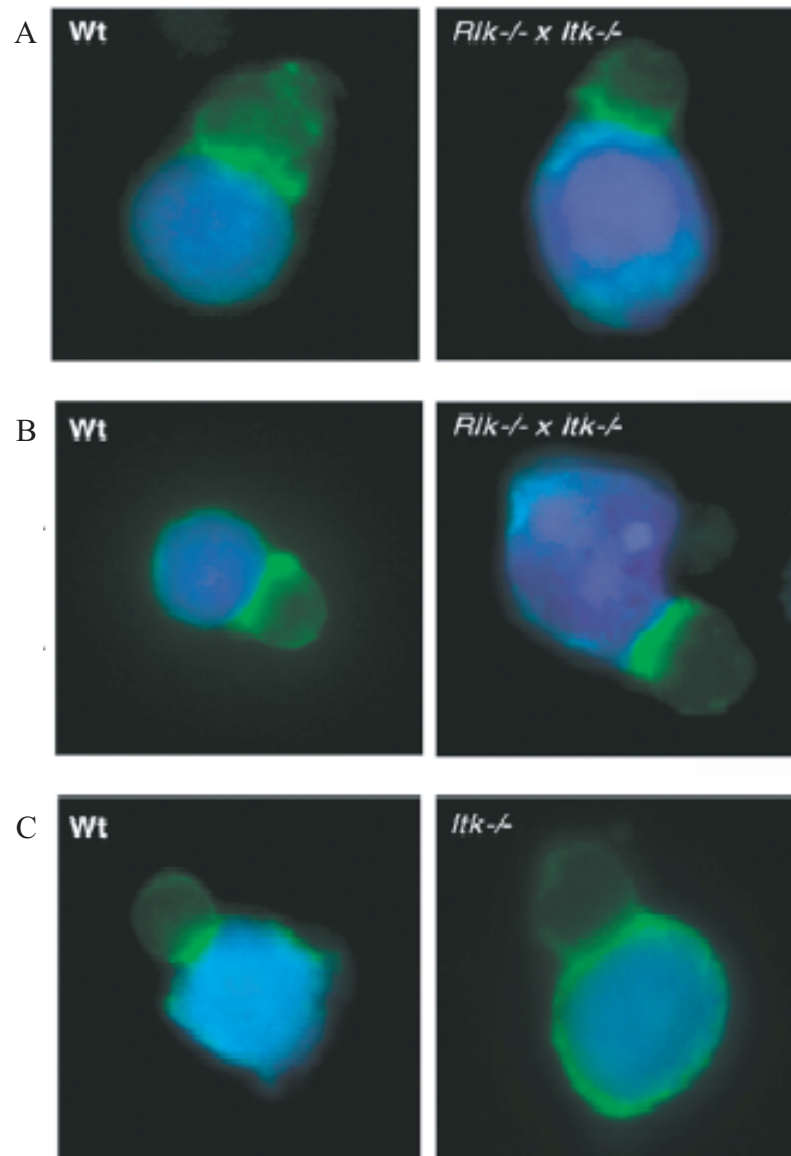


Figure 3-20. WASP is recruited to the immunological synapse independent of Cdc42 (adapted from Labno *et al*, 2003). A. WASP is localized to the immunological synapse in both wildtype and *Rlk*^{-/-} x *Itk*^{-/-} T cells. B. Arp2/3 is also localized to the T cell-APC junction. C. 26E6 mAb labeling shows strong staining of activated WASP only in wildtype cells and not in *Itk*^{-/-} cells.

inactive state and an active state such that the activation of WASP requires a perturbation of this equilibrium, either through covalent modification or ligand binding, to favor the active state. Predictions of the two-state model that WASP affinity for Cdc42, activation by Cdc42, and WASP activity toward Arp2/3 complex are functions of the allosteric equilibrium are all borne out experimentally. Thus, WASP activity is directly coupled to the binding of Cdc42 to WASP. In addition, we have been able to generate a conformation specific reagent with which we can distinguish the active conformation of WASP. The conformational specificity of the 26E6 monoclonal antibody is substantiated both *in vitro* and *in vivo*. While we have examined the regulatory and activation mechanism between WASP and Cdc42 in the actin cytoskeletal signal transduction pathway, there are many additional WASP binding partners or other autoinhibitory systems where the thermodynamic and allosteric properties remain to be characterized. The methods described here can be applied similarly to examine these other systems in order to quantitatively describe how those intra- and inter-molecular interactions work cooperatively to modulate WASP activity.

Materials and Methods (adapted from Leung et al. 2006)

Purification of Human WASP Proteins

We have purified a series of human WASP proteins of varying lengths that contain different domains and mutations. Full-length WASP contains an N-terminal Ena/VASP homology domain 1 (EVH1), a basic region (BR), a GTPase binding domain (GBD), a polyproline linker region (P), and a verprolin homology/central domain/acidic region (collectively termed VCA) at the C-terminus. The most stable of these WASP proteins, GBD-C, is comprised of a truncated GBD tethered to the C region by a GGSGGS linker and forms the minimum unit required for autoinhibition (Kim *et al.* 2000). Expression and purification of GBD-C is relatively straightforward. However, we have found that addition of other domains that are primarily unstructured, including the polyproline linker region, the verprolin homology domain (V), and acidic region (A), results in more difficult bacterial expression and/or purification, as these domains are generally prone to proteolysis and degradation.

Buffers:

A: 20 mM Tris pH 8, 50 mM NaCl, 1 mM EDTA, 2 mM DTT, 1 mM benzamidine, 1

µg/ml pepstatin, 1 µg/ml leupeptin, 1 µg/ml antipain

B: 20 mM Tris pH 8, 50 mM NaCl, 1 mM EDTA, and 2 mM DTT

C: 20 mM Tris pH 8, 1 M NaCl, 1 mM EDTA, and 2 mM DTT

D: 25 mM sodium phosphate pH 7, 150 mM NaCl, 1 mM EDTA, and 2 mM DTT

E: 20 mM Tris pH 8, 1 mM EDTA, 2 mM DTT, 1 mM benzamidine, 1 µg/ml

pepstatin, 1 µg/ml leupeptin, and 1 µg/ml antipain

F: 50 mM Hepes pH 7.25, 500 mM KCl, 5 mM β -mercaptoethanol, 0.01% IGEPAL, 5% glycerol, 1 mM benzamidine, 1 μ g/ml pepstatin, 1 μ g/ml leupeptin, 1 μ g/ml antipain

G: 500 mM imidazole, 500 mM KCl, 25 mM sodium phosphate pH 7, and 5 mM β -mercaptoethanol

H: 25 mM sodium phosphate pH 6, 50 mM NaCl, 1mM EDTA, 2 mM DTT

I: 25 mM sodium phosphate pH 6, 1M NaCl, 1 mM EDTA, 2 mM DTT

J: 20 mM Tris pH 8.5, 1 mM EDTA, 2 mM DTT

K: 20 mM Tris pH 8.5, 1 M NaCl, 1 mM EDTA, 2 mM DTT

L: 20 mM Tris pH 8.5, 2 mM $MgCl_2$, 2 mM DTT, 1 mM benzamidine, 1 μ g/ml pepstatin, 1 μ g/ml leupeptin, 1 μ g/ml antipain

M: 20 mM Tris pH 8.5, 1 M NaCl, 2 mM $MgCl_2$, 2 mM DTT

N: 25 mM sodium phosphate, 150 mM NaCl, 2 mM $MgCl_2$, 2 mM DTT

O: 20 mM Tris pH 8 at 25°C, 0.2 M $(NH_4)_2SO_4$, 0.5 mM NaN_3 , 10 mM DTT

P: 40 mM Tris pH 8, 10 mM EGTA, 1 mM $MgCl_2$, 6.25 μ g/ml pepstatin A, 10 μ M calpain inhibitor II, 10 μ M cathepsin B inhibitor I, 20 μ g/ml leupeptin

Q: 20 mM Tris pH 8, 75 mM NaCl, 1 mM EGTA, 1 mM $MgCl_2$, 1 mM DTT, 2 μ g/ml pepstatin A, 1 μ M calpain inhibitor II, 2 μ g/ml leupeptin

R: 2 mM Tris pH 8, 0.5 mM EGTA, 0.5 mM $MgCl_2$, 1 mM DTT

S: 20 mM Tris pH 8, 1 mM EGTA, 1 mM $MgCl_2$, 1 mM DTT

T: 20 mM Tris pH 8, 1 M NaCl, 1 mM EGTA, 1 mM $MgCl_2$, 1 mM DTT

U: 10 mM PIPES pH 6.8, 1 mM EGTA, 1 mM $MgCl_2$, 1 mM DTT

V: 10 mM PIPES pH 6.8, 150 mM NaCl, 1 mM EGTA, 1 mM MgCl₂, 1 mM DTT

KMEI: 10 mM imidazole pH 7, 50 mM KCl, 1 mM MgCl₂, 1 mM EGTA

Purification of GBD-C

Buffers: A, B, C, D

Overview: DEAE, Mono Q, SD75

The GBD-C (residues 242-310, GGSGGS linker, residues 461-492) protein is expressed from the Novagen pET11a vector in *E. coli* BL21(DE3) cells. Transformed cells are cultured in shaker flasks at 37°C until OD₆₀₀ = 1.0 and induced with 1 mM IPTG for 3 hours. Cells are harvested, resuspended in 20 ml of cold Buffer A per 1 liter of culture, and stored at -80°C. Cells from one liter growth are lysed by sonication and clarified by centrifugation at 39,000 x g for 30 minutes at 4°C. Supernatant is loaded onto a DEAE column (50 ml; XK 26/40 column) (6 column volumes (CV) Buffer B to 30% Buffer C). Peak fractions as monitored by A₂₈₀ and confirmed by SDS-PAGE are pooled and diluted to ~2 mS/cm with 20 mM Tris pH 8. The protein is then loaded onto a Mono Q 10/100 column (12 CV Buffer B to 30% Buffer C). Peak fractions are loaded onto an SD75 26/60 gel filtration column (Buffer D) as a final purification step. GBD-C is flash frozen in liquid N₂ and stored at -80°C. Yield is ~20 mg per liter of culture.

Purification of VCA

Buffers: E, C, B, D

Overview: DEAE, glutathione sepharose, thrombin cleavage, Mono Q, SD75

The isolated VCA domain (residues 420-502) is difficult to purify because it degrades easily, especially in the acidic region. Furthermore, the high acidic content carries many impurities that are difficult to separate. To aid expression and purification,

we express VCA as a GST-fusion protein from a pGEX-2T vector in *E. coli* BL21(DE3) cells. Cells are cultured at 37°C and induced at OD₆₀₀ 0.6-0.8 with 1 mM IPTG for 3 hours. Cultures are harvested, resuspended in 20 ml cold Buffer E per liter of culture, and stored at -80°C. Cells from one liter culture are lysed by sonication and clarified by centrifugation at 39,000 x g for 30 minutes at 4°C. Lysate supernatant is first passed through a DEAE column (50 ml; in XK 26/40 column; 8 CV Buffer E to 40% Buffer C) before peak fractions are collected and incubated in batch with 4 ml of glutathione sepharose beads for 30 minutes at 4°C. We have found that adding a DEAE step prior to glutathione sepharose beads eliminates impurities that are not visible by SDS-PAGE, but which cause VCA degradation over time and inconsistencies in quantitation and assays. The bead suspension is then transferred to a 20 ml disposable column (Bio-Rad), and beads are washed with 3 CV of Buffer B. Beads are resuspended in 20 ml Buffer B and 200 units of thrombin protease (Amersham/GE Healthcare) are added. The suspension is nutated at 25°C for at least 2 hours until cleavage is complete as monitored by SDS-PAGE. VCA is eluted from the beads, diluted to conductivity ~2 mS/cm with Buffer E, and loaded onto Mono Q 10/100 (0.5 CV Buffer E to 20% Buffer C, 20 CV to 50% Buffer C). We have observed that most degradation of VCA occurs at its C-terminus. However, the Mono Q column efficiently separates full-length VCA from its degradation products, which elute earlier since they have lost acidic C-terminal residues. This is a critical step because it eliminates any degradation products that are lacking a full acidic region, including residue Trp500, which are inactive. Finally, the peak fractions from Mono Q are loaded onto an SD75 26/60 gel filtration column (Buffer D). VCA is flash frozen and stored at -80°C. Yields are ~1 mg of VCA per liter of culture.

Purification of GBD-VCA

Buffers: F, G, H, I, J, K, D

Overview: Ni-NTA, desalting, Mono S, Tev cleavage, Mono S, Mono Q, SD75

Expression and purification of GBD-VCA (residues 230-310, GGSGGS linker, 420-502) has the same issue of C-terminal degradation as VCA. To facilitate expression and purification, GBD-VCA was expressed as a (His)₆-fusion from a Novagen pET-15b vector in *E. coli* BL21(DE3) which was modified to include a Tev protease site C-terminal to the (His)₆ tag. We have found that Tev protease produces fewer non-specific cleavage products compared to thrombin and that a (His)₆-tag is easier to separate from GBD-VCA than a GST-tag post cleavage. Transformed cells are cultured at 37°C and induced at OD₆₀₀ 0.6-0.8 with 1 mM IPTG for 3 hours. Cells are harvested, resuspended in 20 ml of cold Buffer F per liter of cells, and stored at -80 °C. Cells from a six liter culture are lysed by sonication and clarified by centrifugation at 39,000 x g for 30 minutes at 4 °C. Lysate supernatant is applied to Ni-NTA beads (8 ml bead volume/6 L cell culture) and incubated in batch at 4°C for 30 minutes. Ni-NTA bead suspension is transferred to a disposable column and washed with additional lysis buffer before elution with 7.5 ml of Buffer G. Eluate is desalted into Buffer H using a High Prep 26/10 Desalting column before loading onto a Mono S 10/10 column (15 CV Buffer H to 35% Buffer I) (Figure 3-21). Peak fractions are pooled, and concentrated to ~2 ml using Amicon Ultra 15 (10,000 MWCO). The pH is adjusted to 8 with Na₂HPO₄ before addition of His-Tev protease (Invitrogen) for incubation at 25°C until the cleavage reaction is complete as monitored by SDS-PAGE. The reaction mixture is loaded onto a Mono S column as above to eliminate any uncleaved protein, His-tag, and His-Tev protease. Flow-through fractions containing GBD-VCA are collected and applied onto a

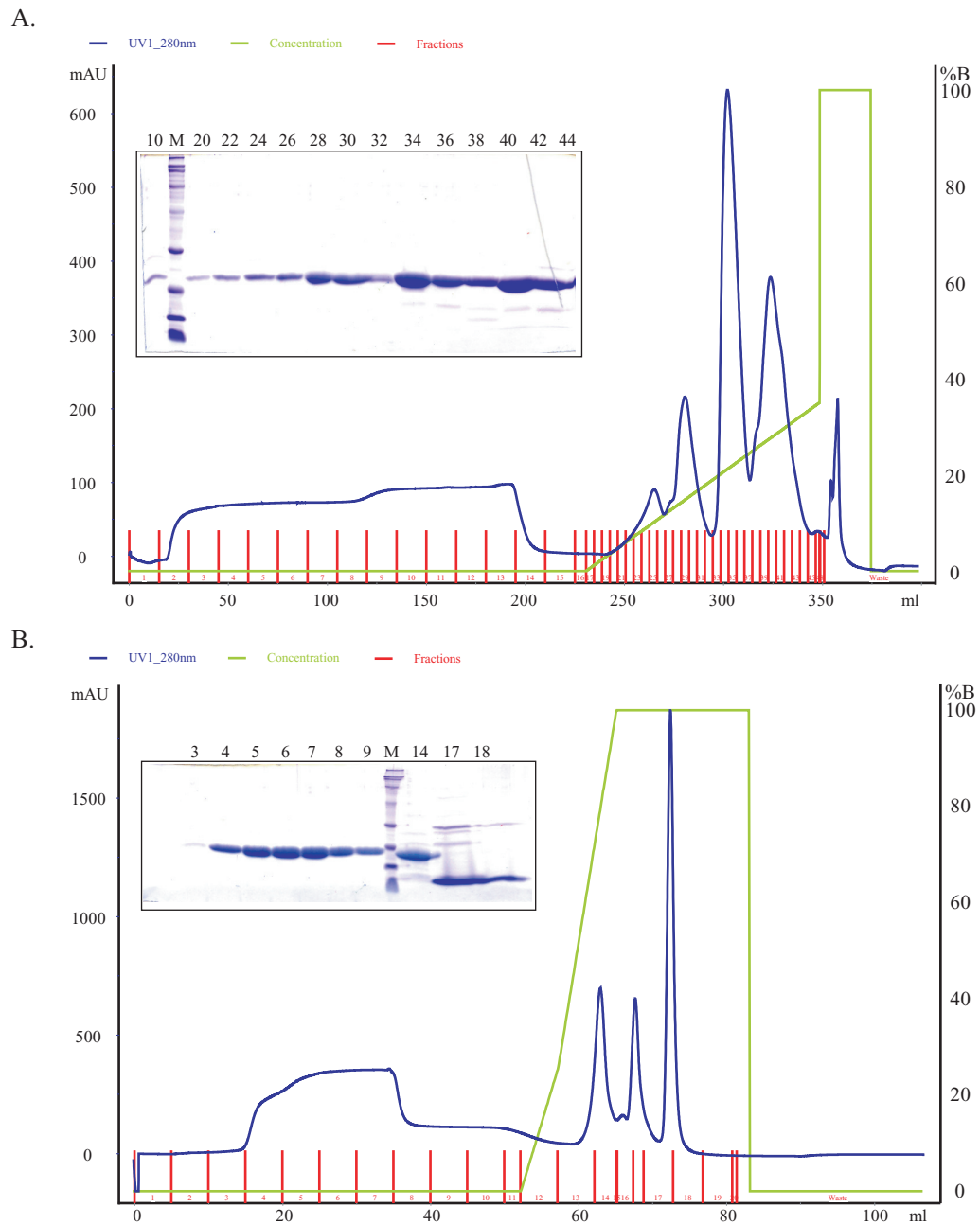


Figure 3-21. Purification of His₆-tagged GBD-VCA. A. Chromatogram of MonoS 10/10 monitoring A₂₈₀. Commassie stained SDS-PAGE of numbered fractions are shown. Fractions 22 to 42 were collected. B. Chromatogram of MonoS 10/10 monitoring A₂₈₀ after Tev cleavage. Fractions 4 to 8 were collected.

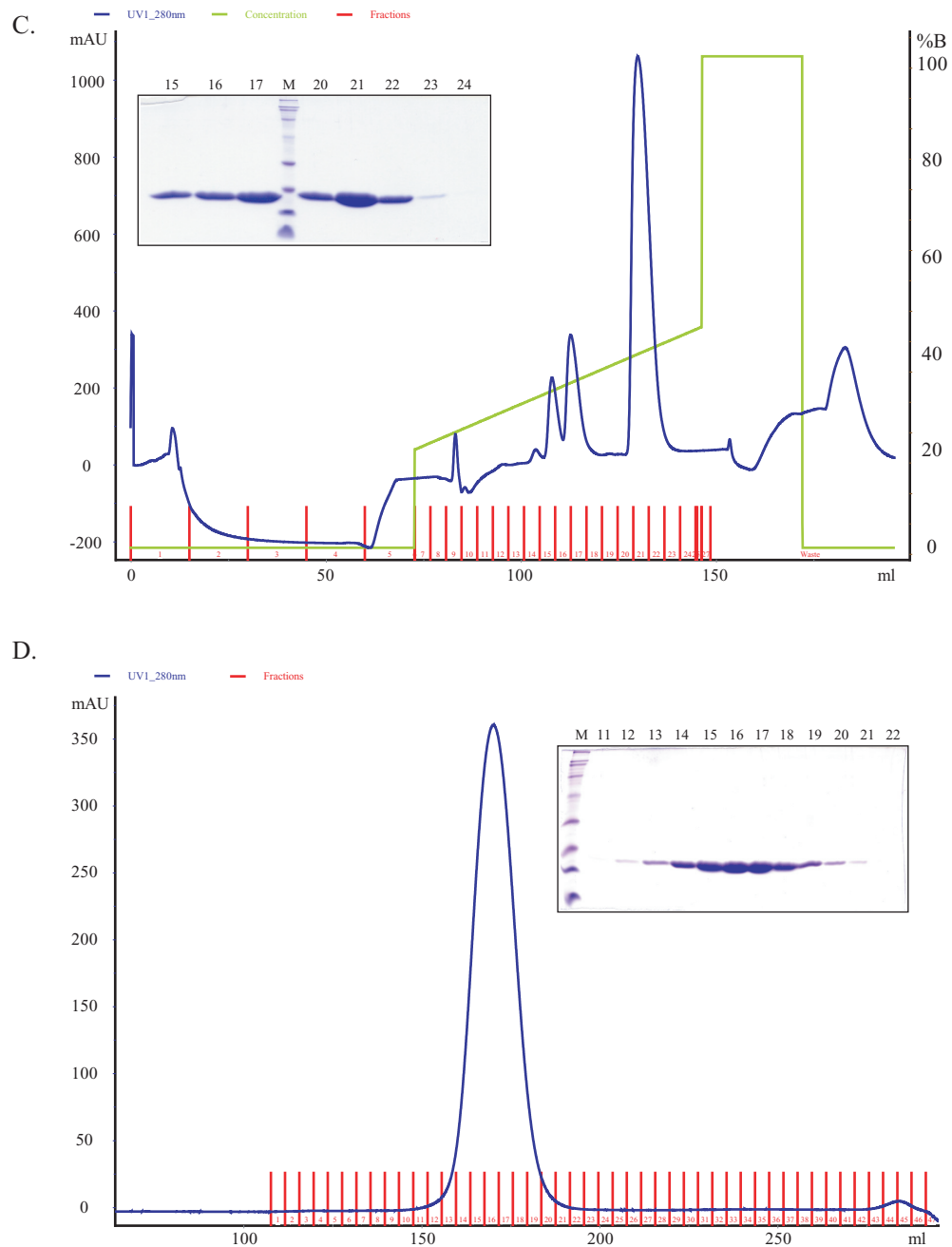


Figure 3-21. Purification of His₆-tagged GBD-VCA. C. Chromatogram of MonoQ 10/100 monitoring A₂₈₀ and separation of C-terminal cleaved protein. Commassie stained SDS-PAGE of numbered fractions are shown. Fractions 20 to 23 were collected. D. Chromatogram of Sephadex (SD) 75 monitoring A₂₈₀. Fractions 13 to 20 were collected.

Mono Q 10/100 where full length GBD-VCA is resolved from proteins that are degraded at the C-terminus (15 CV Buffer J from 20% to 60% Buffer K). Peak fractions are pooled and loaded onto a SD75 26/60 gel filtration column as a final purification and buffer exchange step (Buffer D). GBD-VCA is flash frozen and stored at -80°C. Yields are ~7 mg of GBD-VCA per 6 L of culture.

Purification of Cdc42 (GDP, -GMPPNP, -Mant-GMPPNP)

Buffers: L, M, N (purification); O, N (nucleotide loading)

Overview: DEAE, MonoQ, SD75

Studies in our lab, including fluorescence binding and actin polymerization assays, were conducted using a Cdc42 construct lacking the C-terminal CAAX box (residues 1-179). Cdc42 is expressed from the Novagen pET11a vector in BL21(DE3) cells. Transformed cells are cultured at 37°C until OD₆₀₀ 0.6 and induced with 1 mM IPTG for 12 hours at 25°C. Cells are harvested and resuspended in 20 ml of cold buffer L per liter of culture. The affinity of Cdc42 for nucleotide is sufficiently high that buffers throughout purification do not need to contain excess nucleotide. But buffers do require Mg²⁺ and the absence of EDTA. Cells are lysed by sonication and clarified by centrifugation at 39,000 x g for 30 minutes at 4°C. Lysate supernatant is loaded onto a DEAE column (50 ml in XK 26/40 column; 12 CV Buffer L to 10% Buffer M) (Figure 3-22). Fractions containing Cdc42 are collected, diluted to ~2 mS/cm with 20 mM Tris pH 8.5, and loaded onto Mono Q 10/100 (25 CV Buffer L to 10% Buffer M). It is important that the sample is diluted to very low conductivity, as Cdc42 binds weakly to both DEAE and MonoQ and elutes early in the gradient. Peak fractions are pooled and loaded onto a

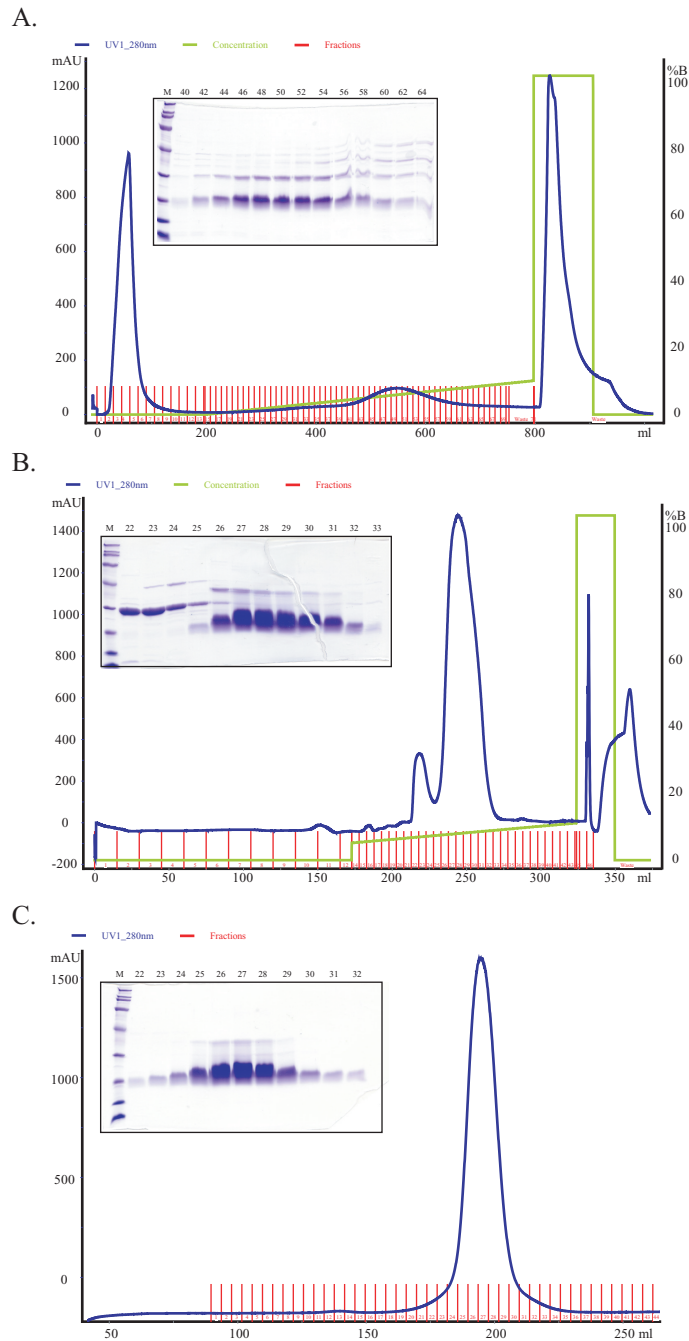


Figure 3-22. Purification of Cdc42. A. Chromatogram of DEAE monitoring A_{280} . Comassie stained SDS-PAGE of numbered fractions are shown. Fractions 44 to 56 were collected. B. Chromatogram of MonoQ 10/100 monitoring A_{280} . Fractions 27 to 31 were collected C. Chromatogram of Sephadex 75. Fractions 25 to 30 were collected.

SD75 26/60 gel filtration column (Buffer N). Cdc42 is flash frozen and stored at -80°C. Yields are ~30 mg per liter of culture.

Cdc42 is loaded with GMPPNP (Pai *et al.* 1990) or mant-GMPPNP (Manor 2000) after desalting into Buffer O using a 5 ml HiTrap Desalting column (Figure 3-23). Fractions containing Cdc42 are pooled together (total 2 ml volume, ~300 μ M) into a 2 ml eppendorf tube. An 8-fold molar excess of nucleotide and 200 units of agarose-bound alkaline phosphatase (Sigma) are added to the eppendorf tube. The loading reaction is nutated at 25° for 4 hours. It is essential that the air space above the solution in the eppendorf tube be minimal, as nutating bubbles will cause aggregation and precipitation of Cdc42 during loading. DTT can be added again halfway into the incubation period to reduce oxidation. The reaction sample is syringe filtered (0.22 μ m) to eliminate the alkaline phosphatase prior to loading onto a SD75 26/60 gel filtration column (Buffer N).

Mant (N-methylanthroniloyl) nucleotides are synthesized from N-methylisotoic anhydride (Molecular Probes) and GMPPNP (Sigma). One liter of 1 M triethylamine buffer (TEAB) is prepared before use by combining 140 ml of triethylamine with 860 ml of ddH₂O in a 2 l flask. CO₂ gas is sparged in TEAB for ~2 hours in a fume hood with vigorous stirring until the pH is ~7-7.5. 25 mg of GMPPNP (Σ_{253} =13,700 M⁻¹) is then dissolved in ddH₂O to 25 mM. The pH of the solution is changed to ~9.5 with 6 M NaOH using pH paper. A 3-fold molar excess of N-methylisotoic anhydride is then added. During the reaction, 5 ml aliquots of 6 M NaOH are added to adjust for changes in pH over time and a sample of the reaction is monitored by chromatography every 30 minutes until the reaction is complete (Figure 3-24). Because the reaction produces both mono- and di-mant products, mono-mant must be purified by chromatography. The

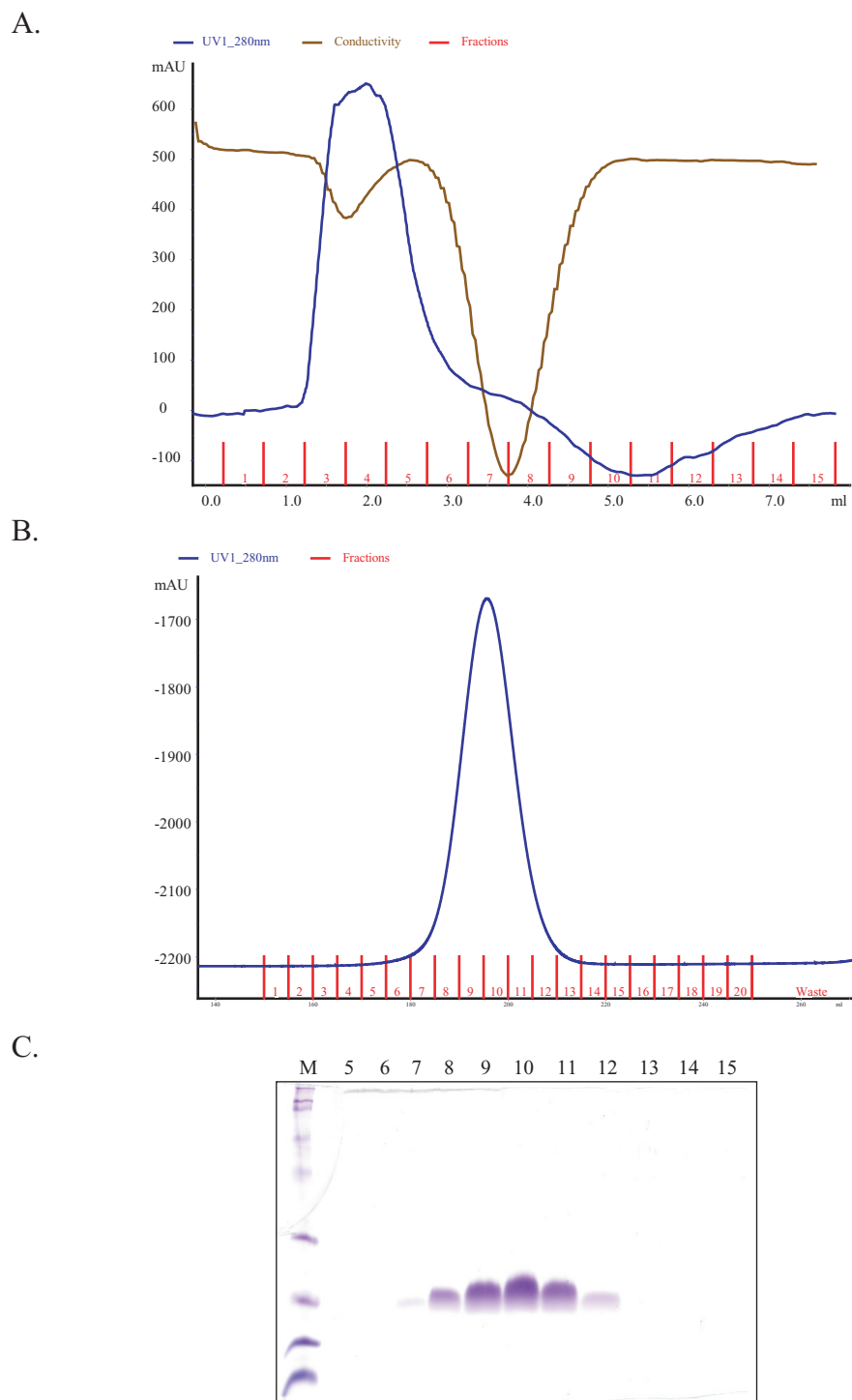


Figure 3-23. Purification of Cdc42 loaded with GMPPNP. A. Chromatogram of HiTrap Desalting (5 ml) column monitoring A_{280} before loading with GMPPNP. B. Chromatogram of Sephadex (SD) 75 after loading Cdc42 with GMPPNP. C. Commassie stained SDS-PAGE of numbered fractions. Fractions 7 to 12 were collected.

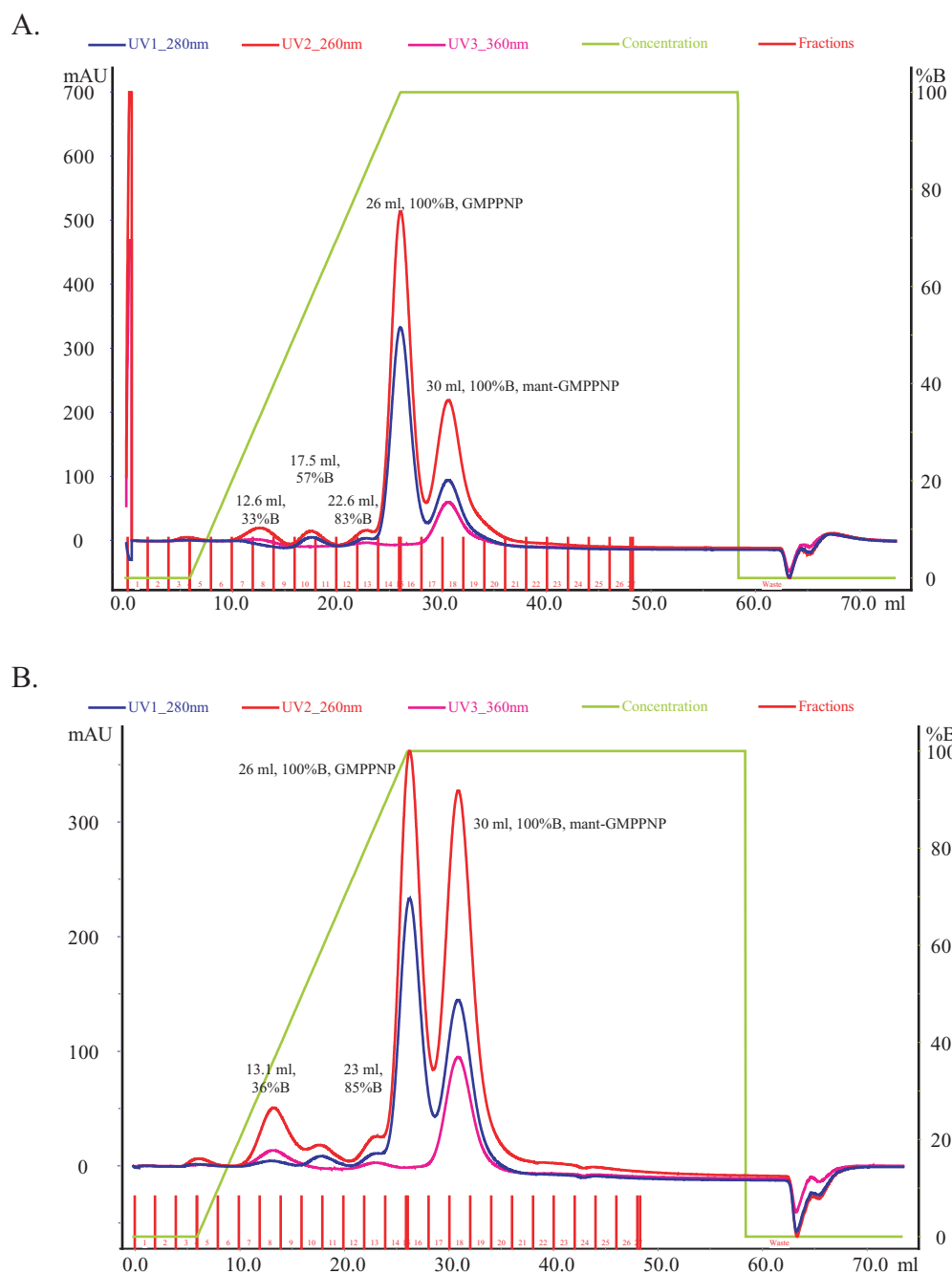
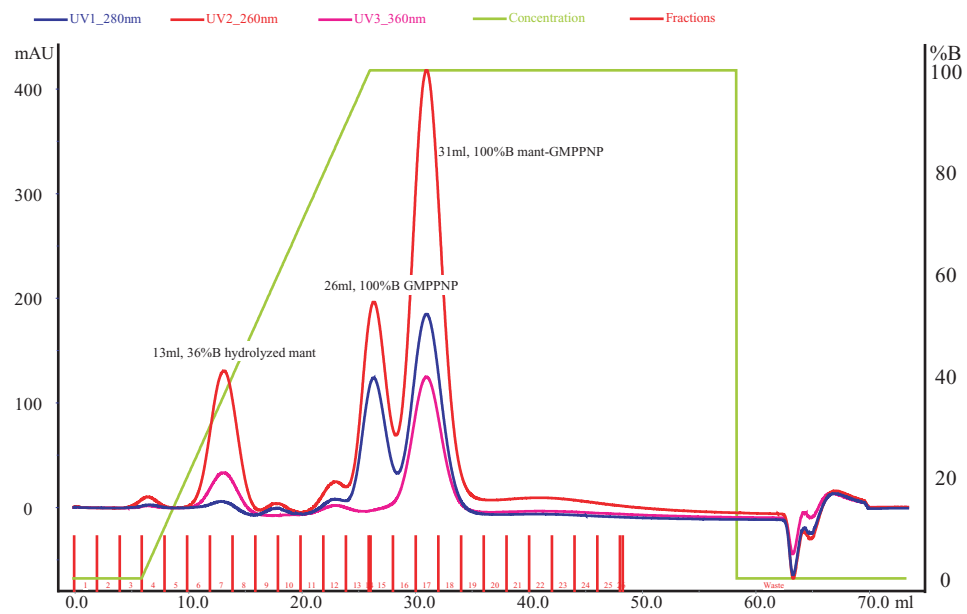
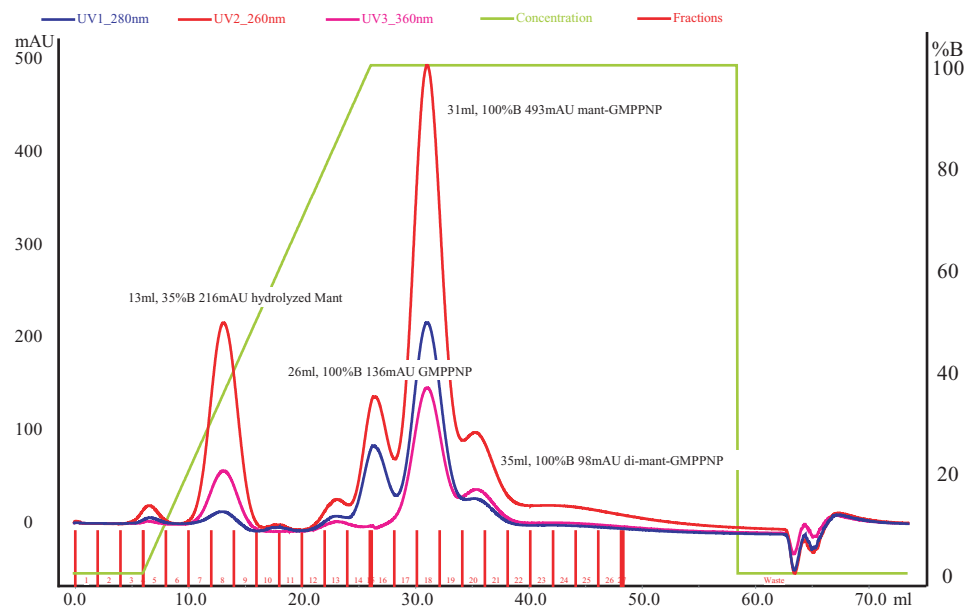


Figure 3-24. Purification of mant-GMPPNP. Chromatogram of HiTrap Q HP monitoring mant absorption at A_{360} and nucleotide absorption at A_{260} . Reaction after A. 30 minutes, B. 60 minutes, C. 120 minutes, D. 180 minutes, E. 240 minutes, and F. >270 minutes.

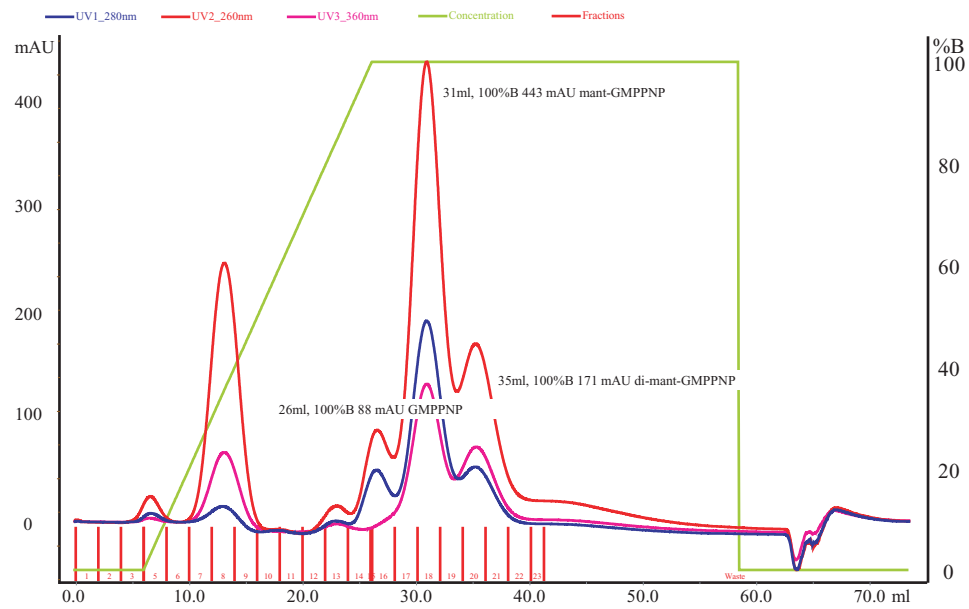
C.



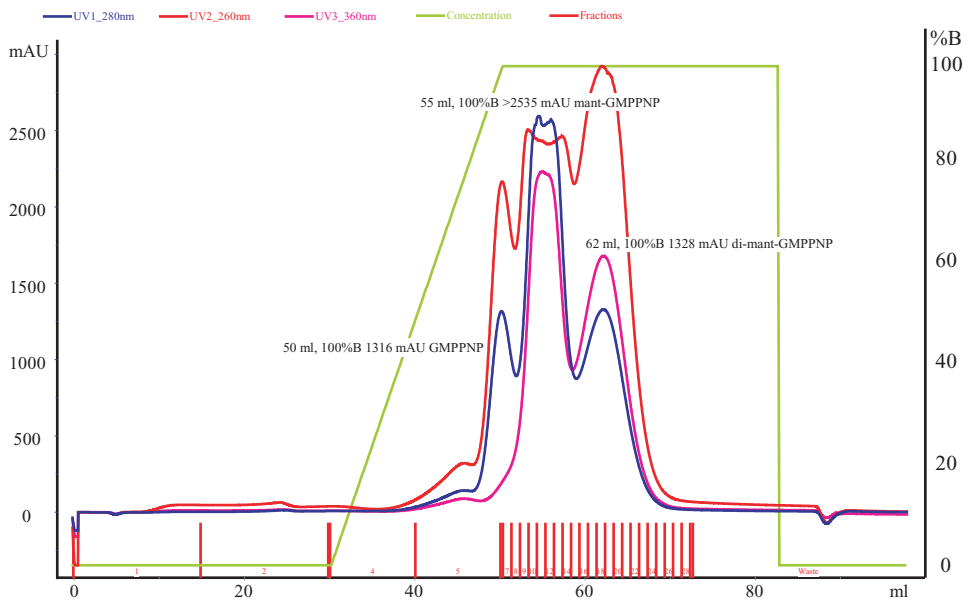
D.



D.



E.



reaction mixture is diluted in 0.2 M TEAB and injected onto a 5 ml Hi Trap Q column pre-equilibrated in 0.2 M TEAB. Mono-mant nucleotides are eluted using a 0.2 M to 1 M TEAB gradient. Hydrolyzed mant elutes first and is followed by unreacted nucleotide and mono-mant nucleotide ($\Sigma_{253}=22,600 \text{ M}^{-1} \text{ cm}^{-1}$, $\Sigma_{350}=5,700 \text{ M}^{-1} \text{ cm}^{-1}$). Di-mant nucleotide elutes last. Fractions containing mono-mant nucleotides are pooled, shell frozen, and concentrated by lyophilization. Pellets are resuspended and lyophilized in ddH₂O to ensure that all buffer is removed.

Purification of bovine Arp2/3 Complex (bArp2/3)

Buffers: P, Q, R, S, T, U, V, KMEI

Overview: Q sepharose, ammonium sulfate cut, Source 15Q, MonoS, SD200

Although there are a number of purification protocols for bArp2/3 complex, we find that we consistently obtain high quality and quantity of the assembly using the protocol outlined by Higgs et al. (Higgs *et al.* 1999). Most steps are performed in a cold room.

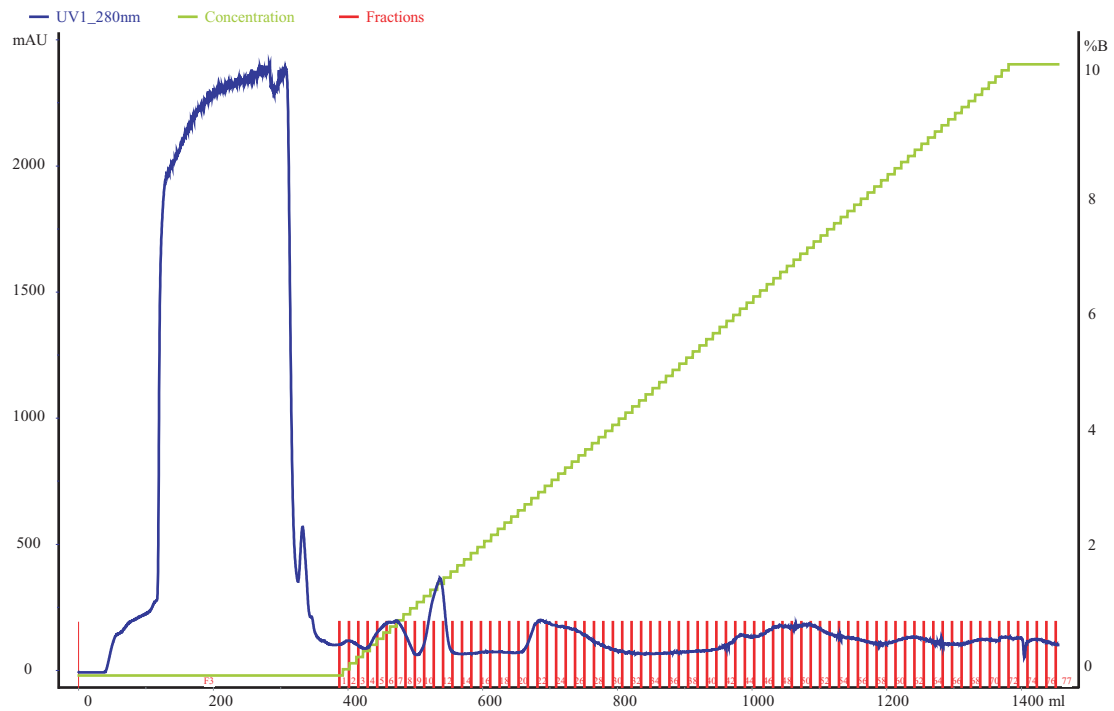
Day 1: Four frozen calf thymuses (Pel-Freez) are roughly broken up and blended in a Waring blender with up to 1.5 L of room temperature Buffer P. The slurry is roughly clarified from fat by centrifugation at 1700 x g for 30 minutes at 4°C. Supernatant is carefully drained from the fat layer and pellet and filtered through cheesecloth into a beaker. Supernatant is centrifuged a second time at 14,000 x g for 15 minutes at 4°C. Supernatant is filtered through cheesecloth and ultracentrifuged at 205,000 x g for 1 hour at 4°C. Supernatant is filtered again through cheesecloth and conductivity (~5.9 mS/cm) is adjusted with 5 M NaCl to a value greater than Buffer Q (~6.3 mS/cm) to prevent Arp2/3 complex from binding to the column. Supernatant is loaded onto a Q-Sepharose

column (180 mL in XK 26/40 column) and flow through containing bArp2/3 complex is collected along with two CV wash with Buffer Q. Next, two ammonium sulfate cuts are performed on the flow through volume. The first ammonium sulfate cut is done to 35% (200 g/L), stirred for 30 minutes, and centrifuged at 14,000 x g for 30 minutes. The second ammonium sulfate cut is done on the supernatant to 55% (150 g/L) to precipitate bArp2/3 complex followed again by stirring and centrifugation. Pellets containing bArp2/3 are resuspended in 20 ml Buffer R and dialyzed (50K MWCO) overnight at 4°C against a total of 12 L Buffer R.

Day 2: The dialysate is pooled and the conductivity is adjusted to less than Buffer S (~0.88 mS/cm) with 2 mM Tris pH 8. The dialysate (~0.5 mS/cm) is filtered through 0.45 µm and loaded onto a Source 15Q (50 ml in XK26/20 column) (Figure 3-25). A gradient of 1000 ml of Buffer S to 10% Buffer T is run. Peak fractions as monitored by absorption at A₂₈₀ and SDS-PAGE are collected (total ~322 ml) and dialyzed (50K MWCO) overnight at 4°C against a total of 12 L Buffer U.

Day 3: The dialysate is pooled, filtered (0.45 µm), and conductivity adjusted to less than Buffer U (~0.94 mS/cm) with 10 mM PIPES pH 6.8. The filtered dialysate is loaded onto a Mono S 10/100 column (30 CV Buffer U to 10% Buffer V) (Figure 3-26). Peak fractions are pooled and loaded onto a SD200 26/60 gel filtration column into Buffer KMEI (Figure 3-27). Fractions containing bArp2/3 complex are pooled (~36 ml) and can be stored on ice at 4°C for approximately one month without significant loss of activity. The assembly should not be frozen, as this decreases activity. Yields are ~20 mg of bArp2/3 per 4 thymuses.

A.



B.

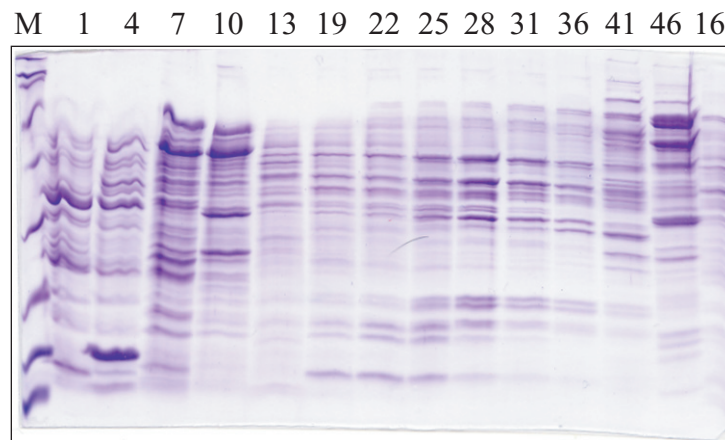


Figure 3-25. Source 15Q purification of bArp2/3 complex from calf thymus. A. Chromatogram monitoring A_{280} . B. Commissie stained SDS-PAGE of numbered fractions. Fractions 15 to 37 were collected (322 ml total).

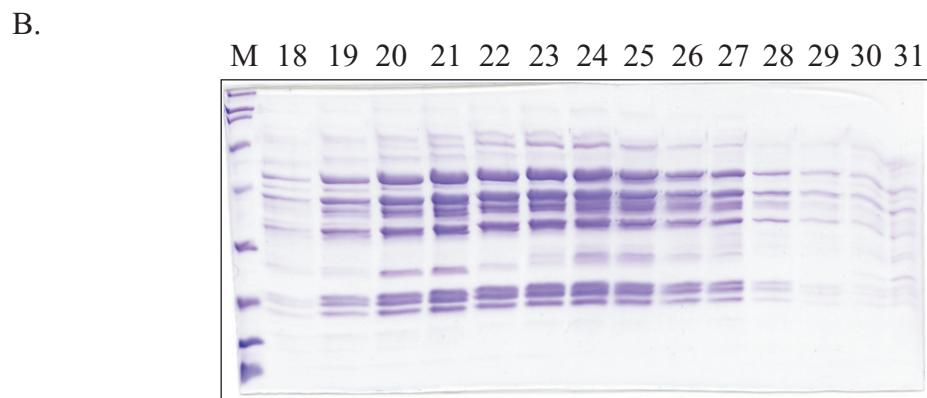
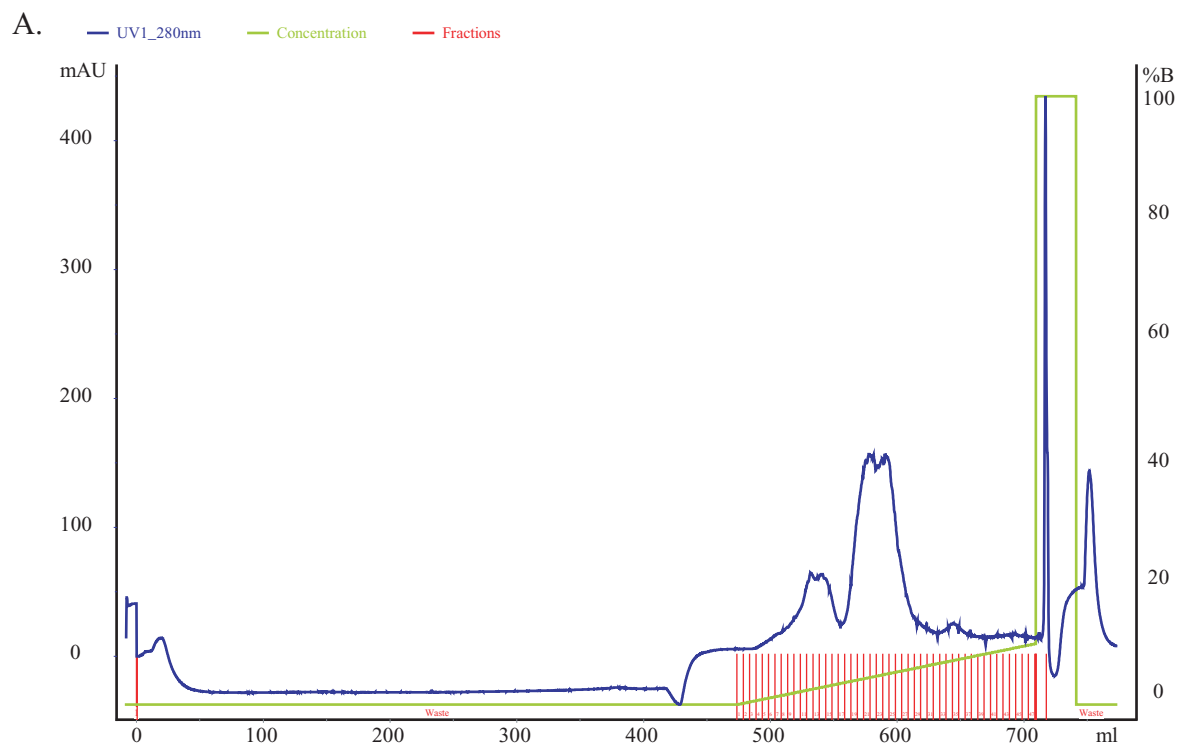


Figure 3-26. MonoS 10/10 purification of bArp2/3 complex. A. Chromatogram monitoring A_{280} . B. Commassie stained SDS-PAGE of numbered fractions. Fractions 19 to 27 were collected (45 ml total).

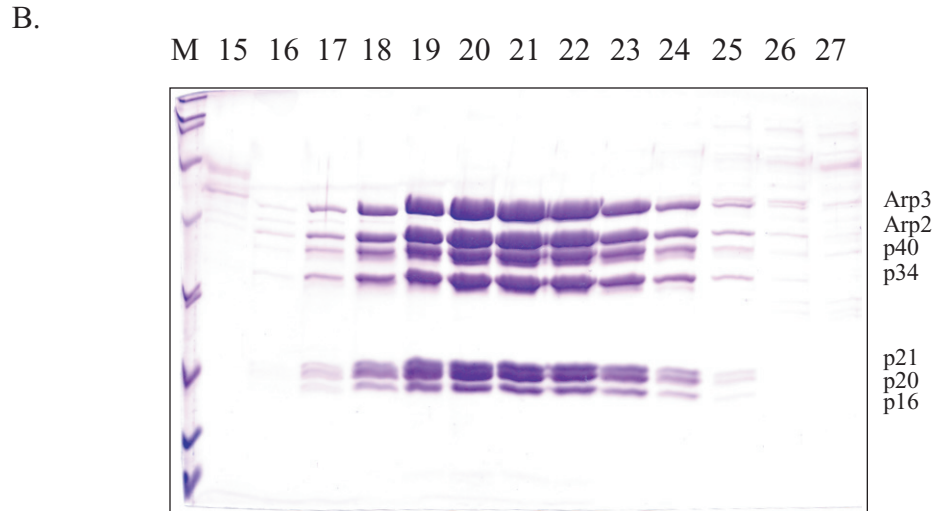
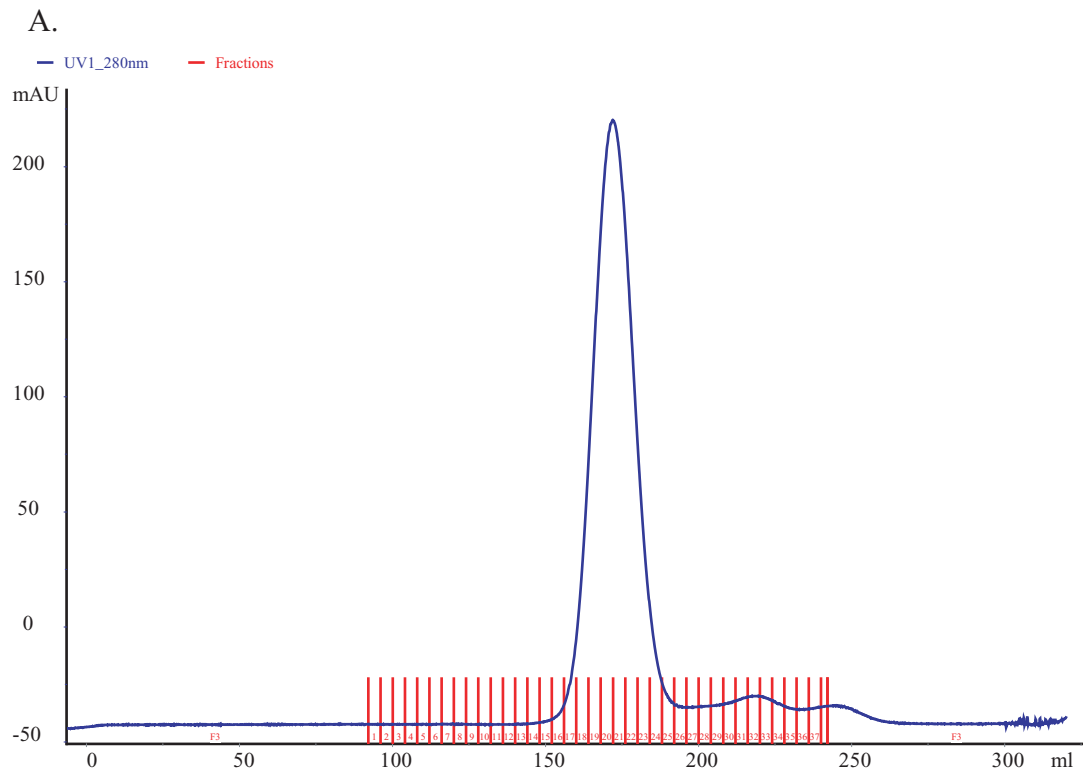


Figure 3-27. Final purification of bArp2/3 complex using gel filtration (Sephadex 200). A. Chromatogram monitoring A_{280} . B. Commassie stained SDS-PAGE of numbered fractions. Fractions 18 to 24 were collected (28 ml total; final amount: 20 mg of bArp2/3 complex).

Purification of Actin and Pyrene-Labeled Actin

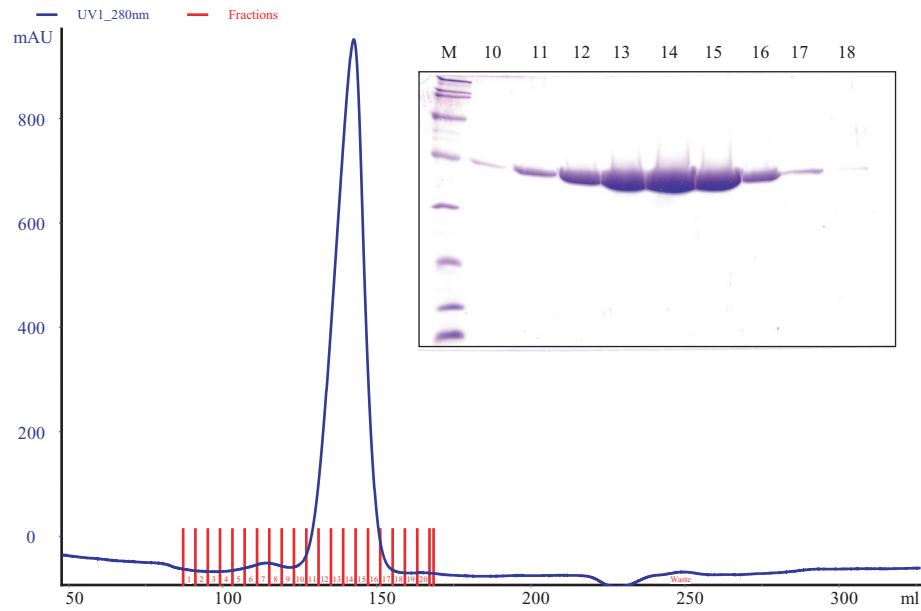
Actin from rabbit skeletal muscle is obtained using the protocol described by Pardee and Spudich and modified by Higgs and Pollard (Pardee and Spudich 1982; Higgs *et al.* 1999). Briefly, skeletal muscle is removed from the two hind legs of a freshly sacrificed rabbit, washed with cold ddH₂O to remove blood and fur, and blended at 4°C. Blended muscle is washed by stirring with 1 L of buffer containing 0.1 M KCl and 0.15 M KPO₄, pH 6.5 for 10 minutes in a cold room and liquid is removed by straining through cheesecloth. The blended muscle is stirred in 2 L of cold 0.05 M NaHCO₃ for 10 minutes at 4°C, strained through cheesecloth. The muscle is transferred to 1 L of cold 1 mM EDTA pH 7 (at 25°C) and stirred for 10 minutes before straining through cheesecloth. The same procedure is repeated two more times with 2 L of cold ddH₂O for 5 minutes and five times with 1 L of chilled acetone for 10 minutes but at room temperature. Acetone is evaporated at room temperature overnight in a fume hood to obtain muscle acetone powder, which is stored at -80°C. Yield is ~80 g.

Actin is extracted from muscle acetone powder with incubation buffer containing 2 mM Tris pH 8 at 25°C, 0.2 mM ATP, 0.5 mM DTT, 0.1 mM CaCl₂, and 1 mM NaN₃ (20 ml/g of muscle) for 30 minutes at 4°C, followed by centrifugation for 30 minutes at 31,000 x g. Extraction and centrifugation are repeated. Pooled supernatants are filtered through cheesecloth and 2 M KCl is added to final concentration of 50 mM, and 1 M MgCl₂ is added to 2 mM. The mixture is allowed to stir for 1 hour at 4 °C to polymerize actin. KCl is added to 0.8 M (5.6 g/100 ml supernatant) and stirred for 30 minutes at 4°C to dissociate tropomyosin from polymerized actin. Supernatant is ultracentrifuged for 2 hours at 142,000 x g. Pellets with a jelly-like consistency are gently washed with Buffer

AB before resuspension in incubation buffer (~3 ml/g of muscle) using a Dounce homogenizer. Actin is dialyzed (12-14 MWCO) against 4 L of incubation buffer overnight at 4°C for 3 nights with changes of fresh Buffer AB to depolymerize actin filaments. The dialysate is recovered and ultracentrifuged at 142,000 x g for 2 hours before loading the top 2/3 fraction of supernatant onto a SD200 26/60 gel filtration column (incubation buffer) to remove traces of capping protein and obtain actin monomers (Figure 3-28A) (Higgs *et al.* 1999).

In order to obtain pyrene-labeled actin, the bottom 1/3 fraction of actin supernatant from the previous ultracentrifugation step can be repolymerized by addition of KCl to 50 mM and MgCl₂ to 2 mM and stirred for 2 hours at 4°C. A 10-fold molar excess (based on ϵ_{actin} of $2.66 \times 10^4 \text{ M}^{-1}$) of pyrene iodoacetamide (Molecular Probes) dissolved in dimethylformamide is added slowly to prevent heavy precipitation of pyrene. The reaction is covered in foil and stirred overnight at 4°C. Labeled polymerized F-actin is centrifuged at low speed for 5 minutes at 3,000 x g to pellet any precipitate, and the supernatant is centrifuged at high speed at 160,000 x g for 2 hours to pellet labeled actin filaments. The pellet is resuspended in incubation buffer using a Dounce homogenizer and dialyzed against incubation buffer for 3 nights to depolymerize actin filaments. Dialysate is centrifuged at 166,000 x g for 2 hours and the supernatant is loaded onto a SD75 26/60 gel filtration column (incubation buffer) to obtain pyrene-labeled actin monomers (Figure 3-28B) (Kouyama and Mihashi 1981; Cooper and Pollard 1982). The percent of pyrene labeling is determined from OD₃₄₄ and OD₂₉₀ and using the following equations:

A.



B.

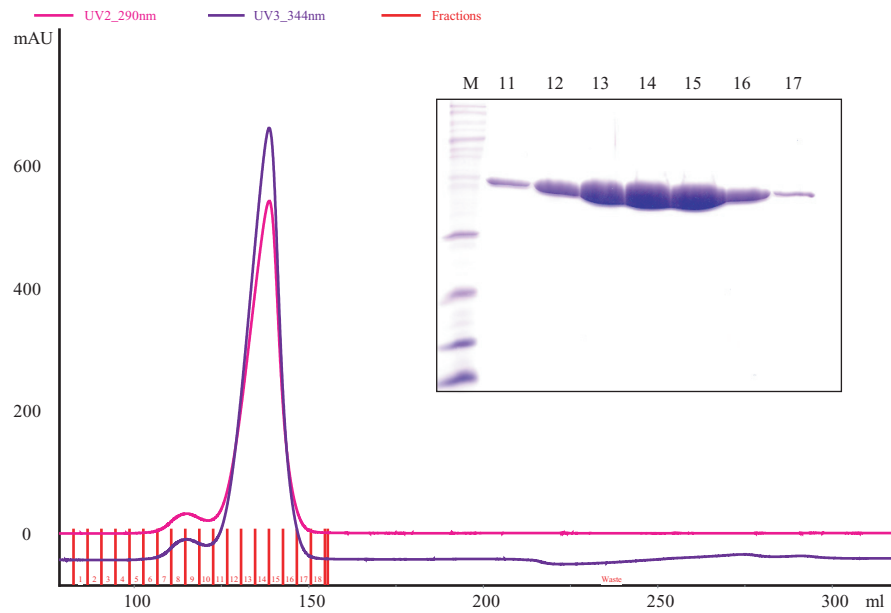


Figure 3-28. Purification of actin and pyrene-labeled actin. A. Chromatogram of Sephadex (SD) 75 monitoring A_{280} . Commassie stained SDS-PAGE of numbered fractions are shown. B. Chromatogram of SD 75 A_{290} and A_{344} .

$$\text{pyrene } (\mu\text{M}) = OD_{344} / 2.2 \times 10^4 (\text{M}^{-1})$$

$$\text{actin } (\mu\text{M}) = (OD_{290} - (OD_{344} * 0.127)) / 2.66 \times 10^4 (\text{M}^{-1})$$

(Eqn. 3-9)

We find that actin and pyrene-actin are best kept stored in dialysis tubing in incubation buffer at 4°C. The buffer should be replaced periodically with fresh incubation buffer and the night before use. Good quality actin can be extracted from muscle acetone powder that has been stored at -80°C for up to 4 months.

Guanidine Hydrochloride or Urea Denaturation of WASP Proteins

The stability of WASP against unfolding can be determined by titration of urea or guanidine hydrochloride (GdnHCl), which can be followed by CD spectroscopy. Both denaturants give similar estimates of WASP stability (Leung and Rosen 2005).

We typically perform chemical denaturant titrations at 25°C on a 10 μM WASP protein sample. The titrant is either 8 M urea or 6 M GdnHCl. To maintain a constant WASP concentration during titration, 10 μM WASP is added to the titrant. Both sample and titrant are allowed to equilibrate at room temperature for 30 minutes before the experiment is begun. The CD signal of the protein is then monitored upon each addition of denaturant at 222 nm or 225 nm for urea and guanidine hydrochloride, respectively, (guanidine hydrochloride absorbs at 222 nm) making sure that the sample equilibrates between additions.

We fit the titration data with the six parameter equation described by C. N. Pace, which takes into account errors in fitting in the pre- and post-transition baselines (Pace 1990):

$$y = \frac{[(y_f + m_f[D]) + (y_u + m_u[D]) (\exp - (\Delta G / RT - m[D] / RT))]}{[1 + \exp - (\Delta G / RT - m[D] / RT)]} \quad (\text{Eqn. 3-10})$$

where y_f and y_u are the slopes of the pre- and post-transition baselines, m_f and m_u are the intercepts of the pre- and post-transition baselines, ΔG is the free energy of unfolding, R is the ideal gas constant, T is temperature, and m describes the dependence of ΔG on the concentration of denaturant.

Fluorescence Experiments

The binding affinity of Cdc42t for WASP can be measured using a number of techniques. We have focused on two methods that utilize a fluorescent molecule to report on the binding interaction. The first method measures affinity by direct binding between WASP and Cdc42t loaded with a GTP analog conjugated to a mant fluorophore. The second method measures affinity by WASP-mediated displacement of Cdc42t prebound to a fluorescent sensor. While the first method is the simpler of the two, we and others have found that the affinities measured in this manner are 7-10 fold weaker than those measured for non-mant labeled nucleotides using alternative assays (Buchwald *et al.* 2001; Buck *et al.* 2001; Leung and Rosen 2005). This may not be a factor when comparing differences in binding affinity among similar effector constructs using the same assay. However, the effect of the mant moiety on binding affinity becomes a greater issue when comparing values obtained from two different assays using mant- or non-mant-nucleotide loaded Cdc42t. An alternative measure of binding affinity in this instance can be found in the second method (Chapter 4 Material and Methods).

Mant Fluorescence Experiments

The binding affinity of GTP-bound Cdc42t for WASP can be measured using GTPase loaded with a fluorescent GTP analog, mantGMPPNP ($\lambda_{\text{exc}} = 360 \text{ nm}$; $\lambda_{\text{em}} = 440 \text{ nm}$). This method and considerations using the mant fluorophore have been described in detail previously (Manor 2000) and will thus be described here briefly. Binding of Cdc42t-mantGMPPNP to WASP proteins is performed in Buffer N by monitoring the decrease of mant fluorescence at 466 nm during titration. Cdc42 is used at concentrations approximately equal to its K_D , and WASP is added from $\sim 0.1K_D$ to $\sim 10K_D$. K_D is obtained by fitting to the quadratic equation describing a single-site binding isotherm:

$$y = F_f + (F_b - F_f) \frac{\left((K_D + [L] + [R]) - \sqrt{(K_D + [L] + [R])^2 - 4[L][R]} \right)}{2[R]} \quad (\text{Eqn. 3-11})$$

where $[L]$ is the total ligand WASP concentration, $[R]$ is the total receptor Cdc42-mantGMPPNP concentration, F_f and F_b are the fluorescence of Cdc42t-mantGMPPNP in the free and WASP-bound states, and K_D is the binding affinity (Marchand *et al.* 2001).

Rhodamine Anisotropy Experiments

The binding affinities of Arp2/3 for I290Q and BGBD-VCA were measured using a rhodamine anisotropy fluorescence assay. A C-terminal cysteine residue was introduced by mutagenesis to I290Q and GBD-VCA to facilitate labeling with tetramethylrhodamine 5'-maleimide. Experiments were performed in the presence of 4

mM actin-latrunculin to approximate the conditions of the polymerization assay and the increase of rhodamine fluorescence anisotropy upon addition of Arp2/3 complex was monitored at 574 nm ($\lambda_{\text{ex}}=552$ nm). Anisotropy data were fit to a single-site binding isotherm (Equation 11).

Pyrene Actin Polymerization Assays

The ability of WASP proteins to activate Arp2/3 complex can be measured using the pyrene-actin polymerization assay that has been described by many labs (Higgs *et al.* 1999; Rohatgi *et al.* 1999; Mullins and Machesky 2000). This assay is based on the increase in fluorescence of pyrene-actin when it incorporates into a filament. Thus, actin polymerization can be measured by following the change in pyrene fluorescence over time in the presence of Arp2/3 complex and activators.

Several experimental parameters should be considered when preparing the assay. Photobleaching of pyrene should be avoided by decreasing the excitation monochromator slit width. The resultant decrease in sensitivity can be offset by increasing the emission monochromator slit width and/or the percentage of pyrene actin (although pyrene-actin doping to >10% can inhibit polymerization). Temperature also affects the reproducibility of polymerization assays. For this reason, all buffers should be equilibrated at room temperature for 30-60 minutes prior to the start of experiments. Protein components that are added in very small volumes are kept on ice until the start of a reaction.

Buffers:

KMEI: 10 mM imidazole pH 7, 50 mM KCl, 1 mM MgCl₂, 1 mM EGTA

Actin-Ca²⁺: 2 mM Tris pH 8, 25°C, 0.2 mM ATP, 0.5 mM DTT, 0.1 mM CaCl₂, 1 mM

NaN₃

Actin-Mg²⁺: 2 mM Tris pH 8, 25°C, 0.2 mM ATP, 0.5 mM DTT, 0.1 mM MgCl₂, 1 mM

NaN₃

10E/1M: 10 mM EGTA pH 8 and 1 mM MgCl₂

A typical polymerization reaction is performed as follows:

1. 32 μ l of 25 μ M Ca²⁺-actin (5% pyrene, stored in Buffer Actin-Ca²⁺) is added to an eppendorf tube. Mg²⁺ is exchanged for Ca²⁺ by addition of 3.2 μ l of Buffer 10E/1M. 64.8 μ l of Buffer Actin-Mg²⁺ is added to bring the volume to 100 μ l, and the mixture is incubated for 2 minutes at room temperature.
2. In a separate eppendorf tube, 2 μ l of 1 μ M bovine Arp2/3, 2 μ l of 50 μ M WASP, 10 μ l of 10X Buffer KMEI, and 78 μ l of 1X Buffer KMEI are mixed together and incubated for 1 minute at room temperature. In reactions with wiskostatin, the small molecule is added to this mixture in DMSO (to give final DMSO < 5% v/v).
3. The contents of both eppendorf tubes are quickly combined to 200 μ l volume and the sample is transferred to a quartz cuvette and into the fluorimeter.

The polymerization reaction here is performed with final concentrations of 4 μ M actin (5% pyrene), 10 nM bArp2/3 complex, and 500 nM WASP in Buffer KMEI. The time it takes to mix the components and start the fluorimeter is noted and must be consistent among experiments in order to obtain reproducible results. Pyrene-actin

fluorescence ($\lambda_{\text{ex}} = 365 \text{ nm}$, $\lambda_{\text{em}} = 407 \text{ nm}$) is measured every second until it plateaus (~50-1000s, depending upon the Arp2/3 complex activator).

Several metrics have been described in the literature to quantitatively analyze Arp2/3 complex-mediated actin polymerization, including maximum polymerization rate (Higgs *et al.* 1999; Prehoda *et al.* 2000), polymerization rate at 50% polymerization (Dueber *et al.* 2003), time to 50% polymerization (Zalevsky *et al.* 2001), and Arp2/3 activation rate constants for nucleation-promoting factors (Zalevsky *et al.* 2001). Our lab favors measurement of maximum polymerization rate, which is converted to concentration of filament barbed ends based on the known rate of actin addition at barbed ends (Higgs *et al.* 1999; Mullins and Machesky 2000). Assuming that each Arp2/3 complex nucleates only a single filament during the assay and that filament growth occurs only at the barbed ends, the maximum concentration of barbed ends is equal to the concentration of active Arp2/3 complex.

The normalized fluorescence values from each actin polymerization curve are converted to actin filament concentrations, and then the rate of filament change with time (elongation rate) is converted to the barbed end concentration using the following equation:

$$\begin{aligned}
 [\text{ends}] &= \frac{\text{elongation rate}}{(k_+ [\text{actin}] - k_-)} \\
 &= \left(\frac{[\text{actin}]_0 - cc}{F_{\text{max}} - F_0} \right) \left(\frac{\Delta F}{\Delta t} \right) * \frac{1}{k_+ \left[\left(\left(\frac{F_{\text{max}} - F_x}{F_{\text{max}} - F_0} \right) ([\text{actin}]_0 - cc) \right) + cc \right] - k_-} \quad (\text{Eqn. 3-12})
 \end{aligned}$$

where $[\text{actin}]_0$ is the initial actin concentration, c_c is the filament barbed end critical concentration (0.1 μM), F_{max} is the maximum fluorescence of the polymerization curve, F_x is the instantaneous fluorescence, $\Delta F/\Delta t$ is the instantaneous slope of the polymerization curve, k_+ is the barbed end Mg^{2+} -actin association rate constant (11.6 $\mu\text{M}^{-1} \text{s}^{-1}$), and k_- is the barbed end Mg^{2+} -actin dissociation rate constant (1.3 s^{-1}). The calculation of barbed ends is greatly affected by noise in the polymerization curve. Thus, we average over a window of points when determining the instantaneous actin concentration and slope ($\Delta F/\Delta t$) at each point of the polymerization curve. Values for F_x and F_{max} are each an average over ten data points and the slope is calculated from a linear fit of at least twenty data points. Furthermore, although spontaneous actin nucleation is negligible when Arp2/3 complex is stimulated by strong activators (e.g. free VCA peptides), this is not the case for weaker activators (e.g. GBD-VCA). Thus, to achieve accurate quantitation across a range of activators, it is necessary to appropriately subtract the concentration of barbed ends generated by actin alone from the Arp2/3-mediated concentration.

References

- Abdul-Manan, N., *et al.* (1999). "Structure of Cdc42 in complex with the GTPase-binding domain of the 'Wiskott-Aldrich syndrome' protein." Nature **399**(6734): 379-83.
- Badour, K., *et al.* (2004). "Fyn and PTP-PEST-mediated regulation of Wiskott-Aldrich syndrome protein (WASp) tyrosine phosphorylation is required for coupling T cell antigen receptor engagement to WASp effector function and T cell activation." J Exp Med **199**(1): 99-112.
- Badour, K., *et al.* (2003). "The Wiskott-Aldrich syndrome protein acts downstream of CD2 and the CD2AP and PSTPIP1 adaptors to promote formation of the immunological synapse." Immunity **18**(1): 141-54.
- Buchwald, G., *et al.* (2001). "Conformational switch and role of phosphorylation in PAK activation." Mol Cell Biol **21**(15): 5179-89.
- Buck, M., *et al.* (2001). "Global disruption of the WASP autoinhibited structure on Cdc42 binding. Ligand displacement as a novel method for monitoring amide hydrogen exchange." Biochemistry **40**(47): 14115-22.
- Buck, M., *et al.* (2004). "A two-state allosteric model for autoinhibition rationalizes WASP signal integration and targeting." J Mol Biol **338**(2): 271-85.
- Burns, S., *et al.* (2004). "Mechanisms of WASp-mediated hematologic and immunologic disease." Blood **104**(12): 3454-62.
- Cannon, J. L. and J. K. Burkhardt (2002). "The regulation of actin remodeling during T-cell-APC conjugate formation." Immunol Rev **186**: 90-9.

- Cannon, J. L. and J. K. Burkhardt (2004). "Differential roles for Wiskott-Aldrich syndrome protein in immune synapse formation and IL-2 production." J Immunol **173**(3): 1658-62.
- Cannon, J. L., *et al.* (2001). "Wasp recruitment to the T cell:APC contact site occurs independently of Cdc42 activation." Immunity **15**(2): 249-59.
- Cooper, J. A. and T. D. Pollard (1982). "Methods to measure actin polymerization." Methods Enzymol **85 Pt B**: 182-210.
- Cory, G. O., *et al.* (2002). "Phosphorylation of tyrosine 291 enhances the ability of WASp to stimulate actin polymerization and filopodium formation. Wiskott-Aldrich Syndrome protein." J Biol Chem **277**(47): 45115-21.
- Devriendt, K., *et al.* (2001). "Constitutively activating mutation in WASP causes X-linked severe congenital neutropenia." Nat Genet **27**(3): 313-7.
- Dueber, J. E., *et al.* (2003). "Reprogramming control of an allosteric signaling switch through modular recombination." Science **301**(5641): 1904-8.
- Gallego, M. D., *et al.* (1997). "Defective actin reorganization and polymerization of Wiskott-Aldrich T cells in response to CD3-mediated stimulation." Blood **90**(8): 3089-97.
- Higgs, H. N., *et al.* (1999). "Influence of the C terminus of Wiskott-Aldrich syndrome protein (WASp) and the Arp2/3 complex on actin polymerization." Biochemistry **38**(46): 15212-22.
- Kim, A. S., *et al.* (2000). "Autoinhibition and activation mechanisms of the Wiskott-Aldrich syndrome protein." Nature **404**(6774): 151-8.

- Kouyama, T. and K. Mihashi (1981). "Fluorimetry study of N-(1-pyrenyl)iodoacetamide-labelled F-actin. Local structural change of actin protomer both on polymerization and on binding of heavy meromyosin." Eur J Biochem **114**(1): 33-8.
- Labno, C. M., *et al.* (2003). "Itk functions to control actin polymerization at the immune synapse through localized activation of Cdc42 and WASP." Curr Biol **13**(18): 1619-24.
- Ladurner, A. G. and A. R. Fersht (1997). "Glutamine, alanine or glycine repeats inserted into the loop of a protein have minimal effects on stability and folding rates." J Mol Biol **273**(1): 330-7.
- Leung, D. W., *et al.* (2006). "Biochemical Properties and Inhibitors of (N-)WASP." Methods Enzymol **406**.
- Leung, D. W. and M. K. Rosen (2005). "The nucleotide switch in Cdc42 modulates coupling between the GTPase-binding and allosteric equilibria of Wiskott-Aldrich syndrome protein." Proc Natl Acad Sci U S A **102**(16): 5685-90.
- Manor, D. (2000). "Measurement of GTPase.effector affinities." Methods Enzymol **325**: 139-49.
- Marchand, J. B., *et al.* (2001). "Interaction of WASP/Scar proteins with actin and vertebrate Arp2/3 complex." Nat Cell Biol **3**(1): 76-82.
- Monod, J., *et al.* (1965). "On the Nature of Allosteric Transitions: a Plausible Model." J Mol Biol **12**: 88-118.
- Mullins, R. D. and L. M. Machesky (2000). "Actin assembly mediated by Arp2/3 complex and WASP family proteins." Methods Enzymol **325**: 214-37.

- Nagi, A. D. and L. Regan (1997). "An inverse correlation between loop length and stability in a four-helix-bundle protein." Fold Des **2**(1): 67-75.
- Pace, C. N. (1990). "Measuring and increasing protein stability." Trends Biotechnol **8**(4): 93-8.
- Pai, E. F., *et al.* (1990). "Refined crystal structure of the triphosphate conformation of H-ras p21 at 1.35 Å resolution: implications for the mechanism of GTP hydrolysis." Embo J **9**(8): 2351-9.
- Pardee, J. D. and J. A. Spudich (1982). "Purification of muscle actin." Methods Enzymol **85 Pt B**: 164-81.
- Prehoda, K. E., *et al.* (2000). "Integration of multiple signals through cooperative regulation of the N-WASP-Arp2/3 complex." Science **290**(5492): 801-6.
- Rohatgi, R., *et al.* (2000). "Mechanism of N-WASP activation by CDC42 and phosphatidylinositol 4, 5-bisphosphate." J Cell Biol **150**(6): 1299-310.
- Rohatgi, R., *et al.* (1999). "The interaction between N-WASP and the Arp2/3 complex links Cdc42-dependent signals to actin assembly." Cell **97**(2): 221-31.
- Torres, E. and M. K. Rosen (2003). "Contingent phosphorylation/dephosphorylation provides a mechanism of molecular memory in WASP." Mol Cell **11**(5): 1215-27.
- Westerberg, L., *et al.* (2005). "Wiskott-Aldrich syndrome protein deficiency leads to reduced B-cell adhesion, migration, and homing, and a delayed humoral immune response." Blood **105**(3): 1144-52.
- Zalevsky, J., *et al.* (2001). "Different WASP family proteins stimulate different Arp2/3 complex-dependent actin-nucleating activities." Curr Biol **11**(24): 1903-13.

Chapter 4 Modulation of the allosteric equilibrium of WASP by Cdc42

(Adapted from Leung and Rosen 2005)

Introduction

The two-state model provides an accurate framework for analyzing the regulation and activation of WASP by activated Cdc42. WASP affinity for Cdc42-GTP and WASP activity toward Arp2/3 complex are functions of the allosteric equilibrium as predicted by the model. Binding of Cdc42-GTP effectively biases the WASP allosteric equilibrium towards the active state of WASP through high affinity interactions with the active state of WASP, thereby providing the basis for WASP activation. Thus, the GTPase behaves as a signaling switch to presumably cycle cellular functions “on” in the GTP-bound state and “off” in the GDP-bound state (Bourne 1995; Hoffman and Cerione 2000). However, WASP, like many other GTPase signaling effectors, is also regulated through autoinhibitory interactions where the GBD forms intramolecular interactions with the C-terminal activity bearing domain. Previous studies examining different GTPase/effector pairs demonstrated that there is a significant difference in GTPase affinity for the corresponding GBD in the full-length effector protein than when the GBD is isolated (Thompson *et al.* 1998; Nomanbhoy and Cerione 1999; Owen *et al.* 2000; Buchwald *et al.* 2001). For example, the binding affinity of Cdc42-GTP for full length WASP is 4 μM , which is ~ 500 -fold higher than the affinity for the isolated WASP GBD ($K_D = 11$ nM) (Buck *et al.* 2001). It is not entirely clear whether the GTPase nucleotide switch, specifically the difference in affinity between the GTP- and GDP-bound states of the

GTPase for the GBD in the full-length protein, is sufficient to trigger activation because a majority of these interactions have not been fully characterized biochemically. In order to further examine the relationship between the GTPase nucleotide switch and the allosteric regulation of WASP, the two-state model was also applied to the GDP-bound state of Cdc42. Results from these analyses have significant and broad implications for the specificity and fidelity of GTPase signaling and for other proteins that function to modulate the WASP allosteric equilibrium.

The biophysical basis of the Cdc42 nucleotide switch on the activation of WASP

The two-state model predicts that an activator can bind to both the inactive and active states of WASP, but preferentially to the active state (Figure 3-1). Consequently, the model also predicts that an activator will shift the WASP allosteric equilibrium toward the activated state according to its C parameter, where C is equal to the ratio of binding affinities of activator for the active and inactive states of WASP. The magnitude of C then dictates the maximum increase in WASP activity that can be achieved by a single agonist. A small C value ($C \ll 1$) signifies a highly effective WASP activator whereas increasingly larger values of C correspond to a decrease in the ability of the activator to stimulate WASP activity. For highly stable proteins, binding of Cdc42-GTP will have a significant effect on the activation state of WASP (Figure 3-13B). As the stability of the protein decreases, saturating concentrations of Cdc42-GTP biases the WASP equilibrium and can gradually lead to the complete activation of WASP. The difference in fractional activity curve of $f_{a,sat} - f_{a,0}$ shows that as the stability of WASP

approaches -3 kcal mol^{-1} , protein activity steadily reaches a maximum (Buck *et al.* 2004). Above -3 kcal mol^{-1} , protein activity appears to decrease but the sharp decline in $f_{a,\text{sat}} - f_{a,0}$ is compensated by a corresponding increase of WASP protein in the active state. However, at much lower Cdc42-GTP concentrations, Cdc42-GTP will affect the stability of WASP (the K_{eq} parameter) but its efficiency at activating and biasing the WASP equilibrium is limited by its value of C and concentration. The constructs most representative of full length WASP, GBDPVCA and GBD-VCA M307A, have stabilities of approximately -3.3 and $-3.4 \text{ kcal mol}^{-1}$, respectively. Both constructs are situated near the beginning region of the fractional activity curve (Figure 3-13C; in the absence of activator) and are fairly stabilized. But the addition of saturating concentrations of Cdc42-GTP can significantly shift the WASP allosteric equilibrium toward the active state. Furthermore, the two-state model predicts that for Cdc42 the GTP-bound state is a better agonist of WASP activation than the GDP-bound state for WASP $K_{\text{eq}} > 50$. Binding of Cdc42-GTP will shift the fractional activity curve considerably towards the left (Figure 3-13C, blue dashed line). Because Cdc42-GDP is predicted to be a poorer agonist of WASP activation, the fractional activity curve in the presence Cdc42-GDP will also shift to the left, but will not exceed that of Cdc42-GTP (Figure 3-13B, green dashed line).

Addition of Cdc42-GMPPNP to the series of WASP GBD-VCA proteins result in an overall increase of activity toward Arp2/3 complex in pyrene-actin polymerization assays. For many of the WASP proteins, activity toward Arp2/3 complex is a linear function of the percent saturation of WASP by Cdc42-GMPPNP (Figure 4-1). WASP proteins that are highly destabilized, such as I290Q and I294A, are predominantly

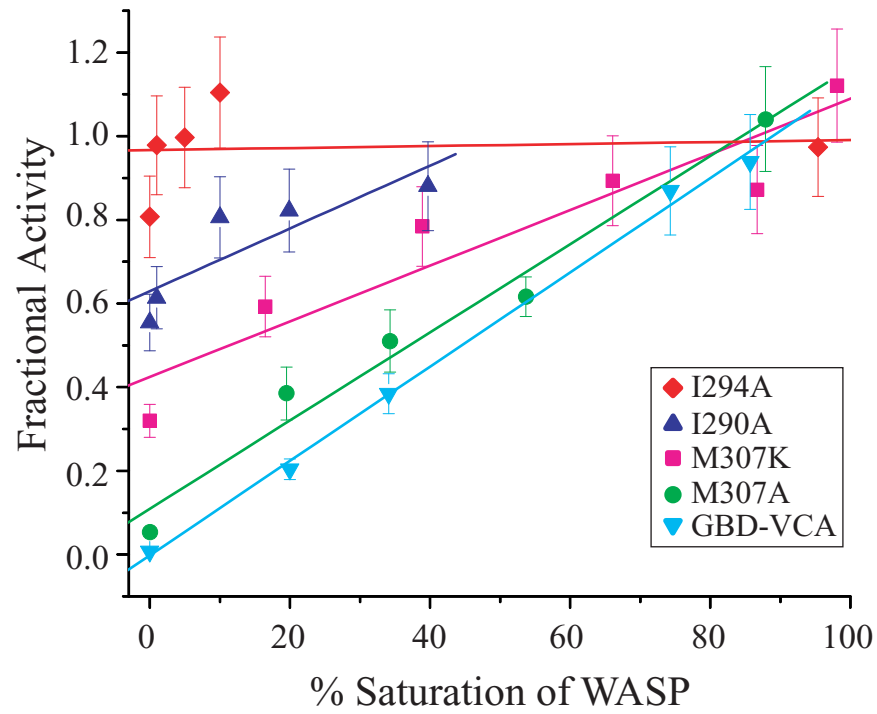


Figure 4-1. Activation of WASP mutants by Cdc42-GMPPNP. Fractional activity of different WASP constructs with increasing fractional saturation by Cdc42-GMPPNP. Lines show linear fits of the data for each protein.

unfolded and primarily occupy the active state and the addition of Cdc42-GMPPNP has very little or no further effect on the WASP allosteric equilibrium or WASP activity. In contrast, addition of increasing amounts of Cdc42-GMPPNP to the most stabilized WASP proteins, such as GBD-VCA or M307A, results in the full activation of WASP and levels of activity comparable to the I294A mutant. These results suggest that $C_{\text{Cdc42,GTP}}$, when coupled with $C_{\text{Arp2/3}}$, provides sufficient driving force to fully overcome WASP autoinhibition for $K_{\text{eq}} \leq 1200$ (GBD-VCA).

Numerous studies have highlighted the role of the GTPase nucleotide cycle in the activation of downstream effectors, where the GDP-bound state of the GTPase requires GEF-mediated nucleotide exchange in order to bind effectors to activate downstream signaling pathways. A number of recent studies indicate that effectors can also bind the GDP-bound state with measurable affinity, but that only the GTP-bound state can effect significant changes in activation (Rohatgi *et al.* 1999; Sondermann *et al.* 2004). To examine these properties in Cdc42 and the biophysical basis of the Cdc42 nucleotide switch on the activation of WASP, the allosteric model was applied to the GDP-bound state of Cdc42. Similar to the studies performed with Cdc42-GTP, we wanted to determine if Cdc42-GDP can shift the WASP allosteric equilibrium and the magnitude of the corresponding C parameter. We expected that the binding affinity of Cdc42-GDP for WASP to be significantly lower than for Cdc42-GTP. Many studies, including those performed in our lab, have shown that the mant moiety when conjugated to GMPPNP results in up to an ~8-fold decrease in affinity between GTPase and its effectors (Rudolph *et al.* 1998), we predicted that similar measurements of WASP affinity for Cdc42-mantGDP would therefore be beyond the limit of accurate detection. In addition, mant

fluorescence can interfere with pyrene fluorescence in pyrene-actin polymerization assays and complicate analysis of the results. Consequently, the affinity of Cdc42-GDP for WASP proteins was measured using a FRET-based fluorescence assay (Seth *et al.* 2003). WASP proteins were fused to a cyan-fluorescent protein (CFP) at the N-terminus and to a yellow fluorescent protein (YFP) at the C-terminus (gift from Abhi Seth). Binding of Cdc42-GDP to WASP was measured by monitoring changes in the ratio of YFP emission at 526 nm to CFP emission at 476 nm (YFP : CFP) after CFP excitation ($\lambda_{\text{ex}} = 433 \text{ nm}$) as a function of Cdc42-GDP concentration (Figure 4-2). The measured affinity of Cdc42-GDP for the most stable, autoinhibited WASP protein ($K_{D,i}$), YFP-GBD-VCA-CFP, was 50 μM , whereas the measured affinity for the representative least stable WASP protein ($K_{D,a}$), YFP-GBD-CFP, was 2.7 μM . The resulting C value for Cdc42-GDP according to Equation 3-4 is:

$$C_{\text{Cdc42-GDP}} = K_{D,a} / K_{D,i} = 5.4 \times 10^{-2} .$$

In order to directly compare the magnitudes of the C parameters for both the GDP and GTP bound states of Cdc42 using the same assay, we also measured the binding affinity of Cdc42-GMPPNP for each of these WASP FRET-proteins. The affinities measured in the FRET assay of Cdc42-GMPPNP for YFP-GBD-VCA-CFP and YFP-GBD-CFP were 2.6 μM and 29 nM, respectively. The corresponding C parameter value is 1.1×10^{-2} , which is 5-fold higher than that measured for Cdc42-GDP.

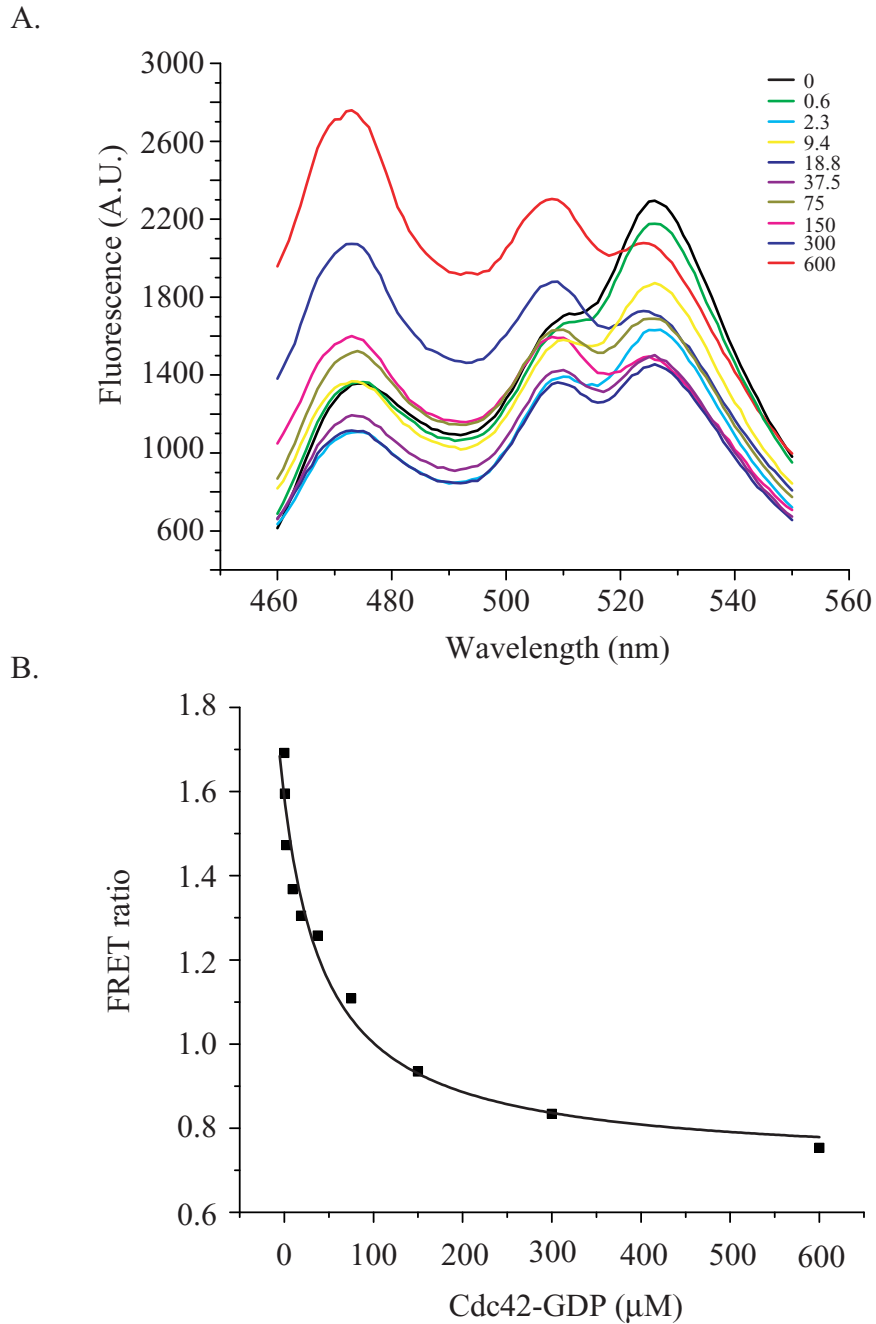


Figure 4-2. FRET-based assay to measure binding affinity of Cdc42-GDP for CFP-GBD-VCA-YFP. A. Titration of increasing amounts of Cdc42-GDP (μM) into 15 nM of WASP FRET sensor. B. Binding affinity measured through changes in FRET ratio of YFP emission (526 nm) to CFP emission (476 nm) after CFP excitation ($\lambda_{\text{ex}}=433$ nm). Data were fit to a quadratic equation for a single-site binding isotherm.

Comparison of these C parameter values suggests that the GDP-bound state of Cdc42 is a poorer activator of WASP than the GTP-bound state of Cdc42 at comparable levels of saturation. To test this, we examined the effect of Cdc42-GDP on the activity of WASP proteins. Consistent with the predictions from the two-state model and observations from previous studies (Rohatgi *et al.* 1999; Sondermann *et al.* 2004), addition of Cdc42-GDP biases the allosteric equilibrium and increases WASP activity toward Arp2/3 complex for $K_{eq} \leq 1200$, analogous to our observations with Cdc42-GMPPNP. However, the level of WASP activation achieved by Cdc42-GDP is significantly lower than that achieved by Cdc42-GMPPNP. For example, addition of equivalent concentrations of Cdc42-GDP and Cdc42-GMPPNP to GBD-VCA M307A in a pyrene-actin polymerization assay indicates that WASP activation levels are lower in the presence of Cdc42-GDP than Cdc42-GMPPNP (Figure 4-3). Furthermore, whereas increasing concentrations of Cdc42-GMPPNP can stimulate maximum levels of activation of GBD-VCA M307A that is comparable to a VCA peptide alone, corresponding levels of Cdc42-GDP result in only a partial activation of GBD-VCA M307A. Even at saturating concentrations, Cdc42-GDP is predicted to only stimulate half-maximal activation of WASP (Figure 4-4). Therefore, the difference in C parameter value reflects the efficiency of activator to bias the allosteric equilibrium of WASP. In this case, Cdc42-GDP is an inferior agonist of WASP and is less effective at coupling the GTPase binding equilibrium to the allosteric equilibrium of WASP than compared with Cdc42-GMPPNP, which is consistent with the predictions of the model.

To understand the structural basis for the difference in C values on WASP activation, we examined the interaction between WASP and the two nucleotide states of

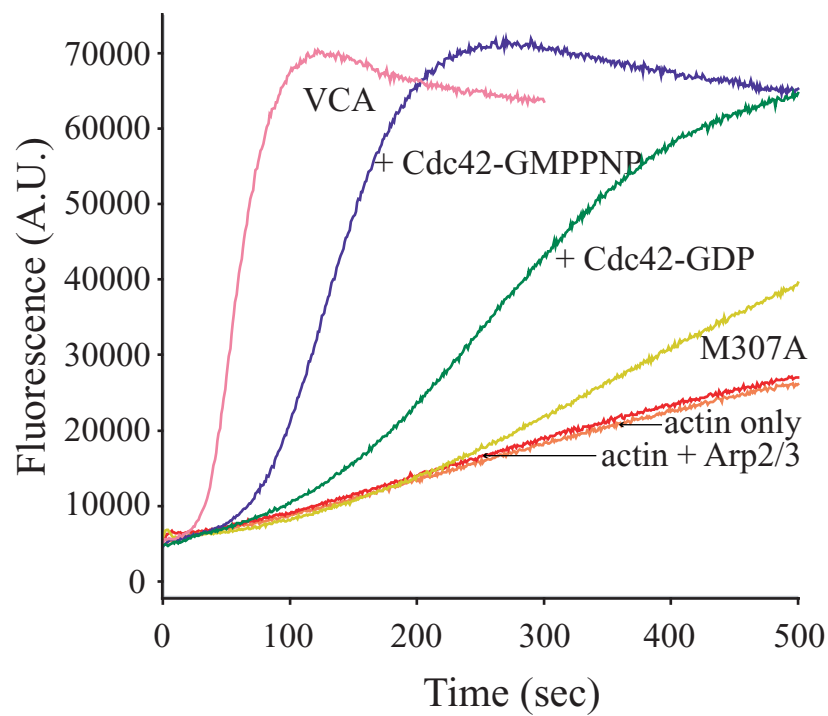


Figure 4-3. Differential activation of GBD-VCA M307A by Cdc42-GDP or Cdc42-GMPPNP. Actin polymerization assay performed in the presence of 500 nM GBD-VCA M307A and 500 nM Cdc42-GDP or 500 nM Cdc42-GMPPNP.

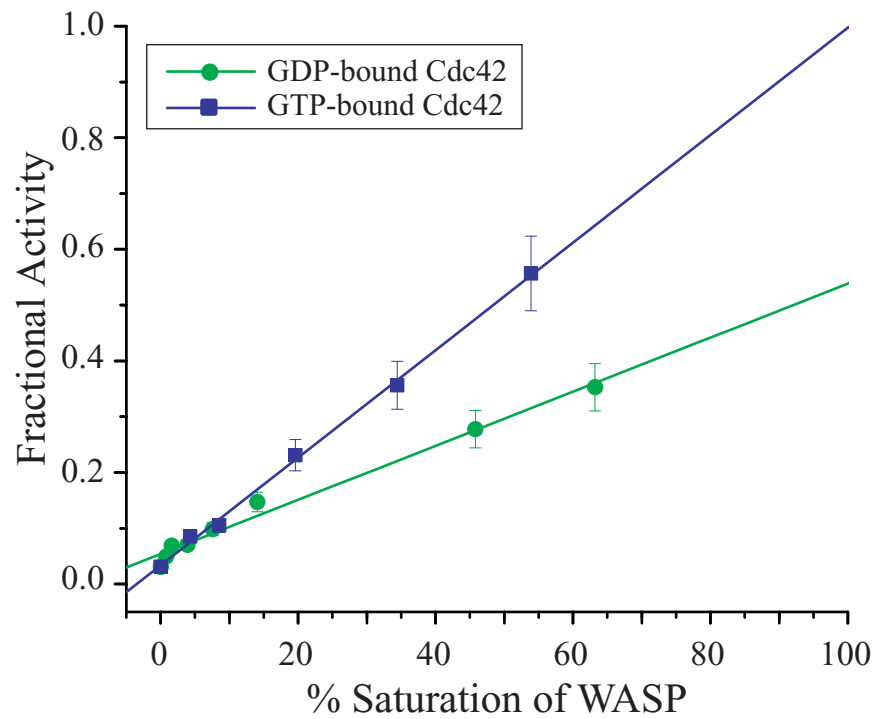
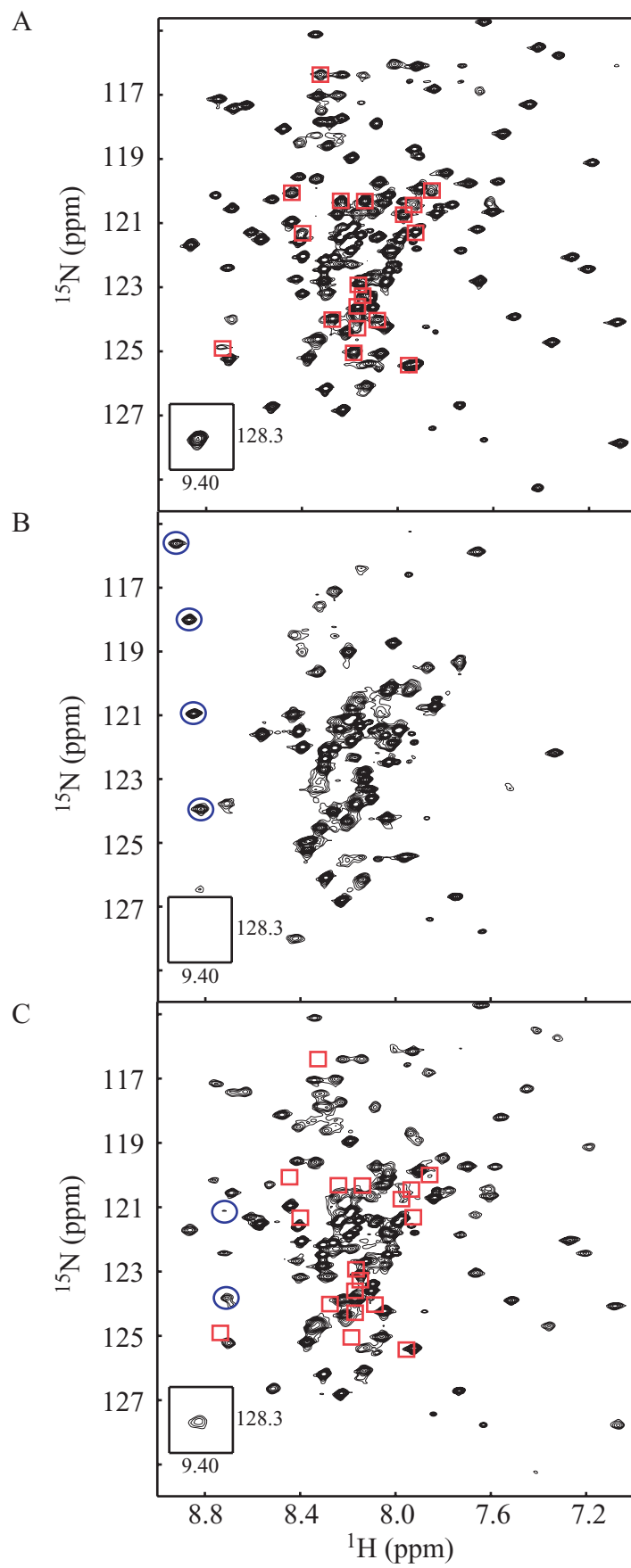


Figure 4-4. WASP activity in the presence of Cdc42-GDP and CDC42- GMPPNP. Actin polymerization assays of GBD-VCA M307A were performed with increasing saturation by Cdc42-GMPPNP (blue) or Cdc42-GDP (green). Data points were fit to a linear slope and extrapolated to 100% saturation.

Cdc42. We acquired $^1\text{H}/^{15}\text{N}$ -TROSY HSQC spectra (Pervushin *et al.* 1997) of $^2\text{H}/^{15}\text{N}$ GBD-VCA alone and in the presence of either Cdc42-GMPPNP or Cdc42-GDP. In the spectrum of free GBD-VCA, the peaks corresponding to the autoinhibited core of WASP display characteristic hallmarks of a well-folded protein (Figure 4-5A). Mainly, the peaks corresponding to the GBD and the C region were well dispersed along both the proton and nitrogen dimensions and displayed near-uniform intensities. In contrast, peaks corresponding to the N-terminal portion of the CRIB motif, the V domain, and the acidic region, which are unstructured in the context of the GBD-VCA construct, displayed higher intensities and were concentrated near the center of the amide region. Addition of Cdc42-GMPPNP to 99% saturation results in severe global broadening of peaks constituting the autoinhibited core of WASP and a general collapse of amide envelope (Figure 4-5B), which are consistent with a two-state conformational equilibrium between folded and unfolded populations on the surface of Cdc42. The indole amide resonance of W252 that was previously located at 9.4 ppm is also severely broadened, indicating that the autoinhibited fold of WASP melts and becomes largely unstructured upon binding to Cdc42-GMPPNP. Four characteristic peaks appear downfield-shifted, from their previous chemical shifts, in the Cdc42-GMPPNP-bound spectrum that are unique indicators of Cdc42-GMPPNP binding to residues of the CRIB motif (Figure 4-5B, blue squares) (Abdul-Manan *et al.* 1999; Buck *et al.* 2001). These observations are in contrast to those obtained from the spectrum of WASP in the presence of Cdc42-GDP (Figure 4-5C). Due to limitations on the solubility of Cdc42-GDP, the spectrum of $^1\text{H}/^{15}\text{N}$ -GBD-VCA was acquired in the presence of only ~90% saturating Cdc42-GDP. Overall, the spectrum of WASP GBD-VCA in the presence of Cdc42-GDP is highly

Figure 4-5. $^1\text{H}/^{15}\text{N}$ TROSY HSQC spectra of $^2\text{H}/^{15}\text{N}$ GBD-VCA in the presence of Cdc42-GMPPNP or Cdc42-GDP (in 90% H_2O , 10% D_2O). A. GBD-VCA (100 μM). B. GBD-VCA (100 μM) in the presence of 500 μM Cdc42-GMPPNP (99% saturation). C. GBD-VCA (100 μM) in the presence of 750 μM Cdc42-GDP (90% saturation). Peaks identified in A (red squares) and superimposed on C are GBD-VCA residues, including the CRIB motif, which broaden severely upon binding to Cdc42-GDP. Additional peaks identified in B and C (blue circles) are new downfield shifted peaks that appear upon binding to Cdc42-GMPPNP (Abdul-Manan *et al*, 1999) and Cdc42-GDP, respectively. Inset shows the GBD-VCA W252 peak that broadens in the presence of Cdc42-GMPPNP.



similar to the free GBD-VCA spectrum. Peaks representative of the autoinhibited core of WASP are well-dispersed and are slightly broadened but remain essentially unaffected by the addition of Cdc42-GDP. Collectively, these data suggest that the surface of Cdc42-GDP is primarily populated with the folded structure of WASP. Closer examination of the Cdc42-GDP spectrum revealed a number of peaks between 7.7 to 8.5 ppm of the spectrum that completely broaden (Figure 4-5C, red squares). In addition, two new peaks that are downfield-shifted appear (Figure 4-5C, blue circles) in positions similar to peaks of the CRIB motif in the Cdc42-GTP/WASP GBD complex, suggesting that Cdc42-GDP also binds to portions of the CRIB motif. Despite severe overlap of peaks at the center of the amide region, we were able to obtain partial assignments for several of residues, as described below. Using uniformly labeled $^1\text{H}/^{13}\text{C}/^{15}\text{N}$ -GBD-VCA and four triple resonance experiments (HNCO, HNCACO, CBCACONH, and HNCACB) (Muhandiram and Kay 1994), we were able to assign a stretch of five residues corresponding to A236 through A240 (Figure 4-6). These assigned residues encompass the N-terminal sequence of the CRIB motif, further substantiating the observation that Cdc42-GDP binds to WASP. The combined results indicate that both nucleotide states of Cdc42 can recognize and bind to regions of the CRIB motif of WASP. However, unlike Cdc42-GTP, the GDP-bound state of Cdc42 cannot induce major structural changes in GBD-VCA or completely destabilize the WASP autoinhibitory core.

Analyses of the NMR spectra indicate that both Cdc42-GDP and Cdc42-GMPPNP binds to the CRIB motif in the WASP GBD. We next wanted to examine if conversely WASP interacts with a defined surface on Cdc42 that is dependent on the nucleotide state. We acquired a $^1\text{H}/^{15}\text{N}$ -TROSY HSQC spectrum of $^2\text{H}/^{15}\text{N}$ -Cdc42-GDP

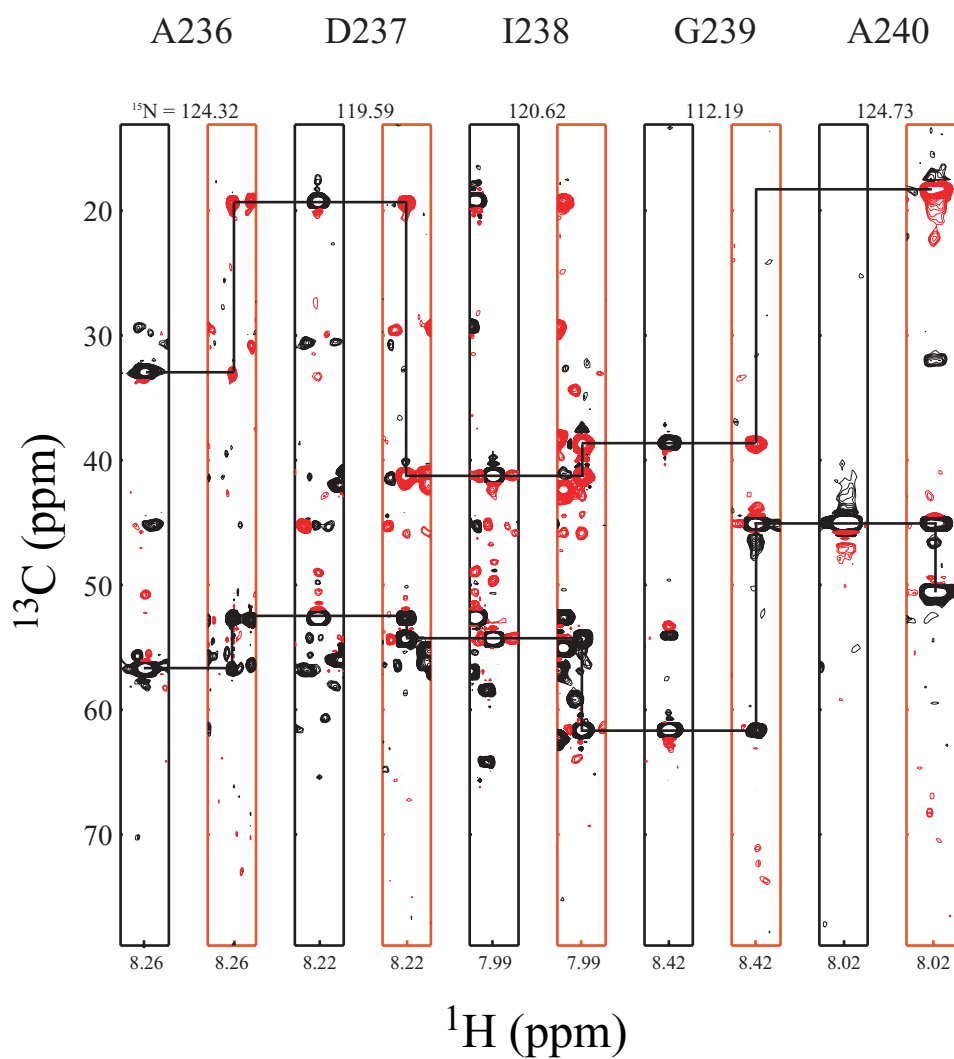


Figure 4-6A. NMR Assignments of $^2\text{H}/^{15}\text{N}/^{13}\text{C}$ -labeled GBD-VCA. CBCA(CO)NH (black) and HNCACB (red) strips shows a partial stretch of assigned CRIB motif residues.

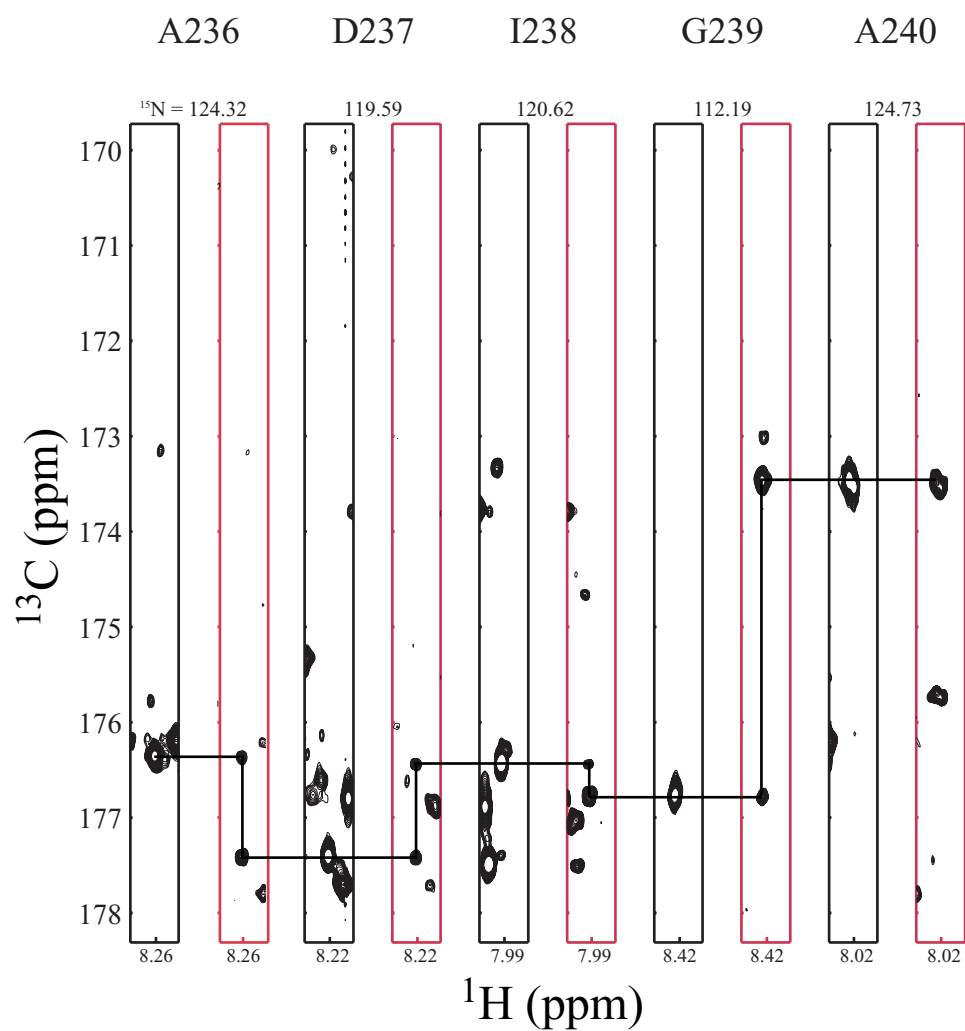


Figure 4-6B. NMR Assignments of $^2\text{H}/^{15}\text{N}/^{13}\text{C}$ -labeled GBD-VCA. HNCOSY (black) and HN(CA)COSY (red) strips show a partial stretch of assigned CRIB motif residues.

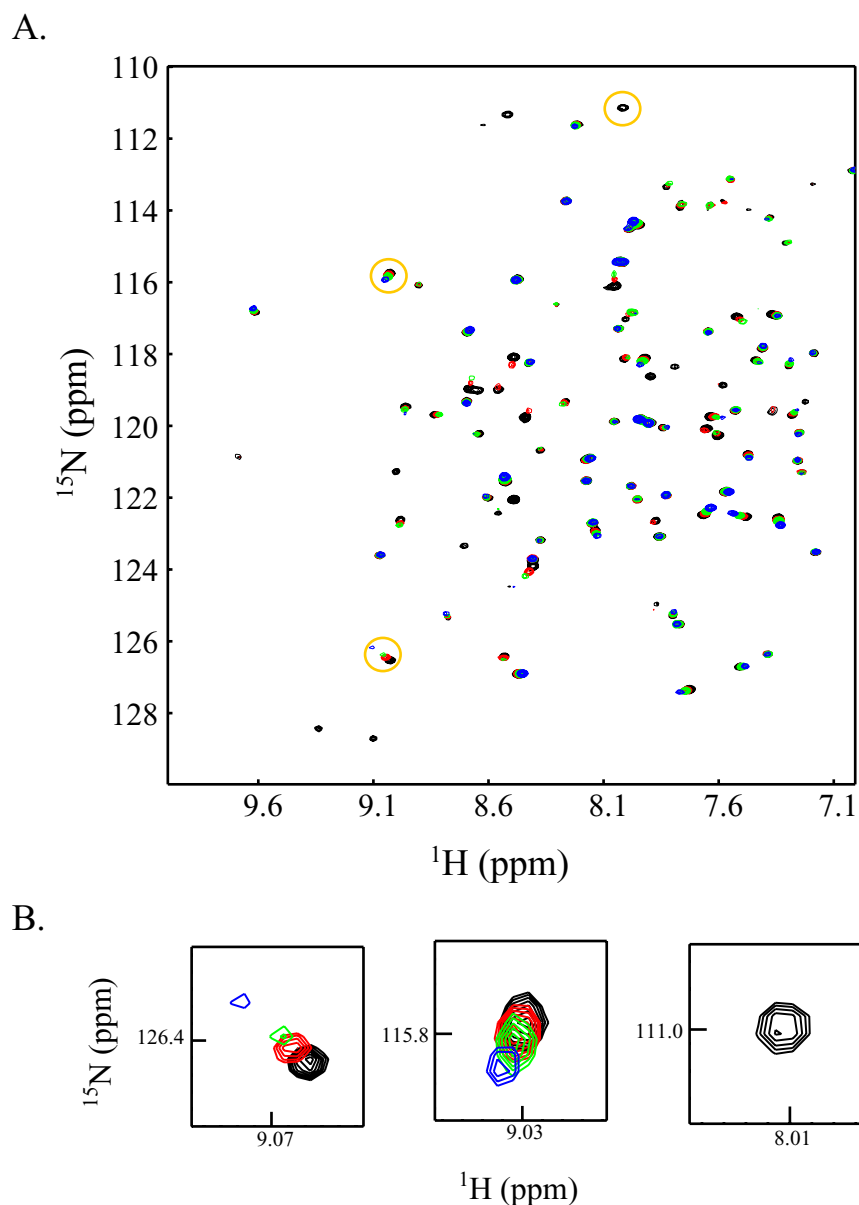


Figure 4-7. NMR analysis of Cdc42-GDP binding to WASP. $^1\text{H}/^{15}\text{N}$ TROSY HSQC spectrum of $^2\text{H}/^{15}\text{N}$ -Cdc42-GDP and increasing concentrations of unlabeled GBD-VCA. A. 100 μM Cdc42-GDP alone (black), with 50 μM GBD-VCA (red), with 100 μM GBD-VCA (green), and with 300 μM GBD-VCA. B. Examples of Cdc42 residues that move or broaden upon addition of GBD-VCA, including I46 (left; located on $\alpha 1$), G164 (middle; located on $\alpha 5$), and T25 (right; located on $\beta 2$).

alone and in the presence of unlabeled GBD-VCA (Figure 4-7). Comparison of the two spectra reveals that the reverse titration of GBD-VCA into $^2\text{H}/^{15}\text{N}$ -Cdc42-GDP (100 μM) results in significant line broadening of resonances around the center of amide region at substoichiometric concentrations of GBD-VCA (50 μM). These include backbone amide resonances of the following residues: G15, C18, L20, and Y23 from the alpha 1 helix; V42, V44, M45, L53, L55, and F56 from the beta 2/beta 3 hairpin; and G165 from the alpha 5 helix (Table 4-1). We also observed a number of peaks whose positions shift by >0.033 ppm (see Table 4-2 legend for chemical shift difference calculation information) in the presence of 300 μM GBD-VCA. These peaks include: T17, I21, S22, T25, and N26 corresponding to the alpha 1 helix; I46, E49, G48, and T52 of the beta 2/beta 3 hairpin; and K166 and E178 of the alpha 5 helix (Table 4-2). These results are summarized in Figure 4-8. In the structure of Cdc42-GMPPCP bound to WASP GBD, the CRIB motif of WASP forms a parallel strand along the beta 2 strand of Cdc42 and that contacts both alpha 1 and alpha 5 helices (Figure 4-9). Elements from the beta hairpin and alpha 1 helix of WASP also make contact with the beta 3 strand. We cannot distinguish the extent of WASP GBD interaction with the switch 1 and switch 2 regions of Cdc42-GDP since most of these resonances in both Cdc42-GDP alone and in the presence of GBD-VCA are not observed due to exchange broadening (Abdul-Manan *et al.* 1999). The similarities between the regions that broaden in the Cdc42-GDP reverse titration with the WASP GBD/Cdc42-GMPPCP structure suggests that the CRIB motif correspondingly binds to a similar surface of Cdc42-GDP. Therefore, the structural details of WASP interaction with Cdc42-GDP indicate that the CRIB motif binds to Cdc42 in a similar fashion analogous to Cdc42-GMPPCP.

Table 4-1. Chemical Shifts (ppm) of Cdc42 residues whose $^1\text{H}/^{15}\text{N}$ TROSY HSQC resonances decrease in intensity by >60% in the presence of 50 μM GBD-VCA.

Residue	HN	N
ALA 13	10.554	124.472
GLY 15	8.623	111.615
CYS 18	9.685	120.869
LEU 19	8.149	122.706
TYR 23	7.896	118.627
TYR 32	7.653	120.074
VAL 42	8.649	119.032
VAL 44	9.337	128.411
MET 45	8.407	123.713
LEU 53	9.443	132.248
LEU 55	8.532	126.420
PHE 56	8.710	123.358
ASP 63	8.556	118.980
ASP 65	7.874	122.639
VAL 93	7.801	125.289
LYS 131	7.978	121.671
THR 141	7.524	119.560
THR 161	8.053	107.756
GLY 164	9.026	115.755

Table 4-2. Chemical Shifts (ppm) of Cdc42 residues whose $^1\text{H}/^{15}\text{N}$ TROSY HSQC resonances shift by >0.033 ppm in the presence of $300\text{ }\mu\text{M}$ GBD-VCA. Differences in ^1H and ^{15}N chemical shifts were determined by using the equation $\Delta\delta=[(\Delta^1\text{H})^2+(\Delta^{15}\text{N}*0.15)^2]^{1/2}$.

Residues		HN	N	HN	N	$\Delta\delta$
		(Cdc42)		(+ GBD-VCA)		
THR	17	8.960	119.458	8.962	119.675	0.0326
ILE	21	8.556	122.442	8.567	122.169	0.0424
SER	22	8.836	119.686	8.784	119.698	0.0521
THR	24	7.613	106.929	7.586	106.712	0.0427
ASN	26	7.522	116.949	7.468	117.200	0.0662
LYS	27	7.634	119.741	7.585	119.755	0.0492
VAL	33	7.727	127.342	7.774	127.423	0.0480
ILE	46	9.026	126.522	9.105	126.174	0.0944
GLY	48	8.515	106.264	8.480	106.121	0.0416
GLU	49	7.665	122.480	7.633	122.300	0.0420
THE	52	8.681	118.966	8.660	118.267	0.1071
GLN	61	8.264	119.309	8.295	119.431	0.0354
GLU	62	8.982	122.620	8.991	122.974	0.0538
TYR	64	8.010	118.137	7.975	117.989	0.0418
LYS	96	7.971	116.838	7.977	116.575	0.0399
GLN	134	8.005	117.025	7.961	116.865	0.0505
LYS	166	8.491	118.084	8.517	118.887	0.1231
GLU	178	7.479	122.531	7.536	122.447	0.0574

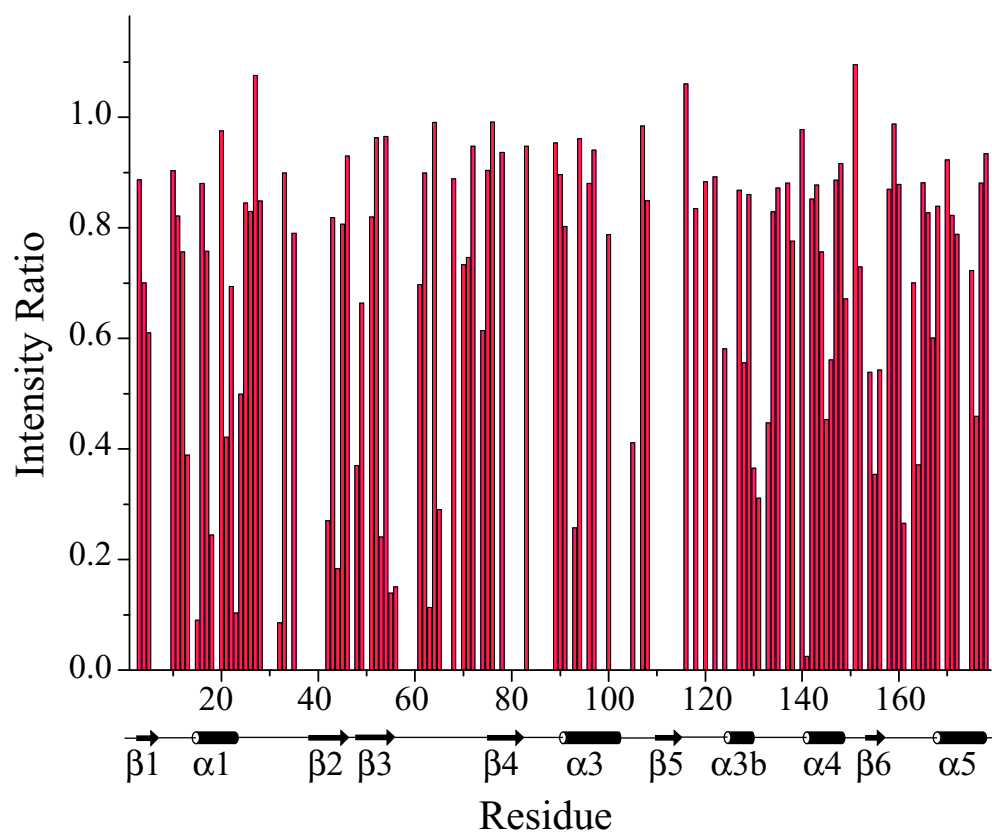
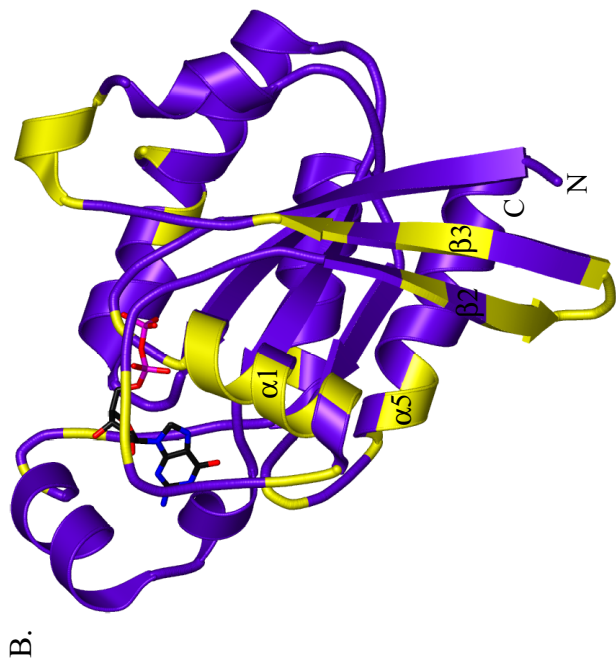
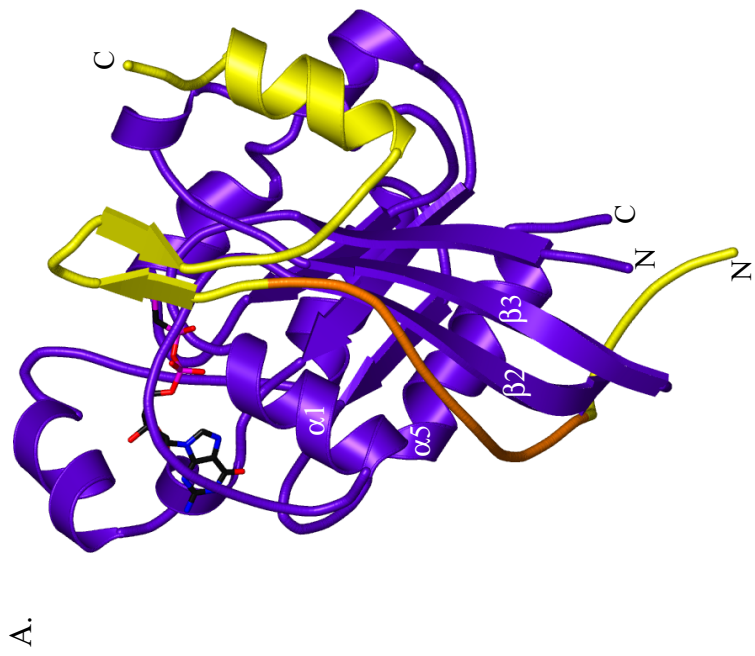


Figure 4-8. Intensity ratios of WASP residues upon binding to Cdc42-GDP. Normalized ratios of $^2\text{H}/^{15}\text{N}$ Cdc42-GDP peak intensities in the presence of GBD-VCA relative to $^2\text{H}/^{15}\text{N}$ Cdc42-GDP peak intensities alone. Cdc42-GDP resonances that were absent from the spectra are indicated by an intensity ratio of 0. The secondary structural elements of Cdc42-GDP are indicated below.

Figure 4-9. Comparison of WASP binding interface with Cdc42-GTP and Cdc42-GDP. A. Structure of a truncated WASP GBD (residues 230-277; yellow) bound to Cdc42-GTP (residues 1-178; purple) (Protein Data Bank ID code 1CEE) (Abdul-Manan *et al*, 1999). The WASP CRIB motif is highlighted in orange. B. The structure of Cdc42-GDP (purple; Protein Data Bank ID code 1DOA) (Hoffman *et al*, 2000). Residues whose $^1\text{H}/^{15}\text{N}$ TROSY HSQC resonances decrease in intensity by >60% or shift by >0.033 ppm when 50 μM GBD-VCA is added to 100 μM $^2\text{H}/^{15}\text{N}$ Cdc42-GDP are colored yellow. Differences in ^1H and ^{15}N chemical shifts were determined by using the equation $\Delta\delta=[(\Delta^1\text{H})^2+(\Delta^{15}\text{N}*0.15)^2]^{1/2}$.



Collectively, these results reveal that Cdc42 is capable of interacting and binding to WASP in both nucleotide states and biasing the allosteric equilibrium towards the active state of WASP. However, the extent of the equilibrium shift is dictated by the magnitude of the C parameter. In the case of Cdc42-GTP, the C parameter is a small value corresponding to a sizable shift in the WASP equilibrium towards the unfolded, active state. Binding of Cdc42-GDP also biases the WASP allosteric equilibrium towards the unfolded, active state, which is reflected by its C parameter value ($C \ll 1$). However, the magnitude of the C parameter for Cdc42-GDP is ~5-fold higher relative to Cdc42-GTP. Thus, the extent of the equilibrium shift is significantly reduced and WASP is heavily populated by the folded, autoinhibited state in the presence of Cdc42-GDP, made evident by the NMR structural analysis. Consequently, Cdc42-GTP is a full agonist of WASP whereas Cdc42-GDP is only a partial agonist.

Conclusion

The Ras family of GTPases is generally considered to function as a molecular switch in regulating signal transduction pathways. The GTP-bound state switches the signaling pathway “on” while the GDP-bound state switches the signaling pathway “off.” This phenomenon has been observed for many Ras superfamily of GTPases, including those in the subfamily of Rho GTPases involved in actin cytoskeletal remodeling. The basis for the nucleotide switch is established from a difference in binding affinity for the effector in the two nucleotide states. The GTP-bound state has a higher affinity for the effector and can therefore bind and activate downstream effectors more effectively than the lower affinity GDP-bound state. This has been demonstrated in several studies of

interactions between Rho GTPases and the isolated GTPase binding domains of signaling effectors (Thompson *et al.* 1998; Nomanbhoy and Cerione 1999; Owen *et al.* 2000; Buchwald *et al.* 2001). Thus, the affinity switch has served as the biochemical basis of GTPase activation and signaling. However, many signaling effectors are also regulated through autoinhibitory interactions where intermolecular GTPase binding must disrupt and replace intramolecular interactions. It is not entirely clear if the canonical view of the nucleotide switch is sufficient to account for the activation of autoinhibited effectors. The collective results from this thesis work challenges this fundamental concept of the GTPase nucleotide switch and suggest that a more complex mechanism is involved in the modulation and activation of autoinhibited GTPase effectors. A quantitative analysis of the interactions between Cdc42 and WASP revealed that the Cdc42-WASP binding equilibrium is coupled to the conformational equilibrium of WASP. Application of the two-state model to GDP-bound state of Cdc42 demonstrated that the nucleotide switch changes the affinity for WASP *and* the ability of Cdc42 to shift the WASP conformational equilibrium toward the active state. Consequently, even at saturating concentrations, Cdc42-GDP is a poor agonist of WASP and can only stimulate partial activity, whereas saturating concentrations of Cdc42-GTP is a significantly better agonist of WASP and is capable of stimulating maximal activity.

What is the physical basis for the stronger coupling observed for Cdc42-GTP and which is absent in Cdc42-GDP? A recent study by Hatley *et al.* (Hatley *et al.* 2003), suggested a potential explanation. They attempted to identify critical interactions between residues that link the regions responsible for nucleotide and effector binding in the G protein family using Statistical Coupling Analysis (SCA) (Hatley *et al.* 2003). The SCA

method provides an approach for approximating the evolutionary coupling between a given pair of residues and the identification of coevolving sequences in multiple sequence alignments (Lockless and Ranganathan 1999; Suel *et al.* 2003). The authors make the assumption that the coevolution of residues in particular positions in the primary sequence is driven by the energetic coupling of residues, defined as ΔG_{stat} in the SCA method, forming a cooperative unit. The authors find that a small number of G protein residues, surrounding the nucleotide and substrate binding sites, behaves as a coevolving unit. In the GTP-bound state, they find that coevolving residues form a physically connected network linking the nucleotide binding site to the effector binding site. In contrast, in the GDP-bound state, this physical connectivity is broken, providing an alternative explanation for the observed differences between the GDP and the GTP nucleotide states. The dependence of network connectivity on the G protein nucleotide state suggests that these residues form a cooperative unit and make up a part of the nucleotide switch. A network of coevolving residues is similarly observed for other distantly related G protein family members, including h-Ras. In the context of Cdc42, it is possible that WASP also biases the equilibrium of Cdc42 in the two nucleotide states, but preferentially binds to the activated GTP-bound state of Cdc42. In the Cdc42-GTP, the nucleotide and effector binding sites form a physically connected network that allows Cdc42-GTP to be more effective at distinguishing between the two states of WASP, bypassing the need for WASP to bias the Cdc42 equilibrium. In contrast, the network connectivity is broken in the GDP-bound state of Cdc42 making Cdc42-GDP less effective at discriminating between the two states of WASP and may also require WASP

binding to shift the Cdc42 equilibrium. As a result, Cdc42-GDP is a poorer agonist of WASP. Further investigations will be required to fully resolve these issues.

The formation of the immunological synapse (IS) between a T cell and antigen presenting cell (APC) conjugate requires the activation of WASP by Cdc42-GTP to mediate the reorganization of T cell receptors, adhesion molecules, and the actin cytoskeleton for sustained T cell signaling. During this process, Cdc42-GTP and WASP are independently localized to the IS. Cdc42 is prenylated at the C-terminus and is attached to the membrane. Local concentration of Cdc42 is mediated through interactions with its guanine nucleotide exchange factor (GEF) to coordinate and activate signaling events. WASP recruitment to the IS does not require interactions between the GBD and Cdc42-GTP. WASP recruitment to the T cell-APC interface is largely regulated through interactions with its proline rich domain and the adaptor protein Nck (Cannon *et al.* 2001; Labno *et al.* 2003; Barda-Saad *et al.* 2005). Additional studies also suggest that a N-WASP/WIP complex is recruited to the IS through interactions with CrkL and ZAP-70 (Sasahara *et al.* 2002). As we have previously shown, the binding affinity of Cdc42-GTP for the GBD in full-length WASP is significantly lower (~100-fold) than compared to the isolated GBD. Thus, it is unlikely that binding energy of Cdc42-GTP is sufficient to both recruit and activate WASP (Buck *et al.* 2001). High local concentrations of both Cdc42-GTP and WASP in a spatially restricted area then result in WASP activation, leading to specific signaling events. If the Cdc42 nucleotide switch were based solely on a change in affinity, then the specificity and fidelity of signaling could be diminished (Figure 4-10). High local concentrations of WASP could overcome a weak affinity between Cdc42-GDP and WASP and result in unregulated and

inappropriate signaling by Cdc42. However, if the Cdc42 nucleotide switch is based on the coupling of binding affinity *and* the conformational equilibrium of WASP, as we have shown here in our biochemical and structural analysis, then the allosteric properties of the system would restrict the ability of a weak agonist Cdc42-GDP to activate WASP. Thus, these properties may guarantee that WASP will be activated only by the appropriate signals, thereby ensuring the specificity and fidelity of GTPase signaling.

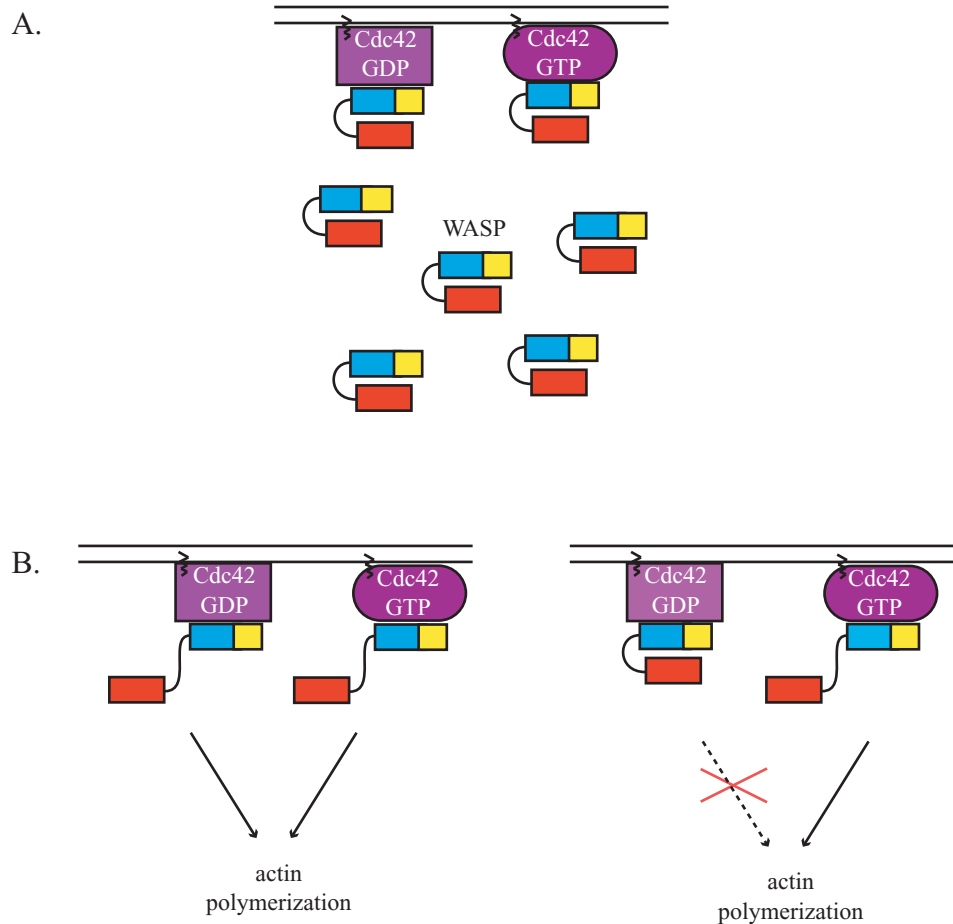


Figure 4-10. Biological implications for the GTPase nucleotide switch. A. Localization of Cdc42 and WASP at the membrane. B. Left. Nucleotide switch based solely on change in affinity. High concentrations of WASP can override the switch and Cdc42-GDP can also activate downstream signaling pathways. Right. Nucleotide switch based on both the change in affinity and efficiency of coupling of Cdc42 binding and WASP allosteric equilibria. Only Cdc42-GTP can activate WASP, therefore maintaining high specificity and fidelity of GTPase signaling.

Materials and Methods

The materials generated and experimental methods used for this chapter follow many of the protocols described in Chapter 3. Additional methods that were used are described in the following text.

Fluorescence Competition Experiments

The binding affinities of WASP proteins for Cdc42t-GMPPNP and Cdc42t-GDP can be determined using fluorescence competition experiments. The basic strategy involves measuring the binding affinity of a receptor for a fluorescent ligand and then determining the affinity of a non-fluorescent ligand for receptor by displacement of the fluorescent ligand. Affinities obtained from fluorescence competition experiments are not as accurate as those obtained from direct binding because of errors in the K_D of the fluorescent ligand. However, by taking effort to obtain a precise measurement of K_D of the fluorescent ligand and by dialyzing all proteins into the same buffer, we can minimize the error propagated into the measurement of the K_D of the non-fluorescent ligand.

To measure WASP affinity for Cdc42t by competition, we used a previously described fluorescence resonance energy transfer (FRET)-based sensor for the GTPase (Seth *et al.* 2003). This reagent consists of the WASP GBD (residues 230-310) flanked by the fluorophores enhanced cyan fluorescent protein (eCFP) and enhanced yellow fluorescent protein (eYFP) at the N- and C-termini, respectively. The isolated sensor has a high FRET value (ratio of YFP emission, 526 nm, to CFP emission, 476 nm) upon CFP excitation ($\lambda_{ex} = 433$ nm) of ~ 2.4 in buffer containing 20 mM Hepes pH 7.5, 150 mM KCl, 2 mM $MgCl_2$, and 2 mM DTT. Binding of Cdc42t changes the FRET value to ~ 1.6 .

Using this sensor, the K_D for Cdc42t can be determined by monitoring the FRET change during titration with Cdc42t. For example, up to 1 μM of Cdc42t-GMPPNP is titrated into a sample containing 15 nM of FRET sensor. The FRET values are plotted against Cdc42t concentration and fit to a single site binding isotherm (Eq. 2, with sensor and Cdc42 as R and L, respectively) to obtain a K_D (29 nM). The K_D of WASP for Cdc42t can subsequently be determined by monitoring the FRET change during titration of WASP, as Cdc42t is displaced from the sensor. For example, up to 50 μM of WASP mutant GBD-VCA I290Q is titrated into a sample containing 15 nM of FRET sensor and a saturating 1 μM of Cdc42t-GMPPNP. Under conditions where the concentration of FRET sensor is significantly smaller than both ligands, such that the free and total ligand concentrations are approximately equal, the competition data obtained is fit according to:

$$y = F_f + (F_b - F_f) / (K_{D,1}([C] + K_{D,2}) / (K_{D,2}[L] + 1)) \quad (\text{Eqn. 4-1})$$

where F_f and F_b are the FRET ratios of the free and Cdc42t-bound sensor, $[L]$ is the total ligand Cdc42t concentration, $[C]$ is the total WASP concentration, $K_{D,1}$ is the equilibrium dissociation constant of Cdc42t-GMPPNP for sensor, and $K_{D,2}$ is the equilibrium dissociation constant of the competing ligand for Cdc42t-GMPPNP (Vinson *et al.* 1998). In cases where these experimental conditions cannot be achieved, the data must be analyzed with the general fourth order equation describing competitive binding, which must be solved numerically (Panchal *et al.* 2003).

NMR acquisition

NMR data were collected on Varian Innova spectrometers operating at 500- or 600-MHz ^1H frequency. All experiments were carried out at 25°C. To probe the structural details of WASP in complexes with Cdc42, $^1\text{H}/^{15}\text{N}$ transverse relaxation-optimized spectroscopy (TROSY) heteronuclear sequential quantum correlation (HSQC) spectra were acquired on 100 μM $^2\text{H}/^{15}\text{N}$ GBD-VCA protein in 10 mM imidazole, pH 7, 50 mM KCl, 1mM MgCl_2 , and 10 mM EGTA in the presence of either 500 μM Cdc42-GMPPNP or 750 μM Cdc42-GDP. To determine the binding interface between Cdc42-GDP and GBD-VCA, $^1\text{H}/^{15}\text{N}$ TROSY HSQC spectra were acquired on a 100 μM sample of $^1\text{H}/^{15}\text{N}$ Cdc42-GDP in 20 mM Tris, pH 7, 100 mM NaCl, 2 mM MgCl_2 , and 5 mM DTT in the presence of increasing concentrations of GBD-VCA (up to 300 μM). Backbone ^1HN , ^{15}N , $^{13}\text{C}\alpha$, $^{13}\text{C}\beta$, and ^{13}CO assignments were obtained for GBD-VCA through the following ^2H -decoupled, triple resonance spectra applied to a $^2\text{H}/^{15}\text{N}/^{13}\text{C}$ -labeled sample: CT-HNCa, CT-HN(CO)Ca, HN(Ca)Cb, and HN(COCa)Cb (Muhandiram and Kay 1994).

References

- Abdul-Manan, N., *et al.* (1999). "Structure of Cdc42 in complex with the GTPase-binding domain of the 'Wiskott-Aldrich syndrome' protein." Nature **399**(6734): 379-83.
- Barda-Saad, M., *et al.* (2005). "Dynamic molecular interactions linking the T cell antigen receptor to the actin cytoskeleton." Nat Immunol **6**(1): 80-9.
- Bourne, H. R. (1995). "GTPases: a family of molecular switches and clocks." Philos Trans R Soc Lond B Biol Sci **349**(1329): 283-9.
- Buchwald, G., *et al.* (2001). "Conformational switch and role of phosphorylation in PAK activation." Mol Cell Biol **21**(15): 5179-89.
- Buck, M., *et al.* (2001). "Global disruption of the WASP autoinhibited structure on Cdc42 binding. Ligand displacement as a novel method for monitoring amide hydrogen exchange." Biochemistry **40**(47): 14115-22.
- Buck, M., *et al.* (2004). "A two-state allosteric model for autoinhibition rationalizes WASP signal integration and targeting." J Mol Biol **338**(2): 271-85.
- Cannon, J. L., *et al.* (2001). "Wasp recruitment to the T cell:APC contact site occurs independently of Cdc42 activation." Immunity **15**(2): 249-59.
- Hatley, M. E., *et al.* (2003). "Allosteric determinants in guanine nucleotide-binding proteins." Proc Natl Acad Sci U S A **100**(24): 14445-50.
- Hoffman, G. R. and R. A. Cerione (2000). "Flipping the switch: the structural basis for signaling through the CRIB motif." Cell **102**(4): 403-6.

- Labno, C. M., *et al.* (2003). "Itk functions to control actin polymerization at the immune synapse through localized activation of Cdc42 and WASP." Curr Biol **13**(18): 1619-24.
- Leung, D. W. and M. K. Rosen (2005). "The nucleotide switch in Cdc42 modulates coupling between the GTPase-binding and allosteric equilibria of Wiskott-Aldrich syndrome protein." Proc Natl Acad Sci U S A **102**(16): 5685-90.
- Lockless, S. W. and R. Ranganathan (1999). "Evolutionarily conserved pathways of energetic connectivity in protein families." Science **286**(5438): 295-9.
- Muhandiram, D. R. and L. E. Kay (1994). "Gradient-enhanced triple-resonance three-dimensional experiments with improved sensitivity." J Magn Res Ser B **103**: 203-16.
- Nomanbhoy, T. and R. A. Cerione (1999). "Fluorescence assays of Cdc42 interactions with target/effector proteins." Biochemistry **38**(48): 15878-84.
- Owen, D., *et al.* (2000). "Residues in Cdc42 that specify binding to individual CRIB effector proteins." Biochemistry **39**(6): 1243-50.
- Panchal, S. C., *et al.* (2003). "A conserved amphipathic helix in WASP/Scar proteins is essential for activation of Arp2/3 complex." Nat Struct Biol **10**(8): 591-8.
- Pervushin, K., *et al.* (1997). "Attenuated T2 relaxation by mutual cancellation of dipole-dipole coupling and chemical shift anisotropy indicates an avenue to NMR structures of very large biological macromolecules in solution." Proc Natl Acad Sci U S A **94**(23): 12366-71.
- Rohatgi, R., *et al.* (1999). "The interaction between N-WASP and the Arp2/3 complex links Cdc42-dependent signals to actin assembly." Cell **97**(2): 221-31.

- Rudolph, M. G., *et al.* (1998). "The Cdc42/Rac interactive binding region motif of the Wiskott Aldrich syndrome protein (WASP) is necessary but not sufficient for tight binding to Cdc42 and structure formation." J Biol Chem **273**(29): 18067-76.
- Sasahara, Y., *et al.* (2002). "Mechanism of recruitment of WASP to the immunological synapse and of its activation following TCR ligation." Mol Cell **10**(6): 1269-81.
- Seth, A., *et al.* (2003). "Rational design of genetically encoded fluorescence resonance energy transfer-based sensors of cellular Cdc42 signaling." Biochemistry **42**(14): 3997-4008.
- Sondermann, H., *et al.* (2004). "Structural analysis of autoinhibition in the Ras activator Son of sevenless." Cell **119**(3): 393-405.
- Suel, G. M., *et al.* (2003). "Evolutionarily conserved networks of residues mediate allosteric communication in proteins." Nat Struct Biol **10**(1): 59-69.
- Thompson, G., *et al.* (1998). "Delineation of the Cdc42/Rac-binding domain of p21-activated kinase." Biochemistry **37**(21): 7885-91.
- Vinson, V. K., *et al.* (1998). "Interactions of Acanthamoeba profilin with actin and nucleotides bound to actin." Biochemistry **37**(31): 10871-80.

Chapter 5 Conclusion of thesis work

The interaction between the intracellular signaling protein WASP and the Rho family GTPase Cdc42 is one of a few examples where the thermodynamic and allosteric properties have been studied rigorously. We have provided a biochemical and biophysical description of the regulation and activation of WASP by Cdc42 using the classical allosteric framework described by Monod *et al.* (Monod *et al.* 1965) in order to understand how Cdc42 binding is coupled to WASP activation. We have shown that the WASP allosteric equilibrium involves transitions between a folded, inactive state and an unfolded active state and that WASP affinity for Cdc42, activity toward Arp2/3 complex, and activation by Cdc42 are all functions of this equilibrium. Furthermore, application of the two-state model to the GDP-bound state of Cdc42 revealed that Cdc42-GTP is more effective at distinguishing between the two states of WASP than Cdc42-GDP and is therefore a full agonist of WASP. Thus, a change in affinity between the nucleotide states in addition to the efficiency of coupling between the GTPase binding equilibrium and the allosteric equilibrium of WASP provide a mechanism that preserves the specificity and fidelity of GTPase signaling in crowded intracellular environments.

The allosteric equilibrium and activity of WASP are ultimately dictated by a balance between two parameters, the equilibrium constant (K_{eq}) and ratio of the binding affinities of the activator for the active and inactive states (C parameter). The combination of these parameters defines the extent of coupling between the conformational equilibrium and the binding of a given input and determines the requirement for activation. For high values of WASP K_{eq} and in the presence Cdc42-GTP, the coupling of C parameters from additional inputs (e.g. C_1 , C_2 , C_3 ,... C_n) can work

in concert to change K_{eq} and allow for the high affinity interaction between Cdc42-GTP and the active conformation of WASP to occur, resulting in the cooperative activation of WASP. We have found with our model that we can artificially modulate the folding stability or K_{eq} of a protein, through the introduction of mutations, to obtain different levels of WASP activity. Multiple inputs can also function in the same manner as mutations and act upon the same allosteric equilibrium to change K_{eq} . The fractional activity of a protein with n inputs can be quantitatively described by the following expression:

$$f_{a,sat(1...n)} = 1 / (C_1 \cdots C_n K_{eq} + 1). \quad (\text{Eqn. 5-1})$$

where C_1 is the C parameter value for the first input and C_n represents the C parameter for n input at saturating concentrations. For example, if the presence of only two inputs is sufficient for activation, then the combination of C_1 and C_2 can shift the allosteric equilibrium completely toward the active state. However, if the two inputs are not sufficient, then the combination of C_1 and C_2 can only partially shift the allosteric equilibrium, leading to limited activation. Thus, depending on the magnitude of each C parameter, a single input can provide partial activation and only the addition of a second input causes significant activation. Alternatively, each ligand alone is not a good activator and only the concomitant addition of both ligands prompts full activation.

In the case of WASP, many studies have suggested that Cdc42 is not sufficient to cause full WASP activation and requires the input of at least one other activator, such as Nck, Grb2, and PIP2 (Higgs and Pollard 1999; Rohatgi *et al.* 1999; Prehoda *et al.* 2000).

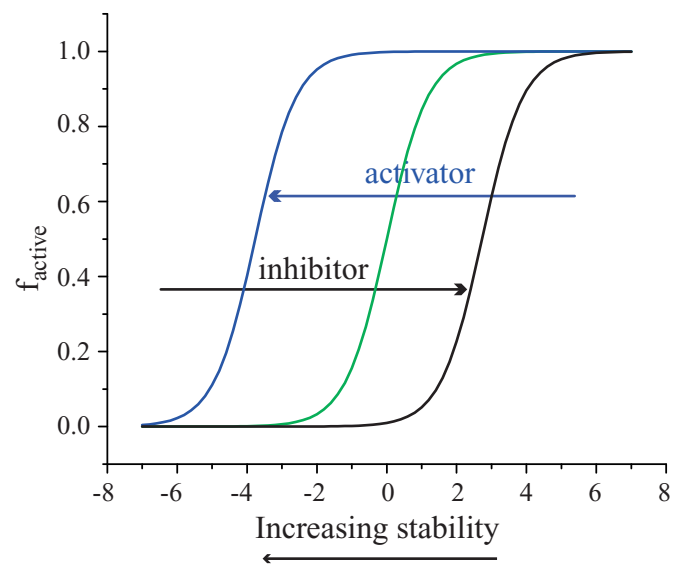


Figure 5-1. Predicted WASP activity in the presence of activators and inhibitors. Difference in fractional activities of WASP (green) in the presence of activator (blue) and in the presence of inhibitor (black).

Under these conditions, a fraction of WASP occupying the inactive state inevitably remains and binding of a second input is required to decrease K_{eq} and completely shift the WASP allosteric equilibrium towards the active state (fractional activity curve toward the left in Figure 5-1). However, the biochemical and mechanistic details of these interactions and exactly how these inputs affect the WASP allosteric equilibrium are not well understood. Both Nck and Grb2 are SH3 domain containing proteins that have been shown to enhance stimulation of N-WASP activation by Cdc42 (Carlier *et al.* 2000; Rohatgi *et al.* 2001; Benesch *et al.* 2002). Binding of Nck and Grb2 to the polyproline region may also regulate the WASP allosteric equilibrium concomitantly with Cdc42, which binds to the GBD. The increased stabilization of the active state of WASP gained through binding of Nck or Grb2 may be sufficient for Cdc42 to induce the full activation of WASP (or vice versa). Interactions with PIP2 may also regulate the WASP allosteric equilibrium by facilitating the disruption of autoinhibitory contacts between the BGBD module and VCA and causing the exposure of the VCA domain. Work in this thesis has shown that the basic region increases the stability of the intramolecular interactions between GBD and VCA, thereby sequestering VCA from interactions with Arp2/3 complex. Binding of PIP2 may function to counteract these effects.

Conversely, inhibitors can also act upon the system and maintain the protein in a stabilized, inactive state. There are many other ligands, synthetic and physiological, that are known to negatively regulate WASP activity, such as wiskotstatin and WIP. The efficiency of an inhibitor on the WASP allosteric equilibrium would be dictated by the magnitude of the C parameter, where increasingly larger values (such that $C \gg 1$) shifts the fractional activity curve proportionally to the right in Figure 5-1, presumably by

stabilizing the inactive state of WASP and effectively raise K_{eq} . Thus, for larger values of C , the inactive, autoinhibited state of WASP would be significantly stabilized and heavily populated through the preferential binding of the inhibitor to the inactive state. Very little WASP would be occupying the active state in the presence of such an inhibitor. Wiskostatin has been shown to prevent actin polymerization mediated by N-WASP in response to PIP2 and Cdc42 *in vitro* (Peterson *et al.* 2001; Peterson *et al.* 2004). Addition of wiskostatin increases the lag time associated with the barrier to actin nucleation and formation of filaments required for Arp2/3 complex branching in pyrene-actin polymerization assays ($IC_{50} \leq 10 \mu M$). Previous NMR data show that the isolated GBD is unfolded in solution (Kim *et al.* 2000; Torres and Rosen 2003). Further NMR analyses demonstrate that addition of wiskostatin induces the folding of the GBD, producing HSQC spectra that are similar to GBD bound to VCA in the autoinhibited conformation (Kim *et al.* 2000). Examination of the solution structure of the WASP/wiskostatin complex reveals that wiskostatin is bound to WASP between the beta hairpin and alpha 3 helix of the GBD (Peterson *et al.* 2004). These results together suggest that wiskostatin directly inhibits WASP through the conformational stabilization of the autoinhibited GBD fold. These data also support the hypothesis that wiskostatin shifts the allosteric equilibrium of WASP toward the autoinhibited state, effectively increasing K_{eq} and antagonizing the allosteric effects of activation by Cdc42 and PIP2. WIP also has been shown to negatively regulate N-WASP activity, although the exact mechanism through which WIP interacts with N-WASP is not fully understood. It is possible that WIP may regulate N-WASP by stabilizing the inactive state of N-WASP. Previous work with the WIP/N-WASP complex *in vitro* (Ramesh *et al.* 1997; Martinez-

Quiles *et al.* 2001) is consistent with a mechanism where interactions with WIP maintains WASP autoinhibited conformation that sequesters the VCA domain from interactions with Arp2/3 complex. Further investigations of the WIP regulatory mechanism, including the quantitation of these biochemical interactions, may further facilitate understanding of how WASP function can be modulated by inhibitors *in vitro* and *in vivo*, although these experiments will be challenging due to material generation.

Ultimately, a different number of inputs, including both activators and inhibitors, may function in combination to cooperatively regulate WASP activity through interactions with the various domains of WASP (Figure 5-1). Interactions of an inhibitor, such as WIP with the EVH1 domain, may stabilize the inactive WASP state and the binding of Cdc42 and PIP2 together to the GBD and basic region are required to work in concert to disrupt these interactions and shift the WASP equilibrium toward the active state. Similar systems where the regulatory mechanism involves a combination of activators and inhibitors have been identified, including the metabolic enzyme aspartate transcarbamylase (ATCase) (Howlett *et al.* 1977). ATCase catalyzes the formation of N-carbamoyl aspartate, a metabolic substrate in pyrimidine synthesis from carbamoyl phosphate (Cbmp) and L-aspartate. In the absence of any ligand, the T state is highly stabilized where the equilibrium constant, K_{eq} , is 250. ATCase is feedback inhibited by the end product of pyrimidine synthesis, CTP, which stabilizes the inactive, T conformation of the protein and results in a 5-fold increase in K_{eq} (from 250 to 1250 with CTP). However, the addition of the first substrate Cbmp, significantly shifts the majority of the ATCase molecules to the R state even in the presence of CTP, where K_{eq} changes from 1250 to 35. ATCase is also allosterically activated by ATP, the end product of

purine synthesis, and favors the active, R state by lowering K_{eq} by ~3.5-fold (from $K_{eq}=250$ to 70 with ATP). Together with Cbmp, ATP shifts the equilibrium completely toward the active state of ATCase (from $K_{eq}=250$ to 2). Thus, different combinations of nucleotide and Cbmp result in differential shifting of the allosteric equilibrium of ATCase.

The modular nature of many autoinhibited proteins provides intrinsic variability and flexibility where the function of a signaling module can easily be modified by the addition or subtraction of other regulatory modules. This type of organizational system allows for additional layers of regulation and for the tuning of activity in accordance to available input. Thus, the modularity of such a system provides a mechanism through which protein properties evolved. We have shown here that the folding stability of WASP can be artificially modulated through the introduction of mutations or by the addition of the basic region of residues N-terminal to the GBD. These perturbations in stability alone can generate very different activities in WASP. Based upon these observations, it is reasonable to speculate that evolution also works in a similar manner to allosterically couple interactions and regulate stability over time in such autoinhibited systems. A protein like WASP can transition among different regimes by increasing stability, from one that requires no ligand for full activity to a regime where multiple signaling inputs are required for full activation. For example, a protein may require one ligand to display partial activity and a second for complete activation, as observed in the case of WASP and PAK (Figure 5-2). Further changes in stability can alter the behavior to require two ligands for significant activation, as observed for Cdk2 (Prehoda and Lim 2002). Thus, evolution can modulate the regulatory equilibrium by shifting along a range

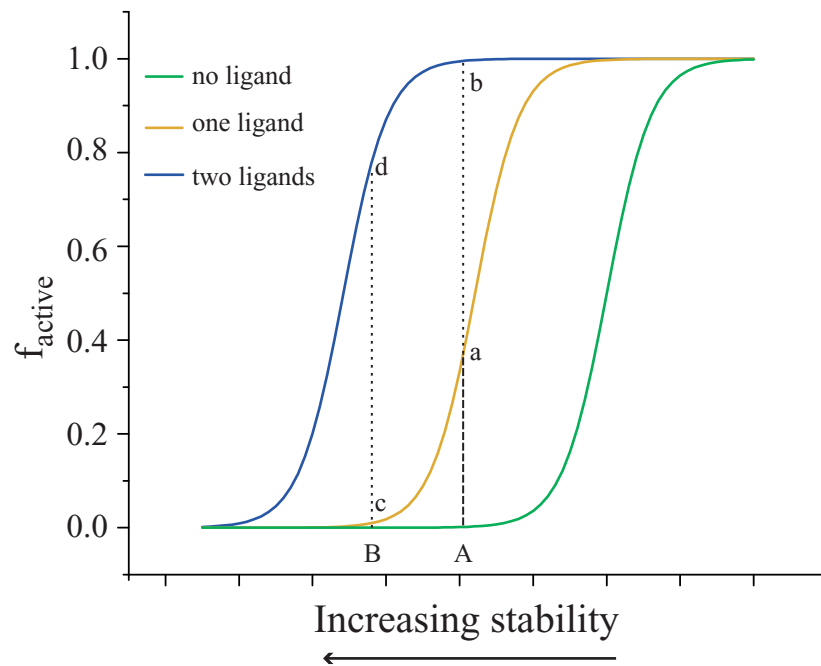


Figure 5-2. Evolvability of protein behavior in a modular system. Fractional activity is plotted as a function of effector stability alone (green), in the presence of one activator (yellow), and in the presence of two activators (blue) (adapted from Buck *et al*, 2004). At stability A, one ligand generates partial activation (a) whereas two ligands effect full activation (b). At stability B, one ligand results in very little activation (c) and requires two ligand to achieve significant levels of activation (d).

of stabilities and tune both the stability of the effector and the allosteric constant of a given ligand (C parameter) to an appropriate range (Buck *et al.* 2004).

Many other GTPase signaling proteins are also regulated through intramolecular interactions. For example, mDia, PAK, and MKL3 are other Rho family GTPase effectors that are also regulated through autoinhibition. Given the similar structural organization of these GTPase effector molecules, it is likely that in many of these proteins the regulatory mechanisms will be similar to WASP, where the specificity and fidelity of GTPase signaling are maintained through a balance of regulatory intramolecular and intermolecular interactions. In addition, the modular architecture of such autoinhibitory effectors affords the protein with the ability to integrate multiple inputs that serve to cooperatively activate and regulate downstream signaling events.

The knowledge and concepts obtained from studies of the allosteric interactions of autoinhibited systems, such as those developed with WASP, can be used to engineer switchable signaling proteins. The generation of a switchable signaling molecule, which can be activated independently of its physiological stimulus, may be used in a variety of investigations in order to further our understanding of how individual proteins affect a signaling pathway and the immediate outcome. Dueber *et al.* recently described an elegant way to design new functionality through the recombination of modular domains (Dueber *et al.* 2003; Dueber *et al.* 2004). The authors combined the N-WASP VCA domain with the heterologous autoinhibitory domains to control activity toward Arp2/3 complex. They demonstrate that by altering binding affinities and the linker lengths between domains the activation levels of N-WASP VCA can be selectively tuned to produce different types of gating mechanisms (Lim 2002; Prehoda and Lim 2002). We

can use a similar approach and apply our understanding of the biochemical and biophysical properties of the highly characterized WASP system described in this thesis work, to engineer a novel, allosterically coupled signaling photoswitch. The activity of WASP may be regulated by a light stimulus through the coupling to known photoreceptor domains, including *A. sativa* LOV2/J α , *A. thaliana* phytochrome B/PIF3, and *E. halophila* PYP, and selectively tuned with the series of destabilized WASP mutants generated in this study. The successful engineering of a photoswitchable WASP protein has the potential to not only expand our biochemical understanding of protein interactions *in vitro* but also allow for diverse applications *in vivo*, including localized activation of WASP mediated signaling in a cell and for detailed examination of the spatial and temporal regulation of elements downstream of WASP. General principles obtained from this system can be readily adapted to other autoinhibited systems, which will allow for the dissection of other cellular signaling pathways.

References

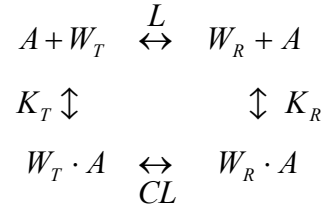
- Benesch, S., *et al.* (2002). "Phosphatidylinositol 4,5-bisphosphate (PIP₂)-induced vesicle movement depends on N-WASP and involves Nck, WIP, and Grb2." J Biol Chem **277**(40): 37771-6.
- Buck, M., *et al.* (2004). "A two-state allosteric model for autoinhibition rationalizes WASP signal integration and targeting." J Mol Biol **338**(2): 271-85.
- Carrier, M. F., *et al.* (2000). "GRB2 links signaling to actin assembly by enhancing interaction of neural Wiskott-Aldrich syndrome protein (N-WASp) with actin-related protein (ARP2/3) complex." J Biol Chem **275**(29): 21946-52.
- Dueber, J. E., *et al.* (2004). "Rewiring cell signaling: the logic and plasticity of eukaryotic protein circuitry." Curr Opin Struct Biol **14**(6): 690-9.
- Dueber, J. E., *et al.* (2003). "Reprogramming control of an allosteric signaling switch through modular recombination." Science **301**(5641): 1904-8.
- Higgs, H. N. and T. D. Pollard (1999). "Regulation of actin polymerization by Arp2/3 complex and WASp/Scar proteins." J Biol Chem **274**(46): 32531-4.
- Howlett, G. J., *et al.* (1977). "Allosteric regulation of aspartate transcarbamoylase. Analysis of the structural and functional behavior in terms of a two-state model." Biochemistry **16**(23): 5091-100.
- Kim, A. S., *et al.* (2000). "Autoinhibition and activation mechanisms of the Wiskott-Aldrich syndrome protein." Nature **404**(6774): 151-8.
- Lim, W. A. (2002). "The modular logic of signaling proteins: building allosteric switches from simple binding domains." Curr Opin Struct Biol **12**(1): 61-8.

- Martinez-Quiles, N., *et al.* (2001). "WIP regulates N-WASP-mediated actin polymerization and filopodium formation." Nat Cell Biol **3**(5): 484-91.
- Monod, J., *et al.* (1965). "On the Nature of Allosteric Transitions: a Plausible Model." J Mol Biol **12**: 88-118.
- Peterson, J. R., *et al.* (2004). "Chemical inhibition of N-WASP by stabilization of a native autoinhibited conformation." Nat Struct Mol Biol **11**(8): 747-55.
- Peterson, J. R., *et al.* (2001). "A chemical inhibitor of N-WASP reveals a new mechanism for targeting protein interactions." Proc Natl Acad Sci U S A **98**(19): 10624-9.
- Prehoda, K. E. and W. A. Lim (2002). "How signaling proteins integrate multiple inputs: a comparison of N-WASP and Cdk2." Curr Opin Cell Biol **14**(2): 149-54.
- Prehoda, K. E., *et al.* (2000). "Integration of multiple signals through cooperative regulation of the N-WASP-Arp2/3 complex." Science **290**(5492): 801-6.
- Ramesh, N., *et al.* (1997). "WIP, a protein associated with wiskott-aldrich syndrome protein, induces actin polymerization and redistribution in lymphoid cells." Proc Natl Acad Sci U S A **94**(26): 14671-6.
- Rohatgi, R., *et al.* (1999). "The interaction between N-WASP and the Arp2/3 complex links Cdc42-dependent signals to actin assembly." Cell **97**(2): 221-31.
- Rohatgi, R., *et al.* (2001). "Nck and phosphatidylinositol 4,5-bisphosphate synergistically activate actin polymerization through the N-WASP-Arp2/3 pathway." J Biol Chem **276**(28): 26448-52.
- Torres, E. and M. K. Rosen (2003). "Contingent phosphorylation/dephosphorylation provides a mechanism of molecular memory in WASP." Mol Cell **11**(5): 1215-27.

Appendix I Derivation of Equations

In the equations below, R and T represents the active and inactive states, respectively, according to the conventions established by the MWC model. WASP is represented by W and activator is represented by A .

Derivation of f_R :



$$\text{fraction in R state} = f_R = \frac{[\text{free R state}] + [\text{bound R state}]}{[\text{total T and R states}]}$$

$$L = [W_T]/[W_R]; \quad X = [A]/K_R; \quad C = K_R/K_T$$

$$[W_R \cdot A] = ([W_R][A])/K_R \Rightarrow [W_R] = ([W_R \cdot A]K_R)/[A]$$

$$[W_T \cdot A] = ([W_T][A])/K_T \Rightarrow [W_T] = ([W_T \cdot A]K_T)/[A]$$

$$[W_R \cdot A] = [W_T \cdot A]/CL$$

$$\begin{aligned}
 f_R &= \frac{[W_R] + [W_R \cdot A]}{[W_T] + [W_R] + [W_T \cdot A] + [W_R \cdot A]} \\
 &= \frac{[W_R] + ([W_R][A])/K_R}{([W_T \cdot A]K_T)/[A] + [W_R] + ([W_R][A])/K_R + [W_R \cdot A]CL} \\
 &= \frac{[W_R] + ([W_R][A])/K_R}{([W_R \cdot A]CLK_T)/[A] + [W_R] + ([W_R][A])/K_R + ([W_R][A]CL)/K_R} \\
 &= \frac{[W_R] + ([W_R][A])/K_R}{([W_R][A]CLK_T)/(K_R[A]) + [W_R] + ([W_R][A])/K_R + ([W_R][A]CL)/K_R}
 \end{aligned}$$

$$= \frac{1+X}{L+1+X+CLX}$$

$$= \frac{1+X}{1+X+L(1+CX)}$$

$$\text{so } f_R = \frac{1+X}{1+X+L(1+CX)}$$

$$\text{where } X = [A]/K_R$$

$$\text{if } [A]=0, \text{ then } f_R = 1/(1+L)$$

$$\text{if } [A]=\infty, \text{ then } f_R = 1/(1+CL)$$

Derivation of K_D :

$$K_D = \text{free} / \text{bound} = \frac{[W_R][A] + [W_T][A]}{[W_R \cdot A] + [W_T \cdot A]}$$

$$= \frac{([W_R] + [W_T])[A]}{[W_R \cdot A] + [W_T \cdot A]}$$

since $C = K_R / K_T$; $L = [W_T] / [W_R]$; $[W_R \cdot A] = ([W_R][A]) / K_R$;

$$[W_T \cdot A] = ([W_T][A]) / K_T$$

$$K_D = \frac{[W_R \cdot A]K_R + [W_T \cdot A]K_T}{[W_R \cdot A] + [W_T \cdot A]CL}$$

$$= \frac{[W_R \cdot A]K_R + [W_R \cdot A]CLK_T}{[W_R \cdot A] + [W_R \cdot A]CL}$$

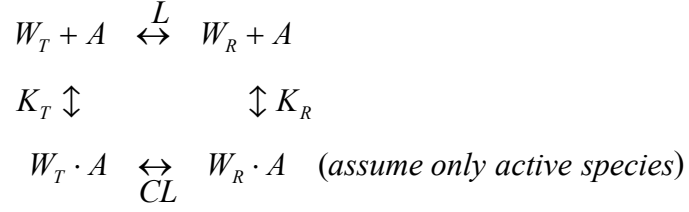
$$= \frac{K_R + CLK_T}{1 + CL} = \frac{K_R + K_R}{1 + CL}$$

$$= \frac{K_R(1 + L)}{1 + CL}$$

if $L \gg 0$, then $K_D = K_R / C = K_{D,T}$

if $L \ll 0$, then $K_D = K_{D,R}$

Derivation of f_R in presence of Arp2/3:



$$C = K_R / K_T; \quad L = [W_T] / [W_R]$$

$$[W_R \cdot A] = [W_T \cdot A] / CL \Rightarrow [W_T \cdot A] = [W_R \cdot A] CL$$

$$[W_R \cdot A] = ([W_R][A]) / K_R \Rightarrow [W_R] = [W_R \cdot A] K_R / [A]$$

$$[W_T \cdot A] = ([W_T][A]) / K_T \Rightarrow [W_T] = [W_T \cdot A] K_T / [A]$$

In terms of WASP:

$$\begin{aligned}
 f_R &= \frac{[W_R \cdot A]}{[W_T] + [W_R] + [W_T \cdot A] + [W_R \cdot A]} \\
 &= \frac{[W_R \cdot A]}{([W_T \cdot A] K_T)[A] + ([W_R \cdot A] K_R / [A]) + [W_T \cdot A] + [W_R \cdot A]} \\
 &= \frac{[W_R \cdot A]}{([W_R \cdot A] CL K_T) / [A] + ([W_R \cdot A] K_R) / [A] + [W_R \cdot A] CL + [W_R \cdot A]} \\
 &= \frac{1}{(CL K_T) / [A] + K_R / [A] + CL + 1} \\
 &= \frac{[A]}{CL K_T + K_R + CL[A] + [A]}
 \end{aligned}$$

therefore, for $[A] = \infty$, $f_R = 1 / (1 + CL)$
for $[A] = 0$, $f_R = 0$

In terms of Arp2/3 complex:

$$\begin{aligned}
f_R &= \frac{[W_R \cdot A]}{[A] + [W_T \cdot A] + [W_R \cdot A]} \\
&= \frac{[W_R \cdot A]}{[A] + [W_R \cdot A]CL + [W_R \cdot A]} \\
&= \frac{[W_R \cdot A]}{([W_R \cdot A]K_R)/W_R + [W_R \cdot A]CL + [W_R \cdot A]} \\
&= \frac{1}{(K_R/W_R) + CL + 1}
\end{aligned}$$

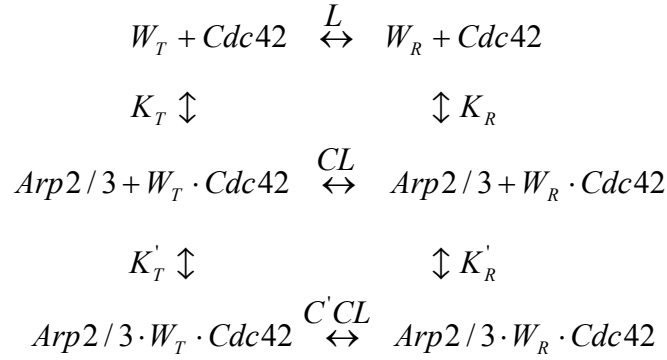
if at $[A] = 0$, for $f_R = (1 + X)/(1 + X + L(1 + CX)) = 1/(1 + L)$ where $X = [A]/K_R$

then $f_R = W_R/(W_R + W_T) = W_R/W_{total} = 1/(1 + L)$, so $W_R = W_{total}/(1 + L)$

therefore, $f_R = \frac{1}{(K_R(1 + L))/W_{total} + CL + 1}$

for $L = 0$, $f_R = 1$; for $L = \infty$, $f_R = 0$

Allosteric model of WASP in the presence of two activators:



$$[W_R \cdot Cdc42 \cdot Arp2/3] = [W_T \cdot Cdc42 \cdot Arp2/3] / C'CL$$

$$[W_R \cdot Cdc42 \cdot Arp2/3] = ([W_R \cdot Cdc42][Arp2/3]) / K'_R$$

$$\begin{aligned}
 f_R &= \frac{[W_R \cdot Cdc42 \cdot Arp2/3]}{[Arp2/3] + [W_T \cdot Cdc42 \cdot Arp2/3] + [W_R \cdot Cdc42 \cdot Arp2/3]} \\
 &= \frac{[W_R \cdot Cdc42 \cdot Arp2/3]}{[Arp2/3] + [W_R \cdot Cdc42 \cdot Arp2/3]C'CL + [W_R \cdot Cdc42 \cdot Arp2/3]} \\
 &= \frac{[W_R \cdot Cdc42 \cdot Arp2/3]}{([W_R \cdot Cdc42 \cdot Arp2/3]K'_R)/[W_R \cdot Cdc42] + [W_R \cdot Cdc42 \cdot Arp2/3]C'CL + [W_R \cdot Cdc42 \cdot Arp2/3]} \\
 &= \frac{1}{K'_R/[W_R \cdot Cdc42] + C'CL + 1}
 \end{aligned}$$

$$\text{if at } [Cdc42] = \infty, f_R = 1/(1 + CL)$$

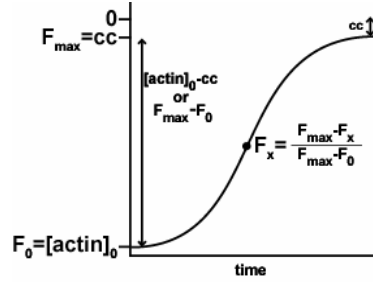
$$f_R = W_R / (W_R + W_T) = W_R / W_{total} = 1/(1 + CL)$$

$$\text{therefore, } W_R = W_{total} / (1 + CL)$$

$$\text{so, } f_R = \frac{1}{(K'_R K_R (1 + CL)) / W_{total} [Cdc42] + C'CL + 1}$$

$$\text{at saturation, } f_R = 1/(C'CL + 1)$$

Derivation of Barbed Ends Equation:



$$\text{elongation rate} = dF / dt = \alpha (k_+ [actin] [ends] - k_- [ends])$$

$$\text{where } \alpha = \frac{F_{\max} - F_0}{[actin]_0 - cc} \text{ and } cc = k_- / k_+$$

$$dF / dt = \left(\frac{F_{\max} - F_0}{[actin]_0 - cc} \right) (k_+ [actin] [ends] - k_- [ends])$$

$$dF / dt = [ends] \left(\left(\frac{F_{\max} - F_0}{[actin]_0 - cc} \right) (k_+ [actin] - k_-) \right)$$

$$\text{therefore, } [ends] = \left(\frac{[actin]_0 - cc}{F_{\max} - F_0} \right) \left(\frac{\Delta F / \Delta t}{k_+ [actin] - k_-} \right)$$

$$[actin] = \left[\left(\frac{F_{\max} - F_0}{F_{\max} - F_x} \right) ([actin]_0 - cc) \right] + cc$$

so if $F_x = F_{\max}$, then $[actin] = cc$ and if $F_x = F_0$, then $[actin] = [actin]_0$

$$\text{therefore, } [ends] = \frac{\text{elongation rate}}{k_+ [actin] - k_-}$$

$$= \left(\frac{[actin]_0 - cc}{F_{\max} - F_0} \right) \left(\frac{\Delta F / \Delta t}{k_+ \left(\left(\frac{F_{\max} - F_0}{F_{\max} - F_x} \right) ([actin]_0 - cc) \right) + cc - k_-} \right)$$

Vitae

Daisy W. Leung was born in Los Angeles, California on September 16, 1975, the daughter of Shun Leung and Yuk-Chun Leung. After completing her work at Benjamin Franklin Magnet High School, Los Angeles, California in 1993, she entered Amherst College at Amherst, Massachusetts. She received the degree of Bachelor of Arts with a major in biology from Amherst College in May 1997. During the following three years she was employed as a research assistant at the University of California, Los Angeles School of Medicine. In August, 2000 she entered the Joan and Sanford I. Weill Graduate School of Medical Sciences of Cornell University in New York, New York. In December, 2001 she transferred to the Graduate School of Biomedical Sciences at the University of Texas Southwestern Medical Center at Dallas. She was awarded the degree of Doctor of Philosophy in December, 2005.

Permanent Address: 6320 Elgin Street
Los Angeles, CA 90042